Thesis report

Investigation of the influence of (auto-)pilot control inputs on helicopter vibrations and ride quality

B.K.F. Yip

TU Delft
AIRBUS HELICOPTERS

Investigation of the influence of (auto-)pilot control inputs on helicopter vibrations and ride quality

Thesis report

by

B.K.F. Yip

to obtain the degree of Master of Science
at the Delft University of Technology,
to be defended publicly on Friday July 6, 2018 at 15:00.

Student number: 4232976
Project duration: August 21, 2017 – July 6, 2018

TU Delft AIRBUS HELICOPTERS

Confidential Clause

The following thesis contains confidential data and information of Airbus Helicopters. Publication or reproduction of all kind – even in digital form or in extracts – is not allowed without express written permission of Airbus Helicopters and the author. Access is granted to the supervisors of the thesis and all persons in charge of its evaluation.

Delft
July 4, 2018

Acknowledgements

This thesis report is written as a part of the graduation project at the faculty of Aerospace Engineering of Delft University of Technology (TU Delft). The graduation project accounts for 54 ECTS (European Credit Transfer and Accumulation System) in which the knowledge and skills obtained during the studies are applied in an individual research project. This document is the final report of my Master's thesis, that I have conducted since August of last year. This thesis also finalizes my Master of Science in Aerospace Engineering, which I started in September 2015.

The topic of this thesis is: 'Investigation of the influence of (auto-)pilot control inputs on helicopter vibrations and ride quality'. My fascination for improving the human experience in complex aerial systems formed my main motivation for choosing this topic. Next to this thesis report, the main contribution is reported in the form of a scientific paper.

For this report, many people provided me with valuable support. I want to thank my supervisor at Airbus Helicopters, Oliver Dieterich for all his support and input throughout the project, and also for bringing me into contact with other colleagues and different departments; most notably German Roth and Robin Lantzsch. I would also like to thank Martijn Priems for arranging this opportunity for me. I want to express my gratitude to my supervisors at the TU Delft as well, Marilena Pavel and Rene van Paassen, for their valuable feedback during this period and arranging the university related side of my thesis.

And finally, I would like to acknowledge all my friends, fellow students and colleagues for creating great memories during my study period. Looking back to my 6 years at Aerospace Engineering, there are too many people to thank specifically. Therefore, I would like to thank the people who started this journey with me during the 'introduction week', the first train trips to Delft and the first year projects. Next to that, I would like to thank the people who provided me the greatest memories during my minor abroad in Singapore and my backpacking experience in South America. These experiences truly opened my eyes on the bigger world we live in. In addition, I would like to thank the project members, who challenged my knowledge during the design of a co-axial hydrogen based helicopter during my Design Synthesis Exercise, and during my time as a member of the Dream Team: Human Power Team. And finally, I am grateful to all the awesome people I met, worked with, had dinner with, partied with, had hiking trips with and celebrated Oktoberfest with during my unforgettable time in Bavaria. Special thanks to all the people who are continuing to answer all my sometimes silly questions, and of course also my little brother for always supporting me.

I especially want to thank my parents for making it possible to earn my Master's degree in Aerospace Engineering. I may be the first in the family line to achieve this, but I have a feeling that many more will follow.

Delft
July 4, 2018

Summary

This project investigates the influence of the helicopter (auto-)pilot control inputs on helicopter vibrations and ride quality. Nowadays the origins and solutions for rotor-induced vibrations in helicopters are well-known. However, non-rotor induced low frequency vibrations still remain a topic of research, although it has proven that these tend to become a dominant source of pilot discomfort, especially in case of turbulence. This research has the aim to reach a conclusion on the effect of (auto-)pilot control inputs on the low-frequency vibrations of the helicopter, and how it influences the ride quality, both in calm and turbulent air. The influence of (auto)-pilot control inputs on the helicopter ride quality is determined in two steps. First, fundamental knowledge about human perception of whole body vibration (WBV) is required to determine the influence of vibrations in helicopters on pilot comfort. Secondly, the pattern and the power of the control inputs and vibration signals are compared to each other. For this, Airbus Helicopters provided flight test data and a non-linear helicopter model.

In this report, first the methods to quantify the helicopter ride quality are critically reviewed. The chosen pilot comfort assessment method is the one described in ISO2631-I. Here, a method is described on how to combine the effects of vibrations from different axes in the form of one parameter a_v, the discomfort value. The sensitivity of the pilot, which is dependent on the frequency, is taken into account with weighting functions.

In order to perform the correlation analysis, the flight test data of two different helicopters are used. The flight test data is analyzed for the EC135 and H145 helicopter. The correlation between the measured control inputs and vibrations is determined in the frequency domain. The correlation analysis is performed by comparing the power of the two signals using Power Spectral Density, and the pattern of the signals using the correlation coefficient. This assessment is done for different rotorcraft configurations and flight conditions. This parametric study shows in which frequency range there is a higher correlation. The similarities and differences in correlation for different configurations and conditions, such as the center of gravity, weight, velocity, rotorcraft mission, flight control system settings and atmospheric conditions are discussed.

The exploitation of flight test data is complemented by related flight mechanics simulations, in order to identify the relationship between control inputs and vibrations under laboratory and thus reproducible conditions. A non-linear helicopter model, including a flight control system and gust model is used for the correlation analysis. The behaviour of a helicopter in flight can be modelled as the combination of a large number of interacting subsystems. The contributions of the main rotor, the fenestron and the airframe are taken into account. As most control inputs occur in the lower frequency domain, only rigid body motions are used. The rotor degrees of freedom considered in this work are the flapping, lead lag and rigid blade torsion. The Dryden wind turbulence model is used to generate turbulence within the helicopter flight simulation. This gust model has been adapated to match the characteristics of a flight-test validated turbulence model developed by Seher-weiss and Gruenhagen [64]. The advantage of using a simulation model is that there are more options for the parametric studies.

Another focus is on the investigation whether the used correlation methods are providing logical and expected results. Knowing the underlying causes for the correlations will help in the process of designing solutions. Elaborations are provided on the pilot inputs, biodynamic feedthrough and the eigenmodes.

Finally, the optimization of the ride quality is discussed. It is determined that the vibrations of a helicopter are dependent on the power of the control inputs and the correlation between the control inputs and the vibrations. The correlation coefficient can be used to measure the susceptibility of a helicopter to vibrations. This parameter is not yet used in the assessment of ride quality, but turned out to be a reliable indicator. Based on this, solutions to improve ride quality are either based on diminishing the amount of control inputs or by designing a helicopter configuration with a low correlation coefficient.

The added value of this thesis is that conclusions are made on where in the frequency domain there are high correlations between the vibrations and the control inputs. Furthermore, the underlying causes for high correlations at certain frequencies are investigated. Knowing where the high correlations come from will help to better understand the causes and therefore provide more guidelines in the process of designing a solution. Finally, the correlation coefficient has been introduced in the research of pilot comfort assessment. It is determined that both a high amount of control input and a high correlation coefficient can lead to higher pilot discomfort. With this knowledge, it becomes easier to design solutions for ride quality improvement.

Contents

List of Figures

List of Tables

Nomenclature

Latin Symbols

a	$[m/s^2]$	Acceleration
a_0, a_1, b_1		Fourier coefficients
a_{L0}	$[2\pi/rad]$	Main rotor blade lift curve slope
a_β	$[m]$	Flapping hinge offset
a_ζ	$[m]$	Lagging hinge offset
a_v	$[m/s^2]$	Vibration Total Value according to ISO 2631-1
a_w	$[m/s^2]$	Weighted Acceleration according to ISO 2631-1
$\vec{b_B}$	$[m/s^2]$	Acceleration of blade element
C_D		Drag coefficient
C_L		Lift coefficient
C_M		Moment coefficient
C_T		Thrust coefficient
c	$[m]$	Blade chord
$c_{\theta B}, c_\beta, c_\zeta$	$[Ns/m]$	Dampers
DA	$[Nm^2]$	Drag area
dD	$[N]$	Drag force of blade element
dL	$[N]$	Lift force of blade element
dM	$[Nm]$	Moment of blade element
$\vec{F}$	$[N]$	Force
$\vec{F_B}$	$[N]$	Force of blade element
f	$[Hz], [1/s]$	Frequency
f_s	$[Hz], [1/s]$	Sampling rate
$\vec{H}$	$[kgm^2/s]$	Angular momentum
H_u, H_v, H_w		Gust Transfer Functions
h_R	$[m]$	Length of rotor mast
I	$[m^4]$	Moment of Inertia
I_β	$[kgm^2]$	Equivalent mass moment for flap
I_ζ	$[kgm^2]$	Equivalent mass moment for lead lag
k_x, k_y, k_z		ISO 2631-1 weighting factors
$k_{\theta B}, k_\beta, k_\zeta$	$[N/m]$	Spring stiffness
L_x, L_y, L_z		Turbulence Scale Length
L	$[Nm]$	Moment around horizontal axis
M	$[Nm]$	Moment around lateral axis
$\vec{M_B}$	$[Nm]$	Moment of blade element
M_β	$[kg]$	Equivalent mass for flap
M_ζ	$[kg]$	Equivalent mass for lead lag
$\vec{M}$	$[Nm]$	Moment
m	$[kg]$	Mass
N	$[Nm]$	Moment around vertical axis
N_B		Number of blades
n		Data points

p	$[deg/s], [rad/s]$	Roll rate
q	$[deg/s], [rad/s]$	Pitch rate
R	$[m]$	Rotor radius
r	$[deg/s], [rad/s]$	Yaw rate
r_{xy}		Correlation coefficient
S	$[m^2]$	Surface area
T	$[s]$	Time Period
T_I	$[s]$	Lag time constant
T_L	$[s]$	Lead time constant
T_R	$[N]$	Thrust
t	$[s]$	Time
U_P	$[m/s]$	Perpendicular speed component
U_T	$[m/s]$	Tangential speed component
$\vec{u}$		Control input vector
u, v, w	$[m/s]$	Speed components
u_g, v_g, w_g	$[m/s]$	Gust speeds
$V, \vec{V}$	$[m/s], [kts]$	Flight speeds
w_d		Horizontal Frequency Weighting according to ISO 2631-1
w_k		Vertical Frequency Weighting according to ISO 2631-1
X	$[N]$	Force in horizontal direction
$\vec{x}$		State variable vector
Y	$[N]$	Force in lateral direction
Z	$[N]$	Force in vertical direction
z_N	$[-]$	Blade number

Greek Symbols

β	$[deg], [rad]$	Flap angle
γ		Lock number
μ		Advance ratio
ρ	$[kg/m^3]$	Density
σ		Gust intensity
θ	$[deg], [rad]$	Control angle
θ_0	$[deg], [rad]$	Collective angle
θ_B	$[deg], [rad]$	Blade torsion angle
θ_L	$[deg], [rad]$	Pitch angle
θ_v	$[deg], [rad]$	Twist angle
θ_α	$[deg], [rad]$	Lateral cyclic angle
θ_β	$[deg], [rad]$	Longitudinal angle
ϕ_i	$[deg], [rad]$	Inflow angle
ϕ_L	$[deg], [rad]$	Roll angle
ψ	$[deg], [rad]$	Azimuth angle
ψ_L	$[deg], [rad]$	Yaw angle
τ_e $[s]$	Effective time delay	
ω	$[deg], [rad]$	Body angles
ω_c	$[rad/s]$	Crossover frequency
ω_{IBC}	$[rad/s]$	Eigenfrequencies rotor modes in individual blade coordinates
$\dot{\omega}$	$[deg/s], [rad/s]$	Body angular rates
Ω	$[rad/s]$	Rotor speed
ζ	$[deg], [rad]$	Lead lag angle

Abbreviations

ADS	Aeronautical Design Standard
ALT	Altitude Hold
ATT	Attitude Hold
ARIS	Anti-Resonance Isolation System
AFCS	Automatic Flight Control System
CETI	Control Equivalent Turbulence Input
CFD	Computational Fluid Dynamics
CSAS	Control and Stability Augmentation System
CSD	Computational Structural Dynamics
CG	Center of Gravity
DISC	Discomfort Unit
DLR	German Aerospace Center
DFT	Discrete Fourier Transform
FEM	Finite Element Method
FFT	Fast Fourier Transform
HDG	Heading mode
HHC	Higher Harmonic Control
IAS	Indicated Air Speed
IBC	Individual Blade Control
ISO	International Organisation for Standardisation
IBC	Individual Blade Coordinate
MBC	Multi-Blade Coordinate
NASA	National Aeronautics and Space Administration
PSD	Power Spectral Density
Rev	Revolution
RMS	Root Mean Square
RMSE	Root Mean Square Error
SAS	Stability Augmentation System
SARIB	Systeme Antivibratoire a Resonateur Integre a Barres
SEMA	Smart Electromechanical Actuators
Sim	Simulation
WBV	Whole Body Vibration

1 Introduction

The purpose of this thesis is to investigate the relationship between flight control inputs and helicopter ride quality. Previous studies on low frequency vibrations has proven that the non-rotor induced vibration is becoming a dominant source of pilot discomfort, especially in case of turbulence, as it is closer to the frequency domain of the human sensitivity. In Section 1.1, the motivation and the relevance of the project are discussed. The research questions and objective are shown in Section 1.2. The outline of the report is explained in Section 1.3.

1.1. Motivation and relevance

Helicopters require a combination of acceptable rotor and airframe loads, an adequate aero elastic stability margin, and low vibrations, in order to be able to profit more from their performance capabilities. For this purpose, the vibrations are a point of attention, as they often define the operating limits of a rotorcraft. Compared to aircraft, the cabin vibration levels of helicopters have always been higher. The main difference between the two is the occurrence of rotor induced vibrations. The main causes of this are the periodic air loads on the rotor blades. Under calm flight conditions, power is generated by the individual rotor blades at multiples of the rpm (revolutions per minute) of the rotor system. Another important type of rotor-induced vibrations is caused by the imbalance and tracking errors of the main rotor. The non-uniformity is due to the variation in manufacturing, and uneven wear/fatigue of the blade as a result of usage. Transmission of these vibrations through the rotor hub will cause vibrations in the fuselage [44]. This will lead to vibrations experienced by the pilots. This can lead to fatigue and health problems. This can also become disastrous with safety related tasks, as the tracking performance of pilot can decrease. Furthermore, the pilot himself will be providing unintentional inputs [50].

While the rotor-induced vibrations are nowadays well-understood, a lesser known area in this field is the influence of non-rotor induced vibrations. This area was in general ignored in the past, but its contribution to vibrations is starting to become more relevant. A study by Rath [51] on this topic concludes that an analysis of flight test data reveals that apart from rotor harmonic vibration, there are other vibration sources that contribute significantly to the vibration discomfort. These vibrations mainly occur in the low frequency domain. The potential causes stated in the research are the elastic tailboom deformations, helicopter flight dynamics and control inputs. It is also stated that with increasing turbulence, the selected non-rotor vibrations tend to dominate the discomfort of the helicopter occupants. Recently, a study was performed by Bernaschek [6] on the influence of the tailboom deformations on the vibrations. Using a FEM Eigenmode analysis and flight dynamics simulations, the different tailboom eigenmodes were identified with the corresponding vibration peaks. The investigation confirms that there is an influence of the tailboom modes on the vibrations and ride quality, and also gives recommendations on how to improve the helicopter ride quality based on a parametric study. In another recent project by Martin [38], the influence of gusts on pilot comfort is discussed. Here it is confirmed that a higher turbulence level causes a higher pilot discomfort. Both a gust model obtained from DLR and the Dryden gust model are used for this study. In order to be able to alleviate low frequency vibrations, the origins of the low frequency vibrations should be well-understood. So far, the influence of helicopter flight dynamics and control inputs on pilot comfort has yet to be investigated.

For this purpose, Airbus Helicopters provides flight test data and a non-linear helicopter model, which makes this project feasible. It is interesting to investigate the causes of vibrations in the low-frequency domain of the vibration spectrum. Although the peaks are not the highest in amplitude compared to the harmonic loads, the affected bandwidth is larger, and the vibrations are close to the frequency domain where the human sensitivity is higher [44]. Furthermore, it would be interesting to investigate whether the pilot comfort can be improved in the low frequency range. To keep this research within the scope of this project; the latter part will only discuss whether the pilot comfort can be improved, instead of providing a mechanical solution.

1.2. Research questions and objective

The thesis should determine the exact correlation between the helicopter control inputs and low frequency vibrations, and find out why there is a correlation. This will be done by investigating both flights under calm and turbulent conditions. Furthermore, it will already provide some initial insights into potential solutions to improve the pilot comfort. Based on this, the research objective for this thesis is:

The research objective of this 9-months master thesis is to come to a conclusion about the effect of helicopter (auto-)pilot control inputs on the low-frequency vibrations, which influences the helicopter ride quality, by determining the correlation between the helicopter (auto-)pilot control inputs to the low-frequency vibrations and turbulence, using existing flight test data and optimized flight dynamics simulations.

Based on this, the main sub-objectives of this thesis are:

1. Based on the flight test data and flight simulations, determine where the correlation between the control inputs and vibrations are in the frequency domain, during both calm and turbulent flights.
2. Investigate the causes for the correlations between the control inputs and vibrations.
3. Use the obtained knowledge to provide recommendations on pilot comfort improvement.

The research questions are:

- How will the helicopter control inputs impact the helicopter ride quality, caused by low-frequency vibrations, during both calm and turbulent flights?
  - In which frequency range can peaks be identified after performing spectral analysis on the flight control inputs?
    - Which variables are able to modify the magnitude of flight control inputs?
    - At which frequency does each of the variables modify the magnitude of the flight control input?
  - What is the correlation between flight control input and vibrations?
    - Which methods can be used to determine the relationship between the helicopter control inputs and the low-frequency vibrations?
    - What is the reliability of the correlation in different flight cases?
  - To which extent do the low frequency vibrations, caused by the helicopter control inputs, have an influence on the helicopter ride quality compared to other vibration sources?
    - What is the most suitable method to measure the low frequency vibrations caused by control inputs in helicopter ride quality?
    - Which parameters will change the extent of the influence?
  - What do we learn about the helicopter ride quality by comparing the results from the correlation analysis during calm and turbulent flights?

1.3. Outline of the report

This thesis is separated into four main chapters, these are the literature review on the state of the art on helicopter ride quality, the flight test data analysis, the flight dynamics simulations and the results analysis. The first main focus is the literature study in Chapter 2, which is already graded for the course AE4020. Here, several pilot comfort assessment methods are reviewed and the most suitable method is chosen. Furthermore, elaborations are provided on the investigation of rotor-induced and non-rotor induced vibrations. Finally, some vibration alleviation methods are explained. The flight test data analysis is presented in Chapter 3. The EC135 and H145 helicopters are analysed, which are both four-bladed twin-engine civil light utility helicopters. In this chapter, different helicopter subsystems are explained. Furthermore, the tools used to perform the correlation analysis are presented. This correlation analysis is also performed on the results of the flight dynamics simulations, which are discussed in Chapter 4. These two chapter should comply with the first sub-objective. The other two sub-objectives are discussed in Chapter 5. Here, the causes for the correlations are investigated and the final evaluation on the pilot comfort is presented. This chapter also includes a discussion the methodology and assumptions. A conclusion is provided in Chapter 6. The accompanying scientific paper is presented in Appendix C.

2

Helicopter ride quality

The cabin vibration levels of rotorcraft are higher in comparison with aircraft. The main reason for higher vibrations is the complex aerodynamic flow field of the main rotor. Changes in this aerodynamic flow field, (auto)-pilot control inputs via the swashplate, and interactions between the rotor blades and vortices of preceding blades are some of the causes for higher amounts of vibrations in the rotor blades. Transmission of these vibrations through the rotor hub will cause vibrations in the fuselage [37]. This influences the comfort of the occupants and can also decrease the performance of the pilot. Long-term exposure to vibrations can also contribute to aircrew occupational health issues including neck strain, back pain injuries and many other human-interface related issues in helicopter operations [9, 27, 28]. Different pilot comfort assessment methods are discussed in Section 2.1. The helicopter vibrations can be divided into two categories: the rotor induced vibrations and the non-rotor induced vibrations. The first group is explained in Section 2.2. The second group, which is close to the frequency domain where the control inputs occur, is discussed in Section 2.3. Some vibration alleviation methods are explained in Section 2.4.

2.1. Pilot comfort assessment

In order to correlate vibrations in helicopters with pilot comfort, fundamental knowledge about human perception of whole body vibration (WBV) is required. The state of the art in research of human vibration perception is summarized by Griffin [44]. There are many ways to measure an oscillatory motion, but the most common way to do this, is by measuring the accelerations. Examples of different types of oscillatory motions are sinusoidal, multi-sinusoidal, transient, shock, stationary or non-stationary motion. Whole-body vibration occurs when the body is supported by a surface which is vibrating. The basicentric coordinate system, shown in Figure 2.1, is useful for these measurements. Next to degraded comfort, other consequences of whole body vibrations can be interference with activities, impaired health, and the occurrence of motion sickness.

Research has been performed between the psychophysical amplitude, representing the human sensitivity, and the measured vibration amplitude [44]. A constant vibration amplitude in each frequency does not produce the same discomfort in each frequency. At low frequencies, below 1 (for x,y-directions) or 2 Hz (for z-direction), the forces acting on the body and the input acceleration have an approximately linear relationship. At slightly higher frequencies , the motion will be amplified due to the occurrence of different body resonance. At even higher frequencies, attenuation will occur. The exact frequencies are of course dependent on a wide range of parameters, such as subject group, seating geometry and backrest conditions. In general, the maximum sensitivity to horizontal translational vibrations (x,y-directions) occurs in the area of 1-2 Hz, if there is no backrest. In the vertical axis (z-direction), the maximum is around 2-6 Hz. Therefore, it can be concluded that the rotor-induced vibrations occur in the area of decreased sensitivity, which is further discussed in Section 2.2. This makes it even more important to investigate the non-rotor induced vibration, which are in the area of maximum human sensitivity.

The sensitivity to rotational vibrations decreases with increasing vibration frequency. Furthermore, the sensitivity to rotational vibrations is dependent on the distance from the center of rotation. If a pilot is located

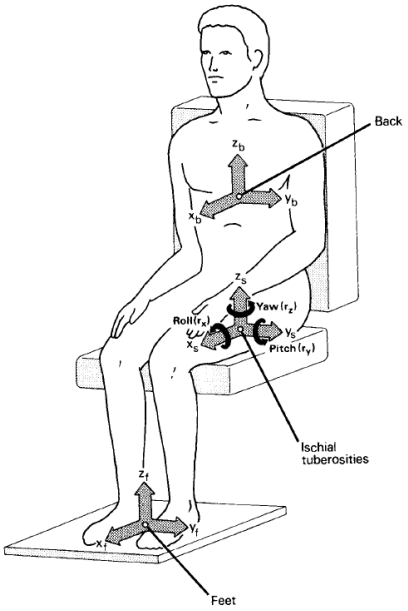

Figure 2.1: A 12-axis basicentric co-ordinate system. The origins of the axes are (i) beneath the ischial tuberosities, (ii) between the back and the backrest and (iii) beneath the feet. [44]

near the center of rotation, almost only pure rotational vibrations will be sensed. However, with increasing distance from the center of rotation, the translational part of the vibration increases as well. The translational vibrations dominate the human perception at distances larger than 1 m, and in many cases even a few centimeters, from the center of rotation, which is the case for pilots in cockpits [23, 44, 49]. Assuming that the center of rotation is near the center of gravity, which is the case when one assumes that the rotational vibrations mainly originate from rigid body rotations rather than elastic motion of the airframe, the rotational vibrations are neglected in this thesis.

Various approaches to evaluate the whole body vibrations have been defined. In order to choose the most appropriate method for this thesis, three common used methods will be discussed [51]. These are the Intrusion Index defined in ADS-27A, the NASA Ride Quality model and the ISO 2631-I.

Intrusion index

The Aeronautical Design Standard 27A-SP defines requirements for rotorcraft vibration specifications, modeling and testing [61]. In this framework, the intrusion index is designed by the US government. The Intrusion index is calculated in the frequency domain and defines the discomfort level of occupants. It assesses the helicopter vibration up to 60 Hz, while treating the 1/rev vibration separately. The frequency spectrum of the helicopter vibrations should be determined first in all three directions. This will be weighted according to certain weighting functions provided in [61]. After this, the root-sum-of-squares of the twelve largest peaks, excluding the 1/rev, is determined. This is the intrusion index. Both this value and the 1/rev value should satisfy the requirements given in [61]. The disadvantage of this method is that it mainly focuses on the rotor-induced vibrations, as it only takes into account large peaks. Furthermore, the weighting factors only start at 5 Hz, which means that lower frequency vibrations are not taken into account. This means that the method is not suitable for this thesis.

NASA Ride Quality model

The NASA Ride Quality model [33] shows a general empirical model for the prediction of passenger ride discomfort in the presence of vibration inputs by combining the results of approximately 2200 test subjects. During the test relevant peaks were selected by the user as input, and it was determined whether the peaks correspond to sinusoidal or random vibration. From the results of the tests, weighting functions can be made. DISC units are defined for the quantification of the discomfort level, which is based on perceived vibrations

after the weighting factor, which is calculated in the frequency domain. A value of DISC = 1 corresponds to 50% of the test subjects feeling uncomfortable. The advantage of this method is that it does take into account rotor and non-rotor induced vibrations. However, just a small amount of low frequency oscillation are considered. This was also the point critized by Stewart [66] for giving inaccurate results in real flight. Furthermore, it has a limited frequency range and number of axis. Frequencies higher than 10 Hz in the y-direction and higher than 30 Hz in the z-direction were not taken into account. Except for 1 frequency point, the x-axis is not considered at all.

ISO 2631-I

The ISO 2631-1(1997) standard is the second edition, which includes the findings summarized by Griffin [44]. In this standard, the method to combine the effects of vibrations from different axes in the form of one parameter a_v, is described. The relevant vibration frequencies for comfort evaluation are in the range of 0.5 Hz to 80 Hz according to ISO 2631. The reference frame at which this filter works is shown in Figure 2.1. The ISO 2631-I is able to consider twelve coordinate systems for comfort evaluation. On the seat the three translational and rotatory vibrations can be taken into account, and at the feet and the backrest only the three translational vibrations. For each location and direction a multiplying factor and weighting function exist. Like the NASA Ride Quality model, it is able to quantify the discomfort caused by non-rotor induced vibrations. Furthermore, it has the advantage of having a weighting function for the x-direction and more tests were applied in the lower frequency domain. A disadvantage is that the inputs were given at one axis at a time, which means that the amount of applicability to multi-axes broadband vibration environment of a helicopter remains unknown. However, none of the commonly used comfort evaluation methods includes this. Another disadvantage is that it is not specifically designed for aerial vehicles. But despite this, when comparing the weighting function of the different methods with each other, as done by Rath [51], the functions are quite close to each other. This is shown in Figures 2.2 and 2.3. Therefore, the decision is made to use the ISO 2631-I for this thesis.

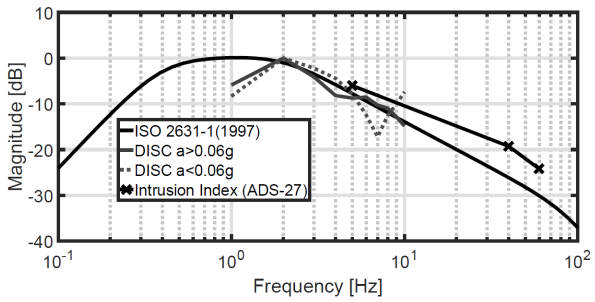

Figure 2.2: Comparison of Weighting Functions (horizontal) [51]

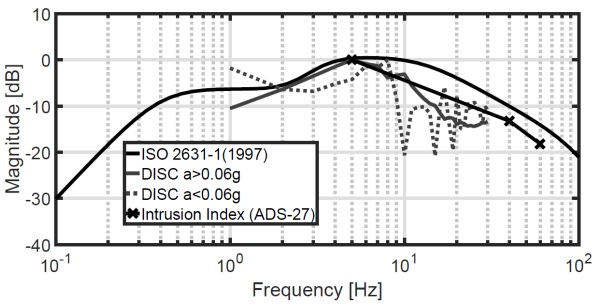

Figure 2.3: Comparison of Weighting Functions (vertical) [51]

Due to availability reasons of sensors in the flight test, only the comfort analysis for the seat location is performed. The vibration on the floor, which is parallel to the positions of the seat surface, is mainly considered. The translational frequency sensitivity weighting curves are shown in Figure 2.4 for x,y-directions and in Figure 2.5 for z-direction. One can notice that the vibrations in x,y-directions are more important for the lower frequencies up till approximately 3 Hz with a peak sensitivity around 1 Hz. After that, the vibrations in z-direction will weight more in the calculation of the discomfort.

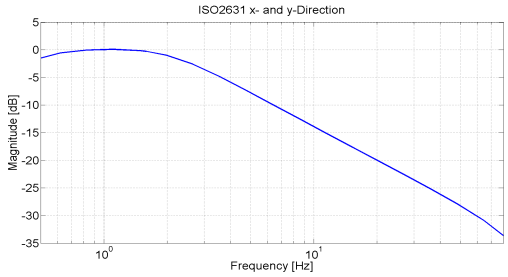

Figure 2.4: Frequency weighting curve for x,y-directions

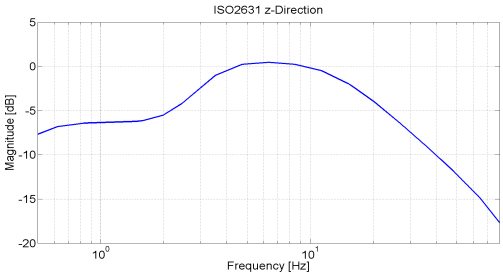

Figure 2.5: Frequency weighting curve for z-direction

The acceleration signal is fed through the filters defined in ISO 2631-1 resulting in the weighted acceleration as a function of time ($\vec{a_w}(t)$). The key indicator for the discomfort level of a vibration signal is the weighted root-mean-square (r.m.s.) acceleration. This is defined as in Equation 2.1, where T is the duration of the measurements in seconds. This equation is only valid if a crest factor of 9 is not reached. This is assumed to be the case for low frequency vibrations. The final evaluation is done by summing the weighted acceleration with a certain multiplying factor. The multiplying factors $k_x = k_y = 1.4$ and $k_z = 1$ as specified in ISO 2631-1 are used. By this definition, the missing influence of the backrest is taken into account. This is shown in Equation 2.2.

$$\vec{a_w} = (\frac{1}{T}\int_0^T \vec{a_w}^2(t)\,dt)^{\frac{1}{2}} \tag{2.1}$$

$$a_v = (k_x^2 a_{wx}^2 + k_y^2 a_{wy}^2 + k_z^2 a_{wz}^2)^{\frac{1}{2}} \tag{2.2}$$

Acceptable values of vibration magnitude for comport depend on many factors which vary with each application. It for example depends on the expectation of the passenger with regards to the trip duration and the type of activities passengers are expected to accomplish. This is why fixed ranges for comfort ratings are hard to define. An indication defined by ISO 2631-I is shown in Table 2.1.

Table 2.1: Comfort rating ISO 2631-I [44]

Range of a_v in m/s^2	Comfort rating
Less than 0.315	Not uncomfortable
0.315 to 0.63	A little uncomfortable
0.5 to 1.0	Fairly uncomfortable
0.8 to 1.6	Uncomfortable
1.25 to 2.5	Very uncomfortable
Greater than 2.0	Extremely uncomfortable

2.2. Rotor induced vibrations

The main causes of rotor induced vibrations are the periodic air loads on the rotor blades. Another important type of rotor-induced vibrations is caused by the imbalance and tracking errors of the main rotor. Both are discussed in this section.

Under calm flight conditions and when rotor blades are undamaged, power is generated by the individual rotor blades at multiples of the rotor rpm (revolutions per minute) of the rotor system due to their periodic physics. This power is displayed at multiples of N/rev, where N is the number of blades. This is a consequence of the orthagonality of the sines applied to the harmonic signals, which blocks certain frequencies from being transmitted from the blades into the fuselage (fixed system) and therefore eliminates other rpm multiples. These N/rev frequencies also contain the highest vibration energies and can have severe consequences [10, 19, 41].

Vibration occurs in the other rpm multiples if there is a variation in manufacturing, and uneven wear/fatigue of the blade as a result of usage. The vibrations regarding this domain occur at frequencies of p/rev where p is an integer value. The most prevalent vibrations of this kind are typically located at a frequency of 1/rev, i.e. the rotor speed [4]. The centrifugal force is one of the basic excitation forces in the rotor blades. Vibrations may originate when the center of gravity of the blades does not exactly coincide with the axis of rotation. Discrepancies may for example occur during design (some parts may not be perfectly symmetrical), during manufacturing (everything is produced with tolerances) or due to technical reason (non-homogeneous material). This can lead to static, coupled or dynamic unbalance. The latter two will mainly have effect on the 1/rev harmonic. Another common fault that can cause vibration is misalignment. Usually it is assumed that the rotor axis is concentric with the axis of housing and bearings and that rotors connected together have a common axis. However, during operations misallignment can occur, which is also called rotor tracking errors. Parallel misallignment mainly has an effect on 1/rev, but it is quite common that the other harmonic

frequences will be affected as well. Angular misallignment will mainly affects the 2/rev harmonic. Interharmonic or subsynchronus vibration may occur due to for example rotor rub, which means a slight contact between a rotor and a stator [7].

2.3. Non-rotor induced vibrations

Since the rotor induced vibrations are a function of the rotor speed, their definition in the frequency spectrum is straightforward. However, the location of the non-rotor induced vibrations is usually harder to locate. Moreover, non-rotor induced vibrations generally have a broader bandwidth, lower amplitudes and are located in the lower frequency domain. As said before, even though the amplitudes of these vibrations are smaller, the effect on the ride quality can still be significant, as it has a larger bandwidth and it occurs closer to the area where human sensitivity to vibrations is higher. In this section, the influence of the tailboom shake phenomenon and the turbulence on the helicopter vibrations is discussed.

2.3.1. Tail boom effects

The focus in this section is on tail-boom-induced vibrations, which are mainly caused by the tail shake phenomenon. This phenomenon can be described as an interaction between aerodynamic excitations due to the rotor wake or gusts and the corresponding structural dynamics response [11]. This interaction can result in the excitation of the lower elastic modes of the tailboom, usually in the vicinity of 1 to 2/rev. A time-resolved coupling framework between Computational Fluid Dynamics (CFD) and Computational Structural Dynamics (CSD) has been implemented by Schäferlein [62] to determine the interaction between the rotor wake and the structural excitation This study was successfully validated against flight test data. The latter allows a physical insight into aeroelastic phenomena on the helicopter airframe. The relevant tailboom motions are the vertical, lateral and torsion modes, with the first mode being the most dominant one. The first vertical bending mode is a two node mode for which an example is provided in Figure 2.6. This means that the vibration is mostly felt in front of the forward node, which is usually the location of the cockpit. An important aspect of the tailboom shake is that it has an unsteady nature, which means that the wake induced excitation is also unsteady of nature. The crew feels “kicks”, sometimes characterised by the crew as a low-frequency vibration, also called buffeting.

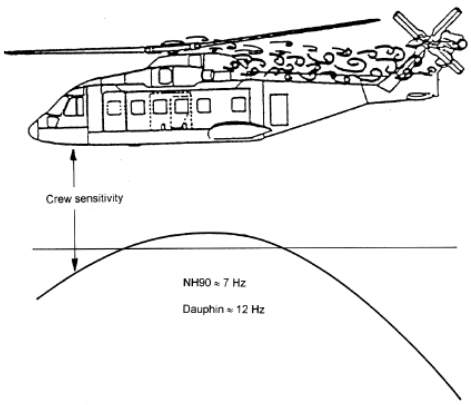

Figure 2.6: First vertical bending mode (2 nodes) [11]

A model to determine tail-boom-induced vibrations in the cabin is developed by Bernaschek [6]. The main excitations in this study are the gusts, and the resulting vibrations are linked to helicopter ride quality. A Finite Element Model (FEM) is used to determine the elastic motions and is validated by an on-ground shake test. The modal masses, eigenfrequencies and the mode shapes of four different locations, including the pilot seat, have been evaluated by an eigenanalysis. These results show that the vertical tailboom mode is indeed the most dominant one, which means that it contributes the highest discomfort to the pilot. The latter is calculated with the ISO 2631-I weighting functions. The effect of turbulence is investigated as well. It shows that higher turbulence results in higher discomfort. The lateral tailboom mode has some influence as well, mainly in the lateral vibrations. However, the human body is the most sensitive in this direction around 1 Hz. This frequency is not close to the structural modes. There is almost no influence on the comfort of the pilot by the torsion mode, due to its mode shape and higher modal mass.

A recommendation was given in the same research how one can improve the pilot comfort. The latter can be achieved by increasing the natural frequency of the vertical tailboom mode. This can for example be done by stiffening the tailboom. However, by doing this the mass will increase. This should therefore be a trade-off. These parameters should also satisfy the handling qualities and other design criteria.

2.3.2. Turbulence

Turbulence can affect the helicopter in two manners. It can both excite the structure directly or perturb the incident flow of the rotor blades. It was stated before that in case of turbulence, the non-rotor induced vibrations tend to dominate the pilot discomfort. Therefore, it is important to compare situations in both calm and turbulent air, and how the latter will have influence on the correlation between the control inputs and the vibrations. For this purpose, the gust modelling and the helicopter gust response are discussed.

Gust modelling

In order to understand the effect of an gust excitation on the response of an helicopter, some investigation has been done on gust modelling first. Figure 2.7 shows how atmospheric disturbances are commonly represented, as a superposition of mean wind, periodic waves and random non-periodic turbulence [67]. In general, the contribution of mean wind and periodic waves have small contributions to the dynamic aircraft response as they vary slowly over time [52]. Therefore, the focus will be on random non-periodic turbulence.

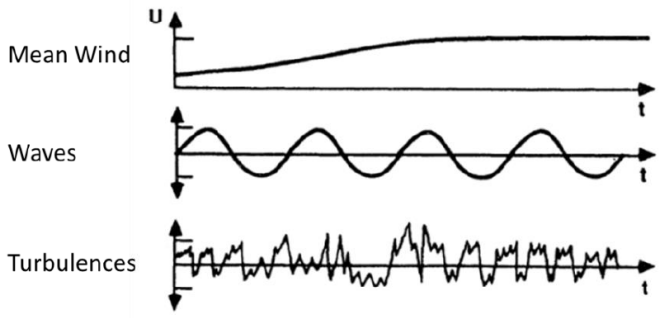

Figure 2.7: Components of atmospheric disturbances [67]

Atmospheric disturbance models can often be categorized into two idealized categories; discrete and continuous. Discrete gusts are generally treated deterministic, having simple forms, and are typically considered in the time domain. Continuous turbulence is treated as a non-deterministic distribution and is considered in either the time domain or frequency domain [52]. Three different discrete gust models have been identified to be relevant in helicopter gust related studies. The first implemented model was the sharp-edged gust model, which models an uniform and instantaneous change in gust velocity [26]. A linear ramped change in gust velocity is modelled as well [25]. Another commonly used model is the 1-cosine shaped model, which consists a sinusoidal representation of the time-varying gust velocity [25, 76]. The latter three models are shown in Figure 2.8.

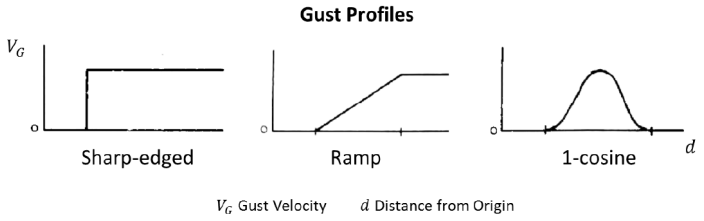

Figure 2.8: discrete gmust profiles, adapted from [24]

Several continuous turbulence models have been developed over the years. The Dryden and Von Karman gust models are the two most common ones used in rotorcraft applications. Both models are defined by using the Root-Mean-Square (RMS) turbulence velocity and a characteristic scale wavelength as function of the

altitude. These parameters are defined in a study by [43]. Both distributions are also defined by their Power Spectral Densies and can be used in both time and frequency domain [25, 76]. Studies have been performed to compare different gust models [73]. The conclusion is that the Von Karman model fits more accurately to measured atmospheric distributions. However, it is also more complex and harder to implement in the time domain as filtered white noise.

Other important aspects on modelling atmospheric disturbances are the reproducibility of the iso-tropy and dimensionality. Principally, the filters in the Von Karman and Dryden model can be used for every direction, as gusts and turbulence tend to be isotropic in the real atmosphere. A notable exception to the isotropy simplification is turbulence due to thermals. The latter is anisotropic and has greater intensity in the vertical direction [25].

For this thesis, the Dryden gust model is used, as it is less complex, and is optimized with the DLR gust model, which has been validated with flight tests for certain flight conditions. Initially, the Dryden model has been designed for planes and not for rotorcraft. Therefore, an adaption to the 135/145 helicopter types is required. This has been performed by Martin [38]. The working principle of the DLR gust model [64] is to produce extra control inputs, which can cause the helicopter to react the same way as in a gust response. The gust model is inspired from the CETI (Control Equivalent Turbulence Input) method [36]. An observer approach, as can be seen in Figure 2.9, can be used to define control inputs related to gusts. The pilot inputs obtained under turbulent conditions are fed into a nominal model of the aircraft to get the response caused by the pilot inputs. The difference between the measured response (which includes the influence of gusts) and the calculated response is consequently determined. This difference is minimized by additional controls calculated in the feedback loop. These time histories will be used to generate white noise driven transfer functions. The DLR gust model has been validated for low altitudes and low speeds for the 135 helicopter types.

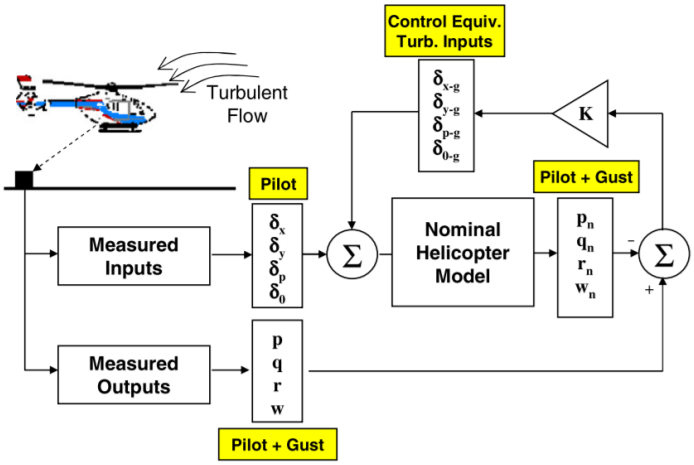

Figure 2.9: Gust extraction by observer [64]

This validated model is used to optimize the translational transfer functions of the Dryden model. The equations are shown in Equation 2.3 - 2.5. The tunable parameters in these equations are the gust intensity (σ) and the wavelength scales (L). These parameters are tuned, such that the Root Mean Square Error (RMSE), as shown in Equation 2.6, between the two models is minimized. This is done with low altitude and low velocity conditions for different turbulence levels. Correct configurations for different altitudes should be obtained as well. This is also defined in [43]. For his research, Martin [38] has used a more linear function between the turbulence intensity and the altitude. Unlike the DLR gust model, the helicopter velocity is a direct variable of the transfer functions, which makes this an easily modifiable parameter. Another advantage of using the Dryden model instead of the DLR gust model, is that the Dryden model adds gust velocity, instead of additional control inputs. The latter would add unwanted signals to the (auto)-pilot control inputs, which are not beneficial for this thesis.

$$H_u(s) = \sigma_x \sqrt{\frac{2L_x}{\pi V}} \frac{1}{1 + \frac{L_x}{V} s} \tag{2.3}$$

$$H_v(s) = \sigma_y \sqrt{\frac{L_y}{\pi V}} \frac{1 + \frac{\sqrt{3}L_y}{V} s}{(1 + \frac{L_y}{V} s)^2} \tag{2.4}$$

$$H_w(s) = \sigma_z \sqrt{\frac{L_z}{\pi V}} \frac{1 + \frac{\sqrt{3}L_z}{V} s}{(1 + \frac{L_z}{V} s)^2} \tag{2.5}$$

$$RMSE = \sqrt{\frac{\sum_{t=1}^{n} (\hat{y}_t - y_t)^2}{n}} \tag{2.6}$$

Helicopter gust response and pilot comfort

In this section, relevant publications about helicopter responses to gusts are discussed. Furthermore, a literature review on the influence of gusts on helicopter ride quality is performed.

At the end of the sixties, in a research by Drees and Harvey et al. [12], the influence of several gust parameters on the gust response of different helicopter configurations were studied. This is done by varying parameters such as forward speed and rotor loading. They find that gradual gust penetration and gust shape have strong influences on helicopter gust loads. In absence of gradual penetration, non-steady aerodynamics becomes more relevant in responses to sudden gusts. The rotor-thrust coefficient and the type of rotor blade (e.g. rigid or articulated, offset flapping hinge) are also major factors. They further show that aeroelastic blade deformation has a relatively small influence on the gust load for rotors with good blade resonance characteristics and high torsional frequency. The effects of the tip speed, forward speed, Lock number and number of blades are also considered small. Additionally, the study concludes that increasing hub stiffness leads to more gust sensitivity.

In a reseach a few years later, Bergquist and Arcidiacono et al. [2] determined the gust response characteristics analytically considering the gust responses shown in Figure 2.8. The principal parameters influencing gust-induced load factor appear to be the non-dimensional blade loading, the proximity of the rotor trim point to blade stall, and the rate of penetration of the rotor into the gust.

Elliot and Chopra found that by increasing flight speed, there will be a significant impact on the helicopter response [13]. On the other hand, Padfield [47] stated that in forward flights with velocities higher than approximately 100kts, helicopters are less sensitive to gusts than airplanes. This is due to the vertical heave damping derivative (Z_w), as can be seen in Figure 2.10. This can be due to the fact that the blade loading of a helicopter is generally higher than the wing loading of an airplane.

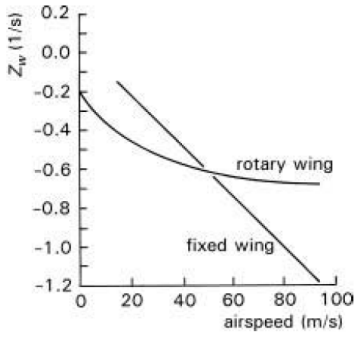

Figure 2.10: Gust response sensibility, heave damping derivative over airspeed [47]

To analyze how the gusts influence the helicopter ride quality, the comfort needs to be quantified. Unlike other vibration sources, there is not a certain frequency range at which the vibrations caused by turbulence

can be generally found. Furthermore, turbulence can have influence on other vibration sources, like tailboom shake or control inputs. Therefore, Martin [38] has performed a parametric study, in which he found in which cases the turbulence will have a large or small effect on the ride quality. Regarding the comfort analysis, the parameters that can influence the helicopter reaction are the weight and balance, as well as the helicopter velocity and the turbulence level. On the other hand, no major differences have been found regarding the lead-lag damping, the stabilizers, the position of the center of gravity or the fuselage moment of inertia.

2.4. Vibration alleviations

The possible benefits from reducing helicopter vibration are as follows: reduced crew fatigue, increased fatigue life, extended flight envelope, and increased passenger comfort [50]. Long-term exposure to vibrations is known to contribute to aircrew occupational health issues including neck strain, back pain injuries and many other human-interface related issues in helicopter operations [9, 27, 28]. As told before, the main focus so far was the alleviation of the harmonic vibrations. The most common alleviation methods will be globally discussed here. The main purpose is to gain some insights into which parameters are tunable for a better ride quality.

Traditional methods to diminish the helicopters vibrations are based on passive approaches, for example structure detuning. This can be achieved in two ways: frequency placement method or by modal orthogonality placement method. In the frequency placement method, structural vibration is reduced by keeping the natural frequency of the structure and the excitation frequency apart from each other. Modal orthogonality placement method involves the maximization of orthogonality of the structural mode shapes to the spatial variability of the applied loadings [22, 35, 54]. This can be done using vibration suppression devices, which means appropriately tuning spring–mass–damper system [72]. Two concepts of isolation systems developed and certified at Airbus Helicopters are the ARIS and SARIB concepts [29]. Vibration isolators try to decouple the dynamics of the main rotor from the fuselage dynamics. This makes the fuselage less susceptible to excitations from the main rotor. Another method is to design the rotor for minimum vibration. Design parameters could for example be the twist or tip sweep. Tailoring of the composite structure could also be an option [18, 21]. Disadvantage of passive systems is that they do not adapt to changing flight conditions.

Numerous active technologies to alleviate the source of the N/rev vibrations have been developed. An example of active vibration control device is the Higher Harmonic Control (HHC) system. Here the blades are oscillated at higher harmonics of the rotor rotational speed. The most popular approach is blade feathering at the root using swashplate oscillations in order to cause unsteady aerodynamic and inertial loads to counteract the existing vibratory blade loads. The latter will cause airframe vibration [46]. Another option is Individual Blade Control, which allows each blade to be controlled separately at a desired frequency [31]. This can be done with servo actuators [56], embedded piezoelectric materials [75] or trailing-edge flaps [17].

To reduce the p/rev vibrations, rotor tracking and balancing methods are used. Examples are using trim tabs as well as pitch rod adjustments for rotor tracking. Furthermore, tuning masses for rotor balancing are used [5].

Next to this, active anti-vibration systems are used as well. The system is based on single-port active devices that are capable to create inertia-based control forces. The latter induce a secondary vibration field to compensate the vibration disturbance [29]. Furthermore, one of the main tasks of the flight control system is to reject disturbances. Note that further research is being developed in this area [47].

Some initial investigations have been performed for the reduction of vibrations caused by the tailboom. The results are, amongst others, to soften the tailboom such that it acts like a vibration absorber. Furthermore the tailboom can be stiffened followed by softening of the fuselage to reduce the vibration at the pilot seat [45].

Vibration control in the fuselage is also possible and is mostly designed to reduce vibrations in a local area. This local area, for instance, could be the instrument panel, a special equipment or the pilot seat. Currently, several adaptive seat vibration isolation devices have been proposed to increase the pilot comfort [74].

3

Flight test data analysis

For this thesis, flight test data and flight dynamics simulation are used in order to check for potential correlations between helicopter control inputs (collective and cyclic main rotor control, pedals for tail rotor control) and low frequency vibrations during calm and turbulent flights. Access to the flight test data of the EC135 and H145 is provided by Airbus Helicopters. The analysis of the data is discussed in this Chapter. In Section 3.1, general information is provided of the EC135 and H145 helicopters. The similarities and differences between the helicopters are explained here. The available flight test data are discussed in Section 3.2. Section 3.3 elaborates on the used methodology to determine the correlation. Results of the spectral analysis, correlation analysis and pilot comfort assessment are discussed in Sections 3.4 and 3.5. Finally, a conclusion on the flight test data analysis is provided in Section 3.6.

3.1. Helicopter types: 135 and 145 helicopter family

For this thesis, the flight test data of the EC135 and H145 helicopters are studied. They are both four-bladed twin-engine civil light utility helicopters, produced by Airbus Helicopters, which was formerly known as Eurocopter. The differences and similarities in the specifications of the helicopters are discussed below. In this discussion, the focus is placed on the main rotor system, the flight controls and the AFCS.

3.1.1. Specifications comparison

The EC135 is a member of the light-medium EC135 helicopter family of Airbus. They are mainly marketed as emergency medical service, for corporate transport, law enforcement, offshore wind applications and flight training. The maximum take off weight is 2980 kg. The maximum range is 609 km, the cruise speed is around 250 km/h and the maximum speed is around 275 km/h. The length of the helicopter is 10.0 m and the width is 2.0 m. The anti-torque system consists of the Fenestron shrouded tail rotor, which provides high efficiency, lower noise and increased safety close to terrain [15]. Furthermore, it contains a bearingless main rotor, which has no main rotor head. This reduces weight and maintenance efforts. The main difference between the version used in this work and the other helicopters in this family is that it has a radius of 5.1 m and end plates on horizontal stabilizer.

The H145 is a member of the EC145/BK117 family. It is primarily used for emergency medical service, on- and offshore missions, in private and business aviation and in law enforcement missions. Compared to the EC135, the H145 is larger and heavier. It has a maximum take off weight of around 3500 kg, a width of 2.4 m and a length of 11.69 m. The maximum range is slightly higher, namely 663 km. The cruise and maximum speeds are comparable to the EC135. As the H145 is larger, it also has larger capacity, which is 9 passengers. For the EC135, this is 7 passengers [16]. The H145 has the same anti-torque system as the EC135, namely the Fenestron shrouded tail rotor, which is also the main difference with the other helicopter types in this family. Pictures of the EC135 and H145 are shown in Figures 3.1 and 3.2 respectively.

For this thesis, it is interesting to know the difference in the approximate frequency tailboom modes, the $1/rev$ and N/rev values. These vibration sources were discussed in Sections 2.2 and 2.3.1 respectively and are listed in Table 3.1.

Figure 3.1: Photo of EC135 [15]

Figure 3.2: Photo of H145 [16]

Table 3.1: Approximate frequencies at which the tailboom modes and rotor-induced vibrations occur, shown in [Hz]

Helicopter Type	**Tailboom modes**			**Rotor-induced vibrations**	
	Vertical	Lateral	Torsion	$1/rev$	N/rev
EC135	5.2	5.6	12.9	6.58	26.3
H145	4.8	5.6	11.3	6.39	25.56

3.1.2. Main rotor system

Both types of helicopters have a four-bladed rotor system. In general, there are two main types of rotor systems: articulated and rigid. In a fully articulated rotor system, each rotor blade is attached to the rotor hub through a series of hinges that let the blade move independently from the others. This means that the blades are able to flap, feather, and lead or lag independently from each other. The term rigid rotor usually refers to a hingeless rotor system. This is also the system that is used in the H145. The blades accommodate the loads, that are caused by flapping and lead-lag by bending, as the blades are flexibly attached to the hub. An advantage of this system is that it is less susceptible to mast bumping. Other advantages are that the weight and drag are reduced, less maintenance is required and that the control inputs can be reduced due to a larger flapping arm. Although the oscillations can be partly eliminated because of the fact that the rotor and fuselage move together as one entity, vibrations are also felt stronger in the cabin as there are no hinges that help absorbing some of the loads. The EC135 helicopter uses a bearingless rotor system. The main difference with the hingeless variant is that it has no feathering bearing. Furthermore, the material inside the cuff is twisted by the action of the pitch change arm as a single entity [8, 48, 63]. The articulated and hingeless rotor systems are shown in Figures 3.3 and 3.4 respectively.

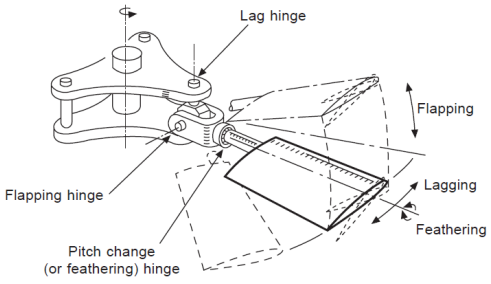

Figure 3.3: Example of an articulated rotor system [8]

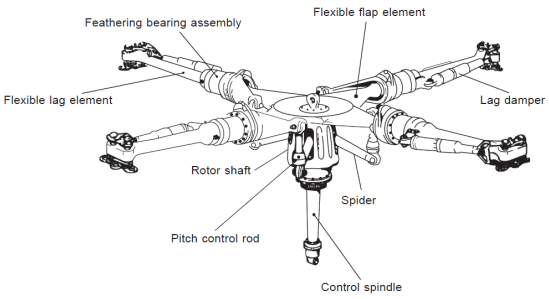

Figure 3.4: Example of a hingeless rotor system [8]

3.1.3. Helicopter flight controls

In general, helicopters have four primary flight controls. The control input for the anti-torque system is given by the pedals. Next to this, there is the collective lever and the cyclic stick. The latter is able to provide longitudinal and lateral cyclic input.

Between the collective and cyclic flight control inputs and the rotor blades is a swashplate. This is a device that translates input from the helicopter flight controls into motion of the main rotor blades. The swashplate consists of two plates, of which the lower plate does not rotate with the shaft, but can be tilted in any direction by the pilot's cyclic control. The upper plate rotates with the shaft but is constrained to remain parallel to the lower plate. Collective pitch is applied by the collective lever which can raise or lower the swashplate without causing further tilt. This will change the pitch angle of all the blades by the same amount [8, 47].

In Figure 3.5 one can see the pilot control inputs being applied to the cyclic stick and collective lever and being transmitted through three ball bearing control cables. These flexballs transmit the control inputs to the input lever of the main rotor actuators. Here the control inputs are transmitted via control rods to the mixing lever assembly. The Automatic Flight Control System generates additional control inputs via the Smart Electromechanical Actuators (SEMA) and trim actuators to the main rotor controls. The tail rotor has the same working principle, except for the fact that the pedals input is sent to the tail rotor actuator [68].

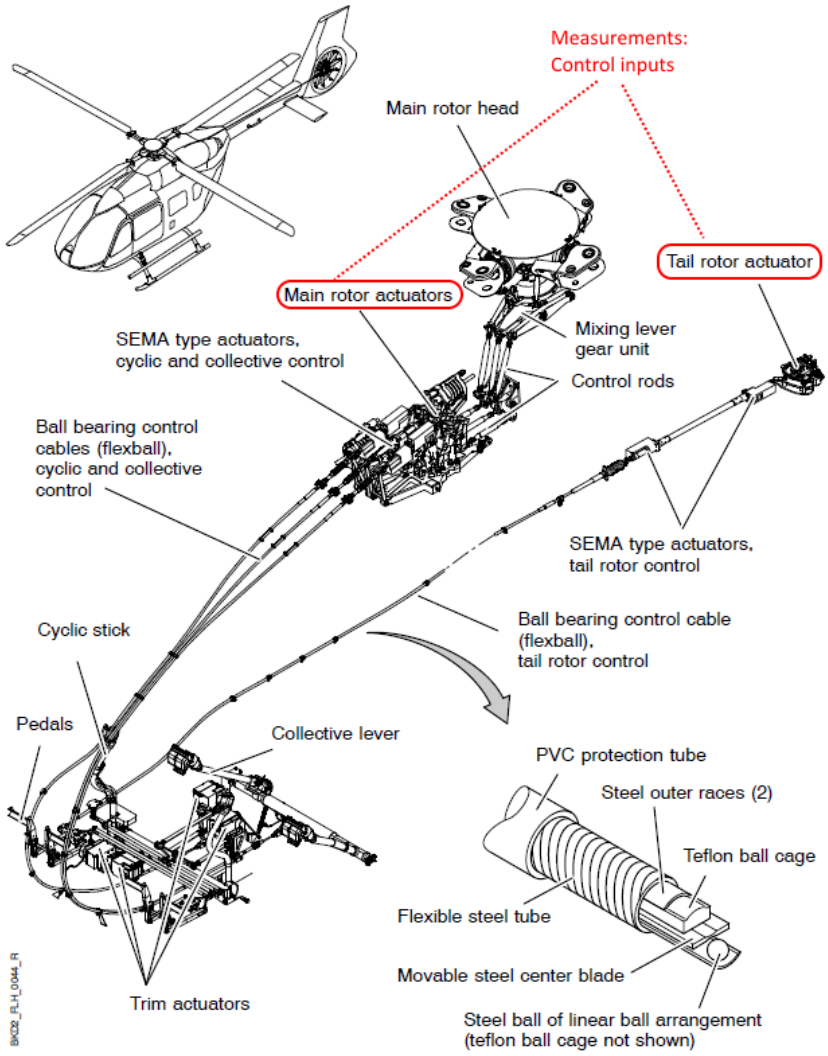

Figure 3.5: Flight control system [68]

3.1.4. Automatic Flight Control System

The H145 is equipped with a 4-axis AFCS for the pitch, roll, collective and yaw axes. The AFCS also regulates both the Smart Electromechanical Actuators and the trim actuators for all four directions. The EC135 can nowadays be equipped with the 4-axis AFCS as well, but for the considered flight tests, the 3-axis AFCS was used. This 3-axes system lacks the regulation of the SEMA for the collective axis and the trim actuator for yaw

[68].

In general, the AFCS settings can be divided into four categories. The first category, which also contains the least or no pilot input, consists of the upper modes. The upper modes include for example the Altitude hold (ALT), the Indicated Air Speed (IAS) and the Heading (HDG) mode. The second category consists of the Attitude hold mode (ATT) when flying with hands off. When the pilot overrides the spring forces, the trim actuator command is automatically disabled and the AFCS will switch to the Control and Stability Augmentation System mode (CSAS). The third category consists of the Stability Augmentation System (SAS). The fourth category means that the AFCS is switched off and that there is only the Integrated Electronic Stand-by Instrument (IESI), which will switch on the back-up SAS [68] if needed. The main difference between the two helicopters in this case is in the upper modes. The 3-axis AFCS is for example not capable to use the ALT and IAS modes at the same time, as it only has pitch control. The 4-axis AFCS is able to use both the pitch and collective for these two modes.

3.2. Flight test data

Flight test data of four different serial numbers of the EC135 and H145 is available. For each serial number, several flight tests are performed at different flight conditions. For each helicopter, data of at least 50 flights tests is available. For each flight test, the helicopter can have a different configuration, such as different take-off weights or center of gravity locations. Furthermore, the flight mission can be different, such as mainly level flight or mainly performing manoeuvres. The investigated flight tests are all level flights, except the one shown in Section 3.5.5. Other examples are different flight speeds, altitudes or AFCS settings. The pilot can differ as well, which is especially important to take into account during flights where the AFCS is off. One should also take into account the turbulence level. Each pilot needs to provide a rating for this. These differences will be discussed in Sections 3.3.2 and 3.5. Measurements of 200 seconds with a sampling rate (f_s) of 400 Hz are performed. The most important measurements for this thesis are listed below:

- Vibrations in x,y,z-direction: Measured with 3-axis accelerometers at several locations in the cabin, including on the floor at the pilot location, which is required for the ISO2631-I calculation.
- Angular rates: The pitch and roll rates were measured with fiber-optic gyro-based sensors during the flight test. Although the rates will not be taken into account during the discomfort calculation, it is still interesting to determine the correlation between the control inputs and the pitch/roll disturbances.
- Control inputs: Linear displacements of the 4 flight controls are measured at the main/tail rotor actuator. This means that the measured value is a combination of the pilot and autopilot control inputs.

These measurement locations are also highlighted in Figure 3.5 for the control inputs, and in Figure 4.2 in Section 4.1 for the vibrations. In that section, the used reference frame will also be discussed. In order to investigate the correlations between control inputs and vibrations, one should know which flight control has influence on which translational or rotational vibration. For this purpose, from Newton's Second Law, shown in Equations 3.1 and 3.2, the equations of motion are derived as shown in Equations 3.3 and 3.4, with the assumption that there is full symmetry in the x-z plane. In this equation, p, q and r are the angular rates in the body axis system and u, v and w are the components of the airspeed (V) in the directions of the body axes. The moment of inertia can be subdivided into $I_{xx}, I_{yy}, I_{zz}, I_{xz}$. Furthermore, m is the mass of the rotorcraft, θ and ϕ are the pitch and roll angle of the body respectively, and X, Y, Z, L, M, N are the forces and moments. These are also variables that are affected by the control inputs.

$$\vec{F} = m \left.\frac{d\vec{V}}{dt}\right|_B + m\vec{\omega} \times \vec{V} \tag{3.1}$$

$$\vec{M} = \left.\frac{d\vec{H}}{dt}\right|_B + \vec{\omega} \times \vec{H} \tag{3.2}$$

$$\begin{bmatrix} X - mg\sin\theta \\ Y + mg\cos\theta\sin\phi \\ Z + mg\cos\theta\cos\phi \end{bmatrix} = \begin{bmatrix} \dot{u} + qw - rv \\ \dot{v} + ru - pw \\ \dot{w} + pv - qu \end{bmatrix} \tag{3.3}$$

$$\begin{bmatrix} L \\ M \\ N \end{bmatrix} = \begin{bmatrix} I_{xx}\dot{p} - I_{xz}\dot{r} + qr(I_{zz} - I_{yy}) - I_{xz}pq \\ I_{yy}\dot{q} + rp(I_{xx} - I_{zz}) + I_{xz}(p^2 - r^2) \\ I_{zz}\dot{r} - I_{xz}\dot{p} + pq(I_{yy} - I_{xx}) + I_{xz}qr \end{bmatrix} \tag{3.4}$$

Fort this thesis, the correlation between the control inputs and all different vibrations is determined. The main focus of this thesis is put on the combinations shown in the list below, since it is expected, based on the previous mentioned equations and flight dynamics [47] that the correlations will be the highest here. This is the case, as the control inputs will influence the forces X, Y and Z. Do note that the combination lateral cyclic and vibration in z-direction is only high with more lateral activity and manoeuvre, which is not the case during many flights.

- Longitudinal cyclic - Vibrations in x,z-direction and pitch rate
- Lateral cyclic - Vibrations in y,z-direction and roll rate
- Collective - Vibration in z-direction
- Pedals - Vibration in y-direction

3.3. Methodology

The measured vibrations and control inputs have different units and therefore suitable statistical methods are investigated for comparison. The control inputs are saved as percentage of their maximum range and the vibrations are saved in m/s^2. First, the data needs to be converted to the frequency domain. And then, the power and the pattern of the signals are compared.

3.3.1. Fourier Transform

First the measurements are converted to the frequency spectrum. The Discrete Fourier Transform (DFT) is determined with a Fast Fourier Transform algorithm [14]. The Fourier transform is a mathematical function that uses a time-based pattern as input and determines the overall cycle offset, frequency and intensity for every possible cycle in the given pattern. In general, it decomposes the waveform into a sinusoid and thus provides another way to represent a waveform. Instead of a continuous function of time, the input for the DFT is a sequence of numbers. In this case, this is the flight test data. The Fourier Transform with discrete signals can be performed with Equation 3.5. In this equation, N_i is the number of time samples, n is the current sample that is being considered, x_n is the value of the signal at time n, k is the current frequency that is being considered, X_k is the amount of frequency in the signal, both amplitude and phase, and is described as a complex number. The $1/N_i$ factor can also be used in the reverse transform (going from frequencies back to time). Using the term in the DFT means that the value at zero Hz is the average value of the measurements. The Inverse Discrete Fourier Transform is shown in Equation 3.6, which transforms the signal from frequency to time domain.

$$X(k) = \frac{1}{N_i} \sum_{n=0}^{N_i-1} x(n) e^{-j2\pi kn/N_i} \tag{3.5}$$

$$x(n) = \sum_{n=0}^{N_i-1} X(k) e^{j2\pi kn/N_i} \tag{3.6}$$

One of the differences between Continuous Fourier Transform and Discrete Fourier Transform is that the spectrum of the sampled continuous-time signal, x(t), is composed of the spectrum of x(t) plus the spectrum of x(t) translated to each harmonic of the sampling frequency [77]. The magnitudes are equal if the pulse width of the sampling function is infinitely small, which is generally the case. After calculating the absolute values of the signal, the spectrum is bandlimitted, which means that only the spectrum around vertical axis is taken into account. In order to have a single-sided amplitude spectrum, the absolutes value of the Fourier transformed sequence are taken first. After that, only the positive frequency range is taken into account. This part is multiplied by two. The frequency spectra of the different vibration and control input signals are calculated in Section 3.4.

There are two main types of DFT errors: aliasing and leakage. If the used samples are not closely spaced enough to represent high frequency components, aliasing occurs in the DFT signals. This means that it is impossible to recover x(t) by filtering. Solutions are either to increase the sampling rate, or to use a pre-filter to minimise the high frequency spectral content. With a sampling rate of 400Hz, the occurrence of aliasing is expected to be negligible. Another effect which can occur is spectral leakage, which means that new frequency components are created. This can for example happen due to the discontinuities in the measurements. As we want to determine the approximate frequency range of correlation, this problem should not alter the conclusion much.

The Fast Fourier Transform uses a greatly reduced number of arithmetic operations. Equation 3.5 can be rewritten into Equation 3.7. The same values of W^{kn} are calculated many times as the computation proceeds. First of all, the integer product nk repeats for different combinations of k and n. Secondly, W^{kn} is a periodic function with only N_i distinct values.

$$X(k) = \frac{1}{N_i} \sum_{n=0}^{N_i-1} x(n) e^{-j2\pi kn/N_i} = \frac{1}{N_i} \sum_{n=0}^{N_i-1} x(n) W^{kn} \tag{3.7}$$

The single summation over N_i samples can be split into 2 summations, each with $N_i/2$ samples, one for k odd and one for k even, assuming that N_i is a power of 2. This is how a 2-point DFT works. In general, the FFT is computed by dividing up, or decimating, the sample sequence X_k into sub-sequences until only 2-point DFTs remain. When N_i=8 for example, only one further stage is required. The amount of stages required can be determined with ($\log_2 N_i$).

3.3.2. Power spectral density

The intensity of a signal can be described with Power Spectral Density [14]. This describes the power per Hz in the signal. The main difference in the calculation is that the square of X_k is taken, and that the value is divided by the sampling frequency. This is shown in Equation 3.8.

$$PSD = \frac{1}{N_i f_s} \left| \sum_{n=0}^{N_i-1} x(n) e^{-j2\pi kn/N_i} \right|^2 \tag{3.8}$$

Still, there is the problem that both variables have different units. This means that you cannot compare the intensity of the two signals directly with each other. Therefore, an analysis is performed on how both signals behave under different circumstances. This can be for example a change in flight condition or rotorcraft configuration. The increase or decrease in vibration level and control inputs is calculated per frequency bin, and it is determined whether there is a positive or negative relationship between the two variables. A list of circumstances that can be changed for the analysis is shown below.

- Rotorcraft configuration (for example weight and center of gravity)
- Velocity
- AFCS setting
- Atmospheric conditions (calm or turbulent flight)
- Rotorcraft mission (level flight or manoeuvre)

To make the comparison easier, the Power Spectral Densities are integrated into small bins. If the bin size of the correlation coefficient is too small, noise correlation will become larger, and if the bin size is too large, some peak correlations with small bandwidth will become unidentifiable. The bin size for this analysis is set at 0.1 Hz. The results are shown in Section 3.5.

3.3.3. Correlation coefficient

The pattern in the frequency spectrum between the control inputs and the vibrations can be determined with the correlation coefficient. Correlation can be described as the degree of association between two variables [34]. This is also independent of the magnitude of the signals, which means that the unit difference will not influence the results. This is also the reason why the covariance solely cannot be used, as it is dependent

on the scale of the signals. The correlation coefficient can be described as the covariance between the two variables, divided by the product between the standard deviation of each of the variables. The Pearson (Product–Moment) correlation r was developed by Pearson and was based on the work of others, including Galton [20], who first introduced the concept of correlation. This calculation is shown in Equation 3.9. In this equation, $(x_1, ..., x_n)$ is the data set of one of the control inputs, and $(y_1, ..., y_n)$ is the data set of the vibration in one direction.

$$r_{xy} = \frac{\sum_{i=1}^{n}(x_i - \bar{x})(y_i - \bar{y})}{\sqrt{\sum_{i=1}^{n}(x_i - \bar{x})}\sqrt{\sum_{i=1}^{n}(y_i - \bar{y})}} \tag{3.9}$$

In general, a value of one means total positive linear correlation, minus one means total negative linear correlation and zero means that there is no linear association between the variables. One of the main disadvantages of this method is noise correlation. This can occur and therefore it is decided not to take correlations lower than 0.3 into account when making conclusions. The approximate strength of correlation is shown in Table 3.2. Furthermore, noise correlation is random, and by taking into account more flight tests, the influence of noise correlation is minimized. The correlation coefficient can also be sensitive to outliers, this can be diminished by increasing the sample size and by taking into account more measurements.

Table 3.2: Strength of correlation [3]

Size of r	Interpretation
0.90 to 1.00	Very high correlation
0.70 to 0.89	High correlation
0.50 to 0.69	Moderate correlation
0.30 to 0.49	Low correlation
0.00 to 0.29	Little if any correlation

For the correlation analysis, the correlation coefficient is calculated in small bins in the frequency spectrum. The minimum amount of data points required can be estimated with Equation 3.10 [30]. This equation is a rule of thumb, which links the amount of data points to the reliability of the correlation coefficient. If one wants the correlation coefficient to be significant from a value of 0.3, at least 45 data points are required.

$$|r_{xy}| > \frac{2}{\sqrt{N_i}} \tag{3.10}$$

3.3.4. Filtering

To calculate the discomfort of the pilot due to helicopter vibrations, the sensitivity weighting function of Section 2.1 can be used. The parameters used for these weighting functions are described in Appendix A. In order to determine the influence of each vibration source, filtering of the signals is required. The Butterworth filter is used for this purpose [57]. It is a signal processing filter designed to have a frequency response as flat as possible in the passband. Other filters that are used are the Notch filter, which can for example be used to filter the harmonic vibrations, and the low pass filter, which is used to filter the low frequency vibrations. With this, one can for example determine the ratio of the discomfort in the lower frequency to the total discomfort.

3.4. Spectral analysis

In this section the spectral analysis of the measurements are discussed. Using the Discrete Fourier Transform, explained in Section 3.3, the measurements are converted to the frequency spectrum. This is shown for one of the flight tests of the H145 at 40 kts in Figures 3.6 - 3.14. One can notice in Figures 3.6 - 3.9 that most of the control inputs happen in the very low frequency domain, around 0-2 Hz, and that after 4 Hz, the amplitude is minimal. Therefore, the focus in this thesis will be on the 0-4 Hz region. One can see that the cyclic control inputs are in this case slightly higher than the collective and pedal inputs. Furthermore, in general the pitch and roll rate also occur in the lower frequency domain, with a peak value around 0.5-1 Hz. This can be seen in the absolute frequency spectra calculated with the FFT algorithms, as shown in Figures 3.10 and 3.11. The vibrations are shown in Figures 3.12, 3.13 and 3.14.

One can notice that the vibration in z-direction is higher. In these vibration spectra, vibrations due to the other vibration sources can be seen as well. This is highlighted in Figure 3.14. At multiples of the rotational speed of the rotor, rotor induced vibrations as discussed in Section 2.2 occur. As shown in the figure, the highest vibration amplitude generally occurs at N/rev. The frequency of the main rotor is shown in Table sc:ftdhelitypes. As said before, although the amplitude of the vibration in the low frequency domain is lower, the broadband is larger compared to the rotor-induced vibrations. This means that it is able to transport more energy. Furthermore, this vibration is closer to the region of human sensitivity. In the vibration spectra, the tail boom modes can also be observed. An example of the vertical tail boom mode is shown in Figure 3.14. Next to these vibration sources, there will also be some influence from measurement noise.

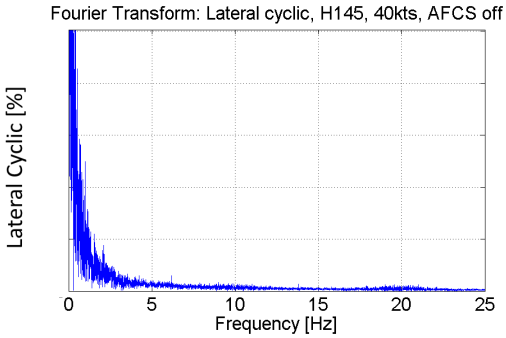

Figure 3.6: Frequency spectrum of lateral cyclic (Flight test data H145)

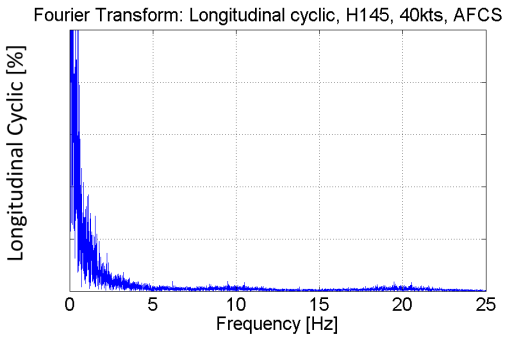

Figure 3.7: Frequency spectrum of longitudinal cyclic (Flight test data H145)

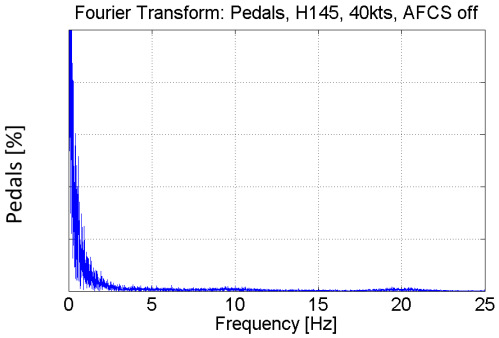

Figure 3.8: Frequency spectrum of pedal input (Flight test data H145)

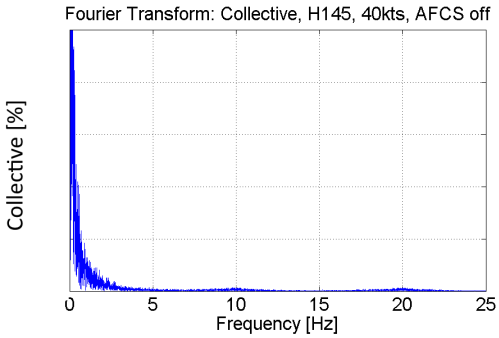

Figure 3.9: Frequency spectrum of collective (Flight test data H145)

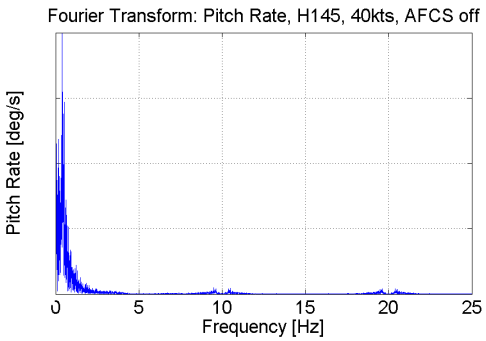

Figure 3.10: Frequency spectrum of pitch rate (Flight test data H145)

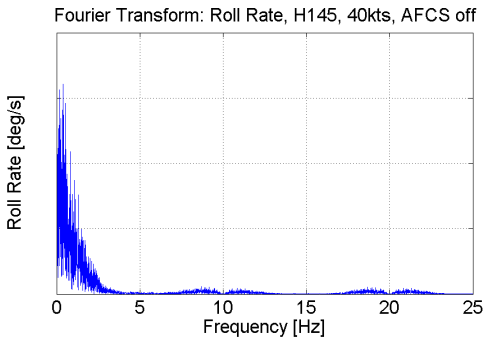

Figure 3.11: Frequency spectrum of roll rate (Flight test data H145)

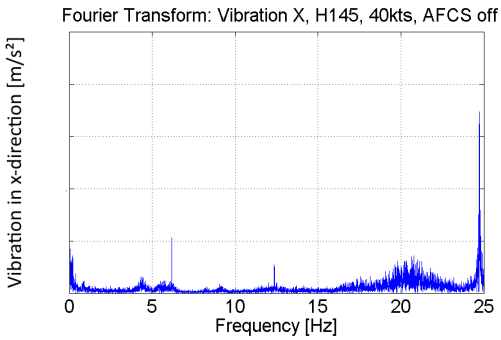

Figure 3.12: Frequency spectrum of vibration in x-direction (Flight test data H145)

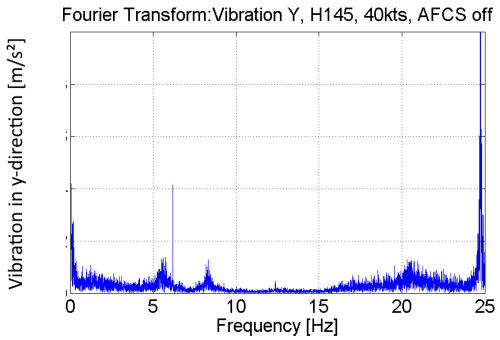

Figure 3.13: Frequency spectrum of vibration in y-direction (Flight test data H145)

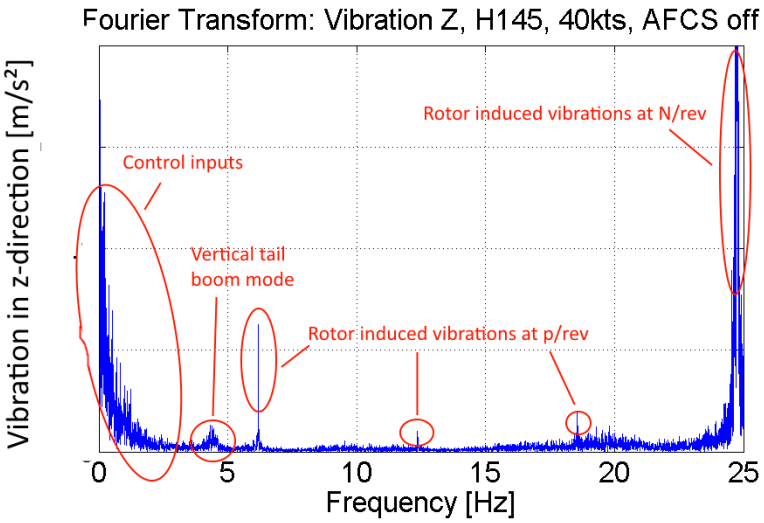

Figure 3.14: Frequency spectrum of vibration in z-direction (Flight test data H145)

3.5. Correlation analysis and pilot comfort assessment

In this section, both the power and pattern comparison are discussed. This is done for different helicopters and flight conditions. The focus is put on the investigation whether there is a correlation between the control inputs and vibrations. It is interesting to find out where in the vibration spectra the correlation occurs. More information on the flight tests used for the parametric study can be found in Appendix B. This includes the serial number, flight test number, the flight speeds and if applicable the helicopter configuration parameters. In many cases, more flight tests have been analyzed than the ones stated in this report before deducing conclusions. However, only the most relevant figures are shown in here.

3.5.1. Rotorcraft configuration

First the correlation coefficients of a EC135 helicopter and the H145 helicopter are discussed. These are shown in Figures 3.15 - 3.21. In these figures, several flight tests with different conditions or configurations are shown for the same serial number. This means that flights 1-5 have different flight speeds and different atmospheric conditions. With these results, several general conclusion can be made first. After that, the flight tests are sorted based on the flight condition or configuration. The correlation coefficients are calculated here for a range of 0 till 15 Hz. It can be noticed that the correlation coefficients between the cyclic controls and disturbances are higher for the lower frequencies, till around 5 Hz. This supports the observation made during spectral analysis, that the control inputs mainly occur in the low frequency domain. This is especially visible in Figure 3.15, where the correlation coefficients between the lateral cyclic and the vibration in y-direction are plotted. The correlation coefficients of the longitudinal cyclic controls, as shown in Figures 3.16 and 3.17, also have a higher correlation with the vibrations in x,z-directions, but in general up to around 2-4 Hz. Also, the correlation with the vibration in x-direction is slightly lower. The pedal inputs show lower

correlations. The collective input does not show any correlation in the lower frequency domain. These are shown in Figures 3.18 and 3.19. Peaks do occur, like almost all correlation coefficients, at the location of the rotor harmonics. In Figures 3.20 and 3.21, one can notice high correlations between the angular rates and the cyclic controls. However, the pedals and collective show no correlations with the angular rates. Furthermore, it was discussed before that the magnitude of the correlation coefficient should be at least higher than 0.3 in order to minimize the influence of noise correlations. It can be concluded that the occurrence of negative correlation correlation coefficients, especially in the lower frequency domain, is negligible.

Another observation that can be made, is that the correlation coefficients of the translational vibrations starts directly at a higher value, while the correlation coefficient of the angular rate has a peak around 0.5 Hz. This can be explained by the fact that when one slowly moves the cyclic stick, the rotorcraft mainly moves in the translational direction, while when one moves the stick faster, one will actually pitch or roll.

One can also notice that that the different flight tests of the same helicopter have a comparable pattern in the correlation coefficient. The lateral correlation coefficients of several flight of the H145 helicopter are shown in Figures 3.22 and 3.23. This holds for both helicopters, even though the conditions of each flight test are different. This might suggest that part of the correlation coefficient can be a helicopter parameter. Further discussion on this point is provided in Chapter 5.

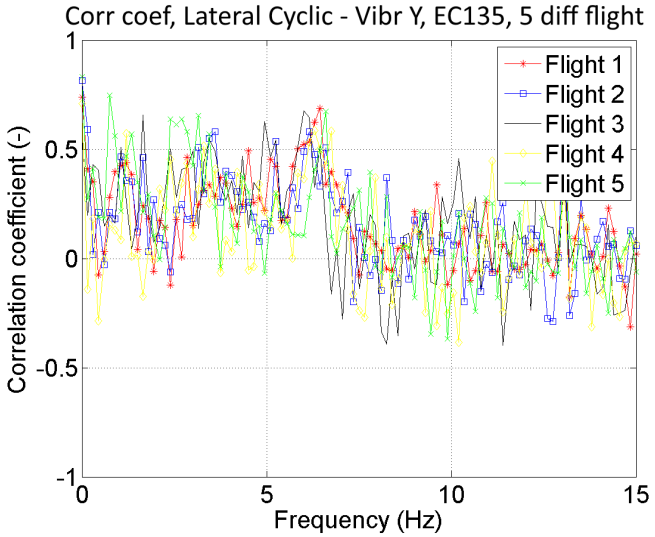

Figure 3.15: Correlation coefficient: Lateral cyclic - Vibration Y (Flight test data EC135)

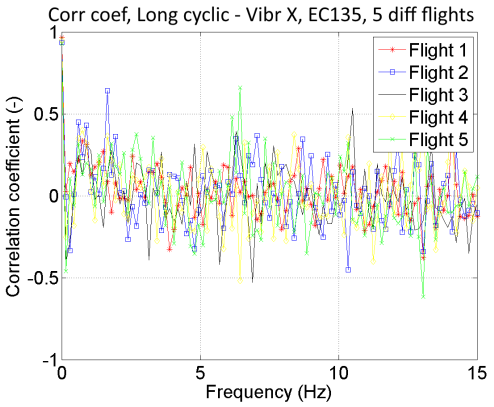

Figure 3.16: Correlation coefficient: Longitudinal cyclic - Vibration X (Flight test data EC135)

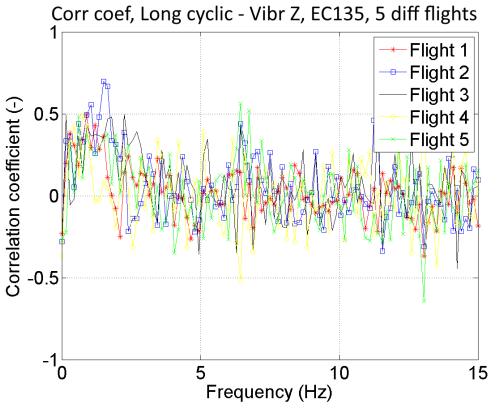

Figure 3.17: Correlation coefficient: Longitudinal cyclic - Vibration Z (Flight test data EC135)

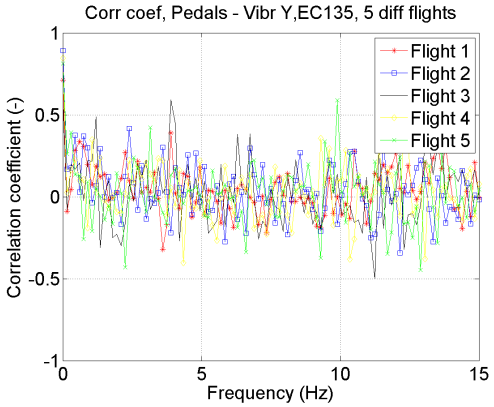

Figure 3.18: Correlation coefficient: Pedals - Vibration Y (Flight test data EC135)

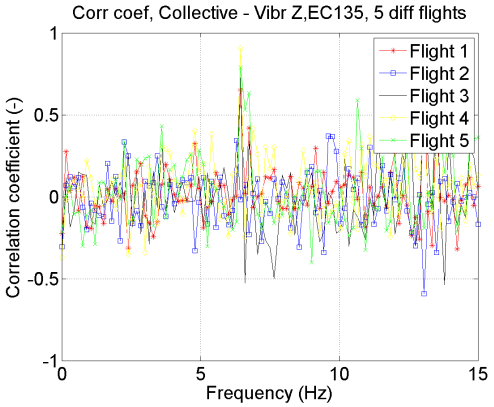

Figure 3.19: Correlation coefficient: Collective - Vibration Z (Flight test data EC135)

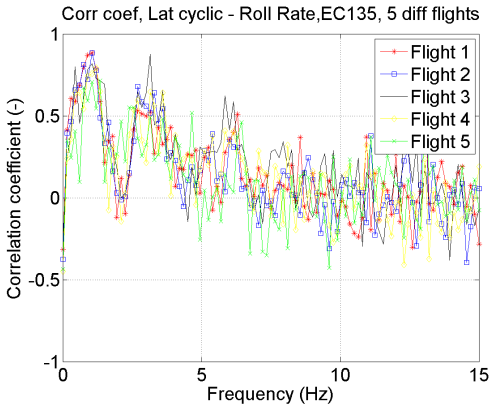

Figure 3.20: Correlation coefficient: Lateral cyclic - Roll rate (Flight test data EC135)

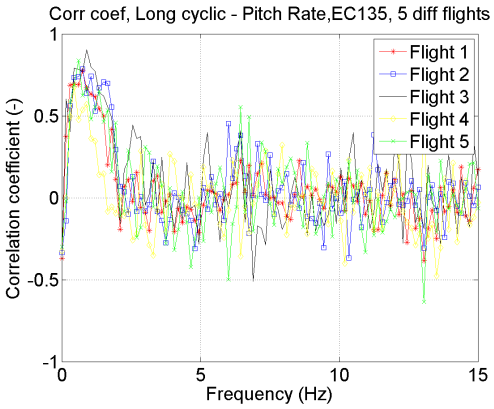

Figure 3.21: Correlation coefficient: Longitudinal cyclic - Pitch rate (Flight test data EC135)

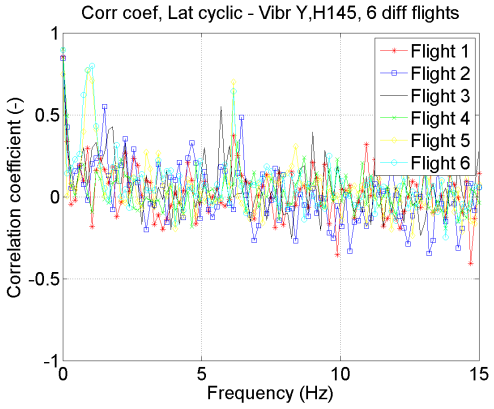

Figure 3.22: Correlation coefficient: Lateral cyclic - Vibration Y (Flight test data H145)

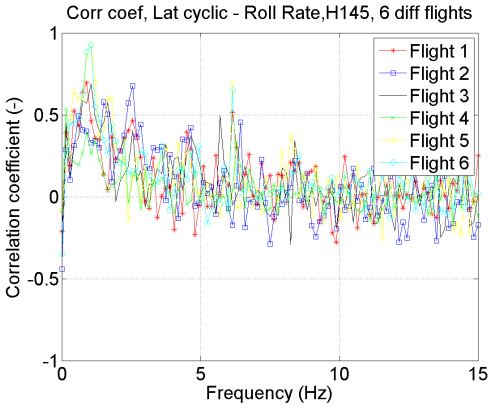

Figure 3.23: Correlation coefficient: Lateral cyclic - Roll rate (Flight test data H145)

3.5.2. Center of gravity

The rotor moment can be approximated as combination of a moment proportional to the disc tilt and one proportional to the rotor thrust. The pitching moment of the helicopter can then be approximated as a combination of the rotor moment, the tailplane moment and the fuselage moment. The tailplane moment is always stabilizing. The contribution from the fuselage is almost always destabilizing. This is because of the fact that the aerodynamic center of the fuselage is in general forward of the center of mass. The rotor moment caused by the disc tilt is stabilizing, as it flaps back with an upward perturbation. Due to the offset of

the thrust from the center of mass, the contribution of the rotor thrust is stabilizing for configurations with a more forward center of gravity. It can be concluded that the more forward the center of gravity is, the more stable the helicopter is [47]. Therefore, it is expected that less control inputs are required with a more forward center of gravity, and that this results in less vibrations. This can indeed be seen in the results; when the center of gravity is shifted 20 cm toward the nose from the original center of gravity, which is 4.2 m, the cyclic control inputs increase, as shown in Figure 3.24, and the vibrations decrease. The pilot discomfort is shown in Figure 3.26. A small change in in the lower frequency domain can be noticed. It can further be concluded that the the change in center of gravity location shifts the peaks of the correlation coefficients, as can be seen in Figure 3.25. This supports the thought that the correlation coefficient could partly be a helicopter parameter. With this knowledge, the peak correlations can be shifted to a frequency with less human sensitivity.

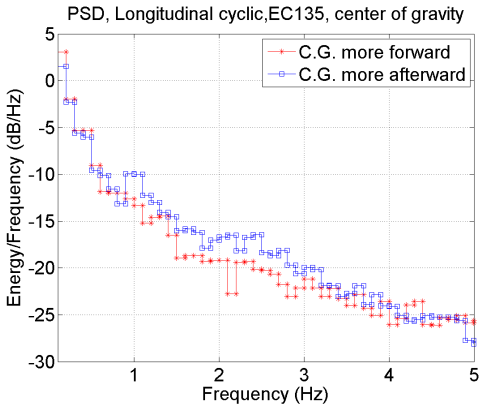

Figure 3.24: Power spectral density: Longitudinal cyclic, center of gravity (Flight test data EC135)

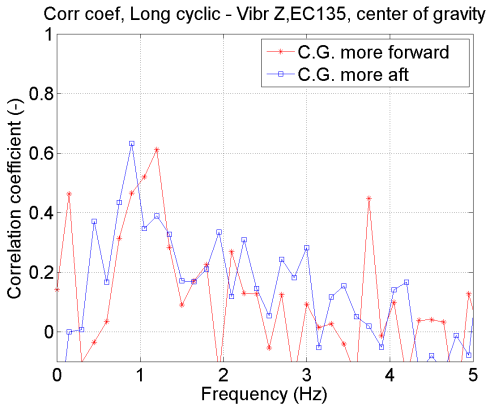

Figure 3.25: Correlation coefficient: Longitudinal cyclic - Vibration Z, center of gravity (Flight test data EC135)

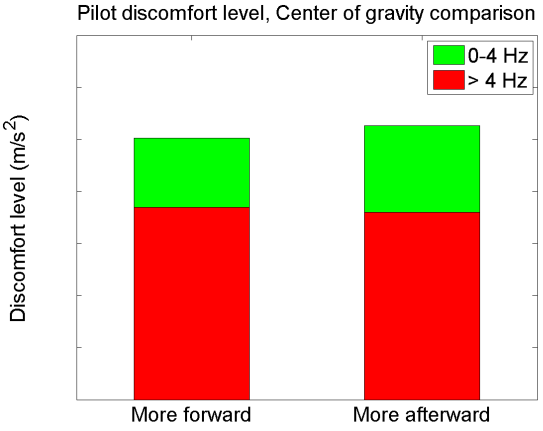

Figure 3.26: Pilot discomfort level for shifts in center of gravity (Flight test data EC135)

3.5.3. Weight

In this section, the influence of different helicopter weights is discussed. Two helicopters, one with a weight of 3800 kg and one with a weight 2700 kg, are compared with each other. It can be seen in Figure 3.28, that for lower weights, the vibration level is higher. This also holds for the other axes. This can be explained by the fact that the helicopter is more susceptible to forces at low weights as can be derived from Equation 3.1. As can be seen in Figure 3.27, the control input is not altered much. In certain frequencies, there is a slight increase. For the lower weight helicopter, the correlation coefficients are higher, as can be seen for example in Figure 3.29. This suggests that the correlation coefficient can potentially measure the susceptibility of the helicopter to vibrations. This suggestion will be investigated in several other sections, and is the main focus of Section 5.3. From the results of the discomfort calculation, shown in Figure 3.30, one can conclude that the control inputs do influence the discomfort level, but they are not the dominant source.

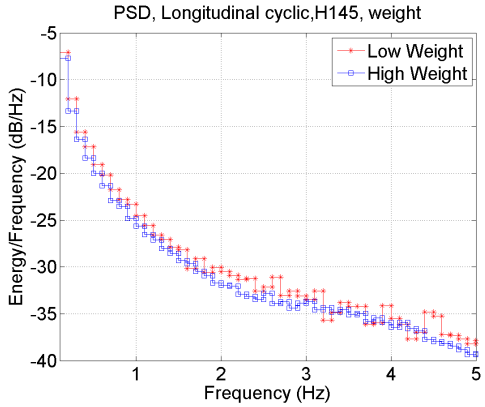

Figure 3.27: Power spectral density: Longitudinal cyclic, weight (Flight test data H145)

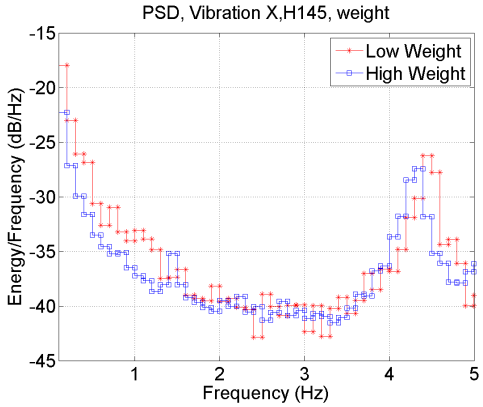

Figure 3.28: Power spectral density: Vibration X, weight (Flight test data H145)

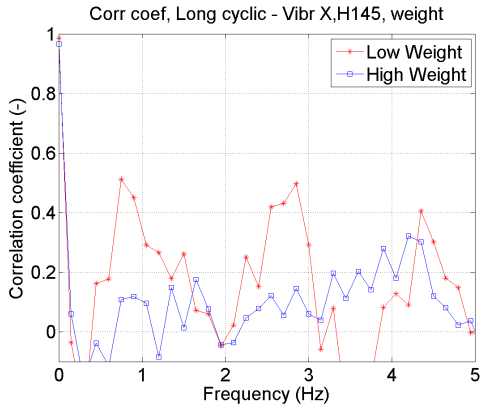

Figure 3.29: Correlation coefficient: Longitudinal cyclic - Vibration X, weight (Flight test data H145)

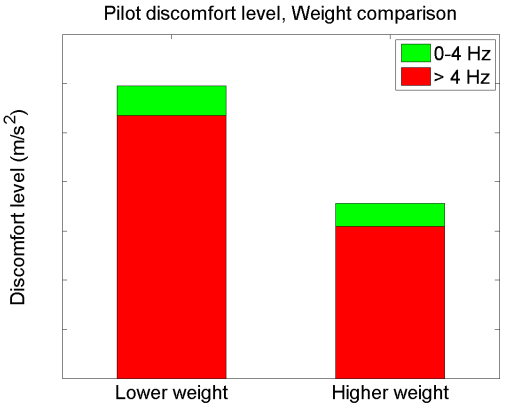

Figure 3.30: Pilot discomfort level for different weights (Flight test data H145)

3.5.4. Velocity

Different velocities are compared with each other during level flight. It is expected that the aerodynamic disturbances are higher for higher speeds. The two main components, rotor thrust and drag, are shown in Equations 4.4 - 4.6 in Section 4. In this section, these equations will be described in more detail. One can notice that both equations are dependent on the square of the velocity. These forces influence the accelerations, as can be seen in Equation 3.1.

Next to this, there is dissymmetry of lift, which refers to an uneven amount of lift on opposite sides of the rotor disc. During hover, the blade tip speed is equal to the rotating speed times the radius. During forward flight, the forward speed is added to the calculation of the blade tip speed of the advancing blade. Next to this, the forward speed is deducted in the calculation of the blade tip speed of the retreating blade. This leads to a dissymmetry in lift. This dissymmetry is countered by blade flapping and cyclic feathering. At high speed, the rotor can experience local blade stall. When moving towards the never-exceed speed, the retreating blade has insufficient net linear speed though the air to generate meaningful lift. This is known as retreating blade stall. This increases the vibrations, as well as the control inputs to restore the proper attached flow [47].

This can also be seen in the results in Figures 3.31 and 3.32. Both the longitudinal cyclic input and the vibration levels increase with higher velocities. The longitudinal cyclic control is also higher in order to correct for the disturbances and stay at level flight. The other inputs do not increase. The pilot discomfort, as shown in Figure 3.34, shows that the discomfort is higher at higher velocities. In general, the discomfort increases in both frequency ranges. However, at 110 kts, the relative amount of discomfort caused in the 0-4 Hz range is larger. This could be explained by the higher amount of longitudinal cyclic input, as shown in Figure 3.31.

The correlation coefficients do not show a clear relationship with the speed level, with in some cases only higher coefficients till 1 Hz for higher flight speeds, as illustrated in Figure 3.33.

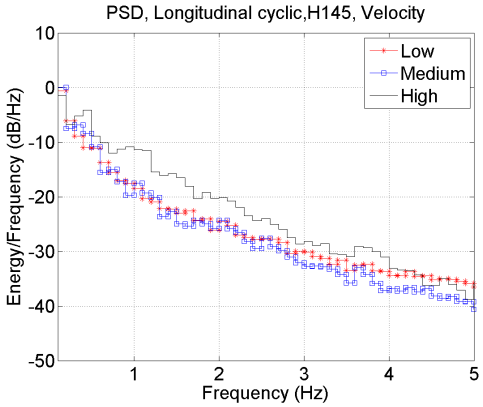

Figure 3.31: Power spectral density: Longitudinal cyclic, speed (Flight test data H145)

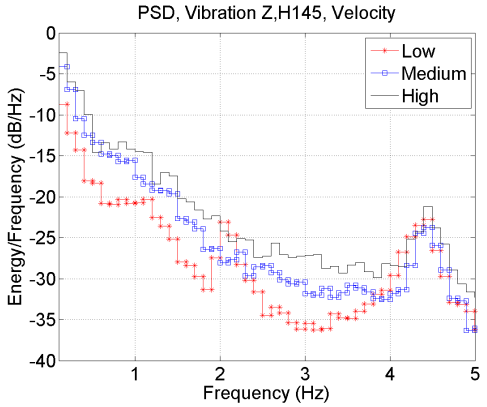

Figure 3.32: Power spectral density: Vibration Z, speed (Flight test data H145)

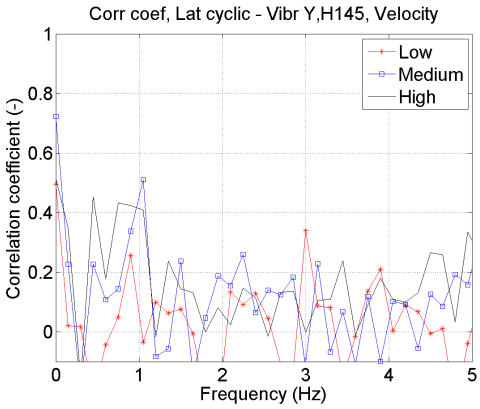

Figure 3.33: Correlation coefficient: Lateral cyclic - Vibration Y, speed (Flight test data H145)

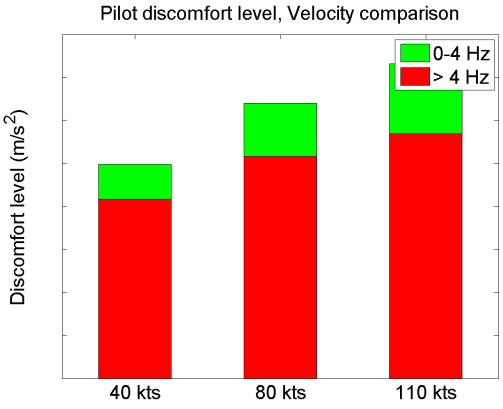

Figure 3.34: Pilot discomfort level for different flight speeds (Flight test data H145)

3.5.5. Rotorcraft mission

In this section, a level flight test will be compared with a manoeuvring flight test. This manoeuvring flight consists of a 90 degrees lateral movement. During a manoeuvre, more flight control inputs are required, especially lateral control inputs. This can also be seen in Figure 3.35. This increase in lateral control input also leads to more movements and more vibrations as can be seen in Figure 3.36. In Figure 3.37, one can also notice that there is an increase in the correlation coefficient. The pilot discomfort level is shown in Figure 3.38. As expected, the flight with a manoeuvre has a higher discomfort level, especially in the lower frequency domain. One should note that, as explained before, the discomfort depends on many aspects, which are not taken into account in the ISO2631-I calculation. During the manoeuvre, the pilot expects more activity, which means that the discomfort level could be lower. However, this point is not taken into account during this thesis.

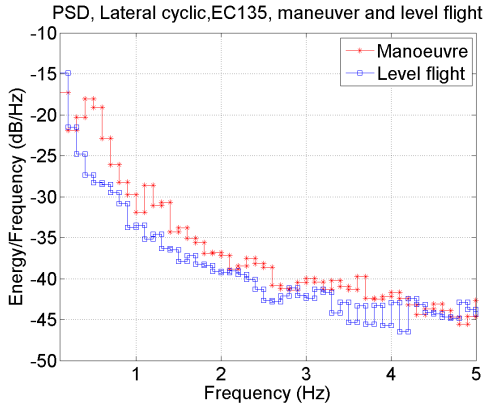

Figure 3.35: Power spectral density: Lateral cyclic, mission (Flight test data EC135)

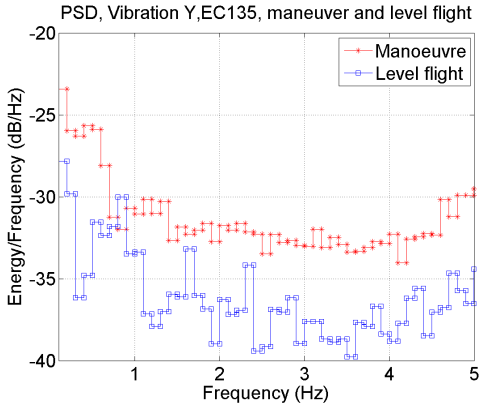

Figure 3.36: Power spectral density: Vibration Y, mission (Flight test data EC135)

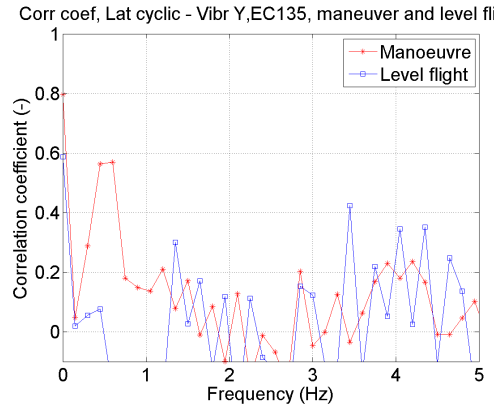

Figure 3.37: Correlation coefficient: Lateral cyclic - Vibration Y, mission (Flight test data EC135)

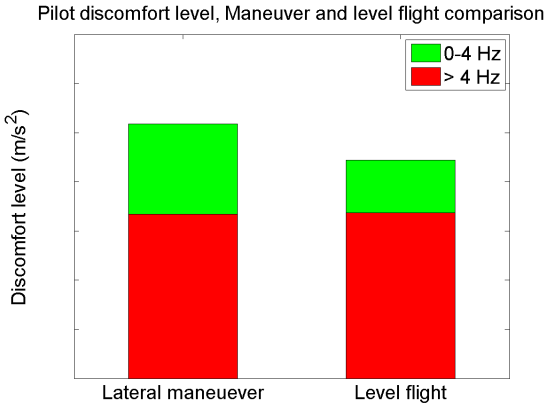

Figure 3.38: Pilot discomfort level for different flight missions (Flight test data EC135)

3.5.6. AFCS setting

The different AFCS settings were discussed in Section 3.1.4. It can be concluded that when the autopilot is turned off, the cyclic control inputs and pedal inputs are higher. The collective input is slightly lower. The reason for this is that in general pilots tend to use the cyclic stick more, as it is more convenient. When the AFCS is turned on for the H145 in the upper modes, the power of the collective input in the frequency domain will increase and the power of the cyclic controls and pedals will decrease. For the EC135, the collective will not increase in power, as it uses the 3-axes AFCS, which does not include the collective input. The cyclic control power decreases slightly, as the AFCS is probably able to control the disturbances more efficiently. However, the decrease is smaller than when a 4-axes AFCS system is used.

The results of the vibration measurements of one EC135 flight tests are shown in Figures 3.43 - 3.45. In these figures, a flight with autopilot is compared with a flight where the autopilot is switched off. One can notice that the vibrations in y,z-directions decrease in case the autopilot is switched on. In Figures 3.41 and 3.42 the PSDs of the control inputs are shown. In general, the control inputs are slightly higher in case the autopilot is switched off. When there is no increase in longitudinal cyclic inputs around 1-2 Hz, there is also no increase in vibration in z-direction. This is the same for the lateral case, around 3 Hz. This confirms the relationship between the cyclic control and the vibrations even more. One can see that the correlation coefficients corresponding to the cyclic controls are slightly lower when the AFCS is used, which coincides with the observations made before. An example of this is shown in Figure 3.39. In the case shown, the correlation coefficient between the vibration in x-direction and longitudinal cyclic input is higher for the case when the autopilot is used, after 1 Hz. If it is true that the correlation coefficient can be used as a measure for susceptibility to vibrations, this could explain why there is an increase in vibration in x-direction, as more control inputs are

translated into vibrations in this case.

When comparing the other AFCS settings (SAS and attitude mode), it can be concluded that the higher the automation level, the lower the amount of cyclic inputs and vibrations compared with when the flight control system is switched off. The discomfort level between the AFCS off mode and the autopilot are compared in Figure 3.46. It can be seen that only the discomfort in the lower frequency domain is influenced. This strengthens the idea that the control input is the dominant source for discomfort in this region.

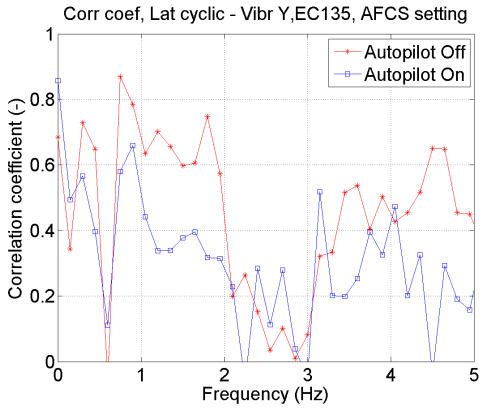

Figure 3.39: Correlation coefficient: Lateral cyclic - Vibration Y, AFCS (Flight test data EC135)

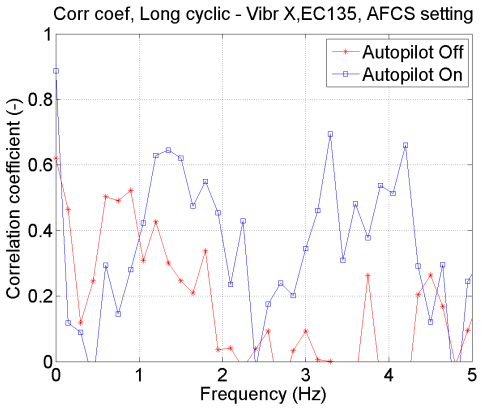

Figure 3.40: Correlation coefficient: Longitudinal cyclic - Vibration X, AFCS (Flight test data EC135)

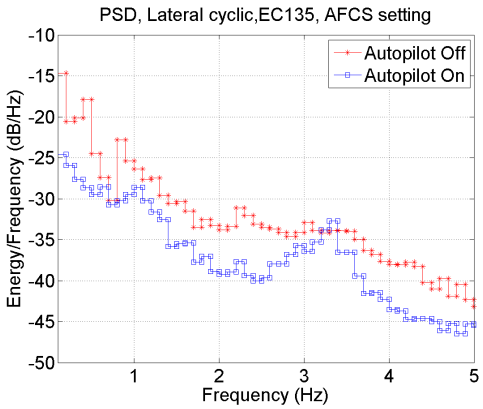

Figure 3.41: Power spectral density: Lateral cyclic, AFCS (Flight test data EC135)

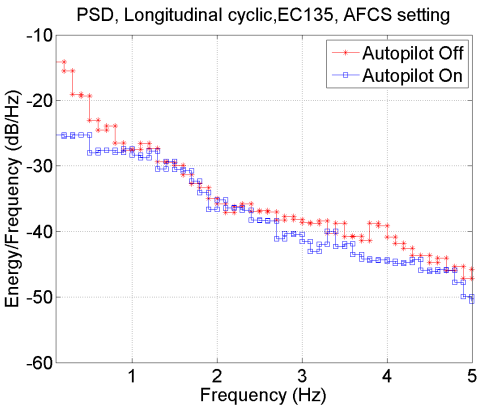

Figure 3.42: Power spectral density: Longitudinal cyclic, AFCS (Flight test data EC135)

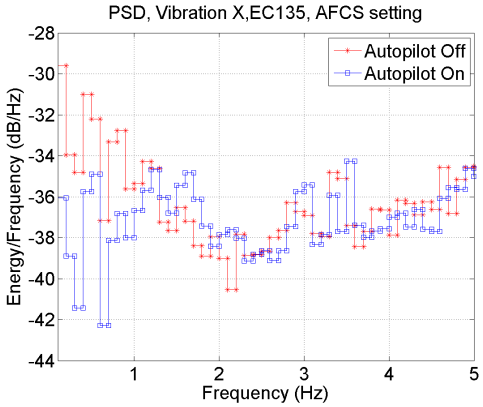

Figure 3.43: Power spectral density: Vibration X, AFCS (Flight test data EC135)

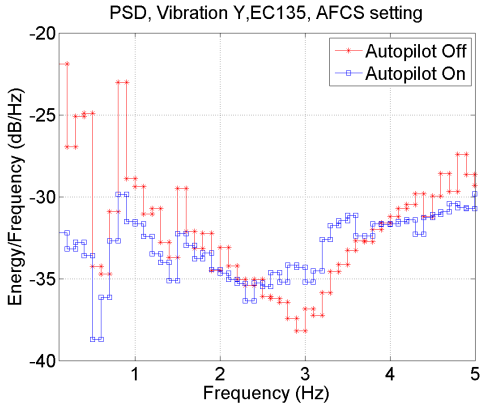

Figure 3.44: Power spectral density: Vibration Y, AFCS (Flight test data EC135)

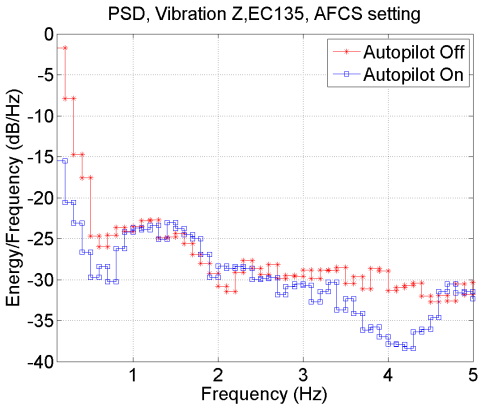

Figure 3.45: Power spectral density: Vibration Z, AFCS (Flight test data EC135)

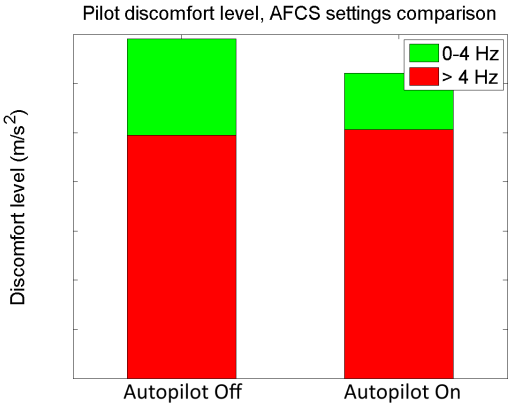

Figure 3.46: Pilot discomfort level for autopilot on and off (Flight test data EC135)

3.5.7. Atmospheric conditions

As said before, during turbulent flights, non-rotor induced vibrations tend to dominate the pilot discomfort level. Gust modelling and gust response of a helicopter have been elaborated on in Section 2.3.2. It was already concluded in previous research citemartinthat a higher turbulence level results in higher discomfort for the pilot. This section focuses more on the effect of turbulence in the lower frequency domain and the influence on the control inputs. It is first important to determine which flights one should categorize as a turbulent flight. After each flight test, the pilots were required to provide a rating of the turbulence level. This is a subjective approach, and a more objective measurement was unfortunately not yet available at the time of testing. Turbulence can affect the control inputs in different ways. First, the pilot inputs will be higher, if the frequency is low enough for a pilot to handle it. For higher frequencies, the pilot will try to keep the stick in the same position, in order to avoid inducing more oscillations. Secondly, the autopilot will react to the disturbances. Finally, biodynamic feedthrough can occur when the vibrations of the helicopter feed through the pilot's body and cause involuntary motions of limbs, which will result in involuntary control inputs. This topic will be further discussed in Section 5.1.

The PSDs are plotted for the EC135 and H145. The average is taken from both the calm flight and the turbulent flight. Unfortunately, these flights were not specifically designed to measure the influence of turbulence, which means that the flight speeds and the AFCS settings are mixed. From the PSDs shown in Figures 3.49, 3.50, 3.59 and 3.60, it can be seen that the cyclic control inputs increase in case of turbulence. This increase is in general from zero till around 3 Hz. However, there was no increase in collective and pedal input, and in some cases even a decrease. This can be seen in Figures 3.51, 3.52, 3.61 and 3.62. The reason for this is that in case of turbulence, pilots tend to use the cyclic stick more, as this is more convenient. From the flight test

data, it can be seen that for most turbulent flights, there was also an increase in roll and pitch disturbance. This can be seen in Figures 3.53, 3.54, 3.63 and 3.64. There is an increase in the translational vibrations up to around 3 Hz. The correlation coefficients are higher as well as can be seen in Figures 3.65 - 3.72. In general, they increases up to around 3 Hz for the correlation coefficients with the angular rates, and even till higher frequencies for the coefficients with the translational vibrations. One can conclude that the correlations are indeed higher at exactly the same frequency range as the turbulence has influence. This supports the statement that in case of turbulence, the non-rotor induced vibrations tend to dominate the pilot discomfort. These objective measurements could actually also be used as an objective rating to the turbulence level. More flight tests are needed to confirm whether the rating given by the pilots really coincides with the increase in intensity of the vibrations and control inputs, and the increase in correlation coefficient.

And finally, the pilot discomfort is calculated and shown in Figure 3.73. These results indeed show that in case of turbulence, the lower frequencies will dominate the pilot discomfort. This is especially true in the case of the H145, where the discomfort in the region of 0-4 Hz is larger than the discomfort in the rest of the frequency spectrum. One can also notice that the vibration level of the H145 is in general higher, although the reason is not due to the lower frequencies.

3.6. Conclusions on flight test data analysis

From the flight test data analysis, one can determine in which frequency area there is a correlation between the control inputs and the vibrations. This is analyzed by comparing the power and the pattern between the signals. It is concluded from spectral analysis that the control inputs occur in the region of 0-4 Hz. When determining the correlation coefficients, one can notice that there is a higher correlation between the two signals up to 4 or 5 Hz. Furthermore, the occurrence of negative correlation coefficients in this frequency domain is negligible. This has been done for different flight tests. One can also notice that the correlation coefficients have comparable shapes depending on the helicopter type, when plotted along the frequency range. This suggests that part of the shape of the correlation coefficients is dependent of the rotorcraft configuration.

The center of gravity is also investigated. It showed that the less stable the helicopter is, the more control inputs it requires. This also results in more vibrations. A shift in the correlation peaks can also be noticed in the frequency domain. This could be due to the fact that due to the changed rotorcraft configuration, the eigenfrequencies could be shifted as well. Furthermore, the damping of the eigenmodes can be changed. This topic is further investigated in Section 5.1.3. This is the reason why this point will be investigated with the simulation model. If this is true, a suggestion could be made to try to shift the peaks towards a frequency domain with lower human sensitivity. One can then try to tune the other helicopter parameters as well. Another interesting parameter was the change in weight. Although the control inputs are not altered much, the vibrations are clearly higher for reduced weight. Interestingly, the correlations coefficients are higher as well. This could suggest that a higher discomfort level can be proven by either a higher increase of control inputs or a higher correlation coefficient of the helicopter between the control inputs and vibrations. If this turns out to be true, one could try to improve the ride quality by lowering the correlation coefficient along the frequency range. This point is investigated in Chapter 5.3.

Both the velocity and rotorcraft mission investigations show expected results. In cases where more control inputs are required, the discomfort is higher. The most interesting results are the results from the comparison between the AFCS settings and the atmospheric disturbances. When comparing the AFCS, one can for example conclude that the cyclic control inputs are more correlated with the vibrations than the collective and pedal inputs. The results show that even when the collective is used more, the discomfort is not be influenced much. Furthermore, the Power Spectral Densities show that at frequencies where there is a lot of input from cyclic stick, the vibrations are also higher. Furthermore, the switch between AFCS on and off only influences the pilot discomfort from energy in the lower frequency domain.

When comparing flights during turbulent air with calm air, one can indeed conclude that in case of turbulence, the pilot discomfort in the lower frequency domain increases. In some cases, it even becomes the dominant source of discomfort. From the results, it is determined that the cyclic control inputs are higher as well during turbulent flights. An increase in inputs cannot be noticed for the other controls. Turbulence

mainly occurs in the frequency range from zero till approximately three Hz.

And finally, it is impossible to have flight tests where only one parameter (flight condition or helicopter configuration) is varying. Some results are more reliable than others, for example the parametric study of the flight speed. Here the same helicopter is used during the same flight test. However, the comparison of the atmospheric conditions is done with several flight tests, which are performed at different days and have different flight conditions. Furthermore, the conclusions made in this chapter are based on more flight tests than the ones showed, except for the parametric study of the weight and center of gravity. In these cases, only one flight test was available. Therefore, it is necessary to complement these results with the correlation analysis performed with flight simulations. These results will be compared in Section 5.2.

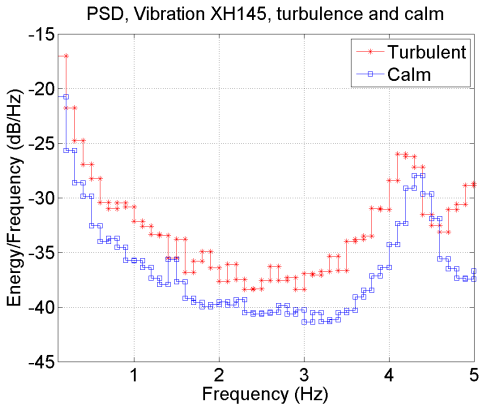

Figure 3.47: Power spectral density: Vibration X, turbulence (Flight test data H145)

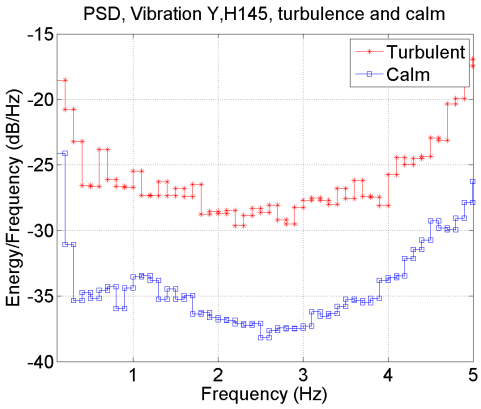

Figure 3.48: Power spectral density: Vibration Y, turbulence (Flight test data H145)

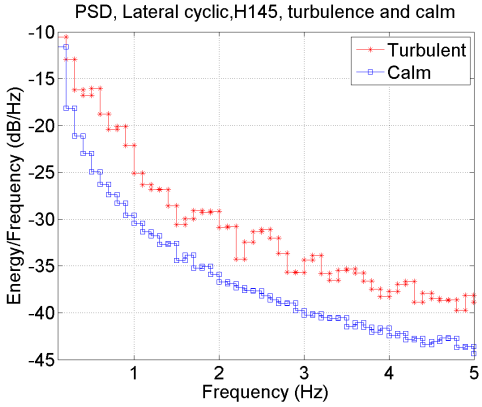

Figure 3.49: Power spectral density: Lateral cyclic, turbulence (Flight test data H145)

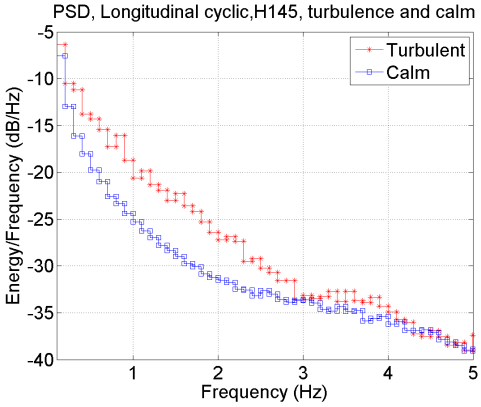

Figure 3.50: Power spectral density: Longitudinal cyclic, turbulence (Flight test data H145)

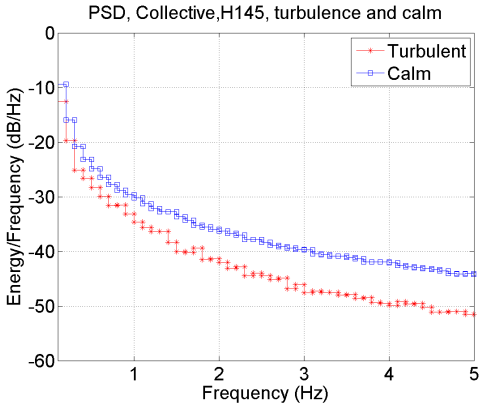

Figure 3.51: Power spectral density: Collective, turbulence (Flight test data H145)

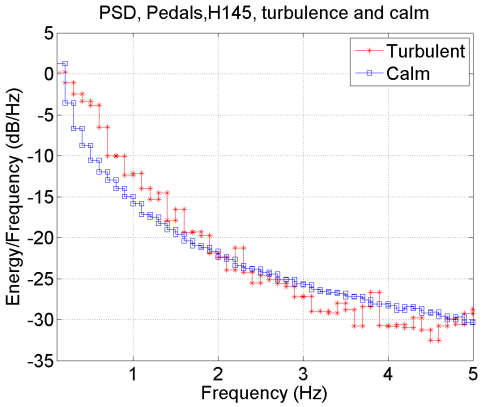

Figure 3.52: Power spectral density: Pedals, turbulence (Flight test data H145)

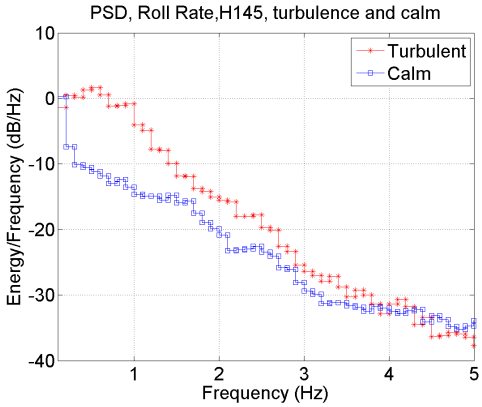

Figure 3.53: Power spectral density: Roll rate, turbulence (Flight test data H145)

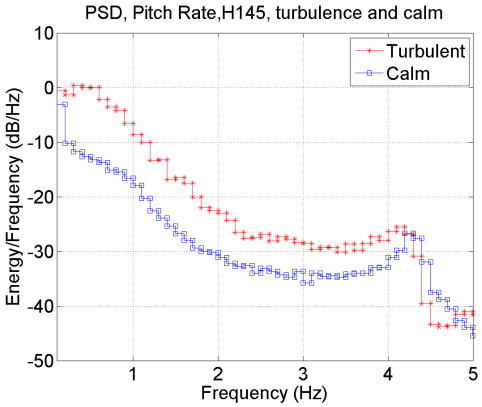

Figure 3.54: Power spectral density: Pitch rate, turbulence (Flight test data H145)

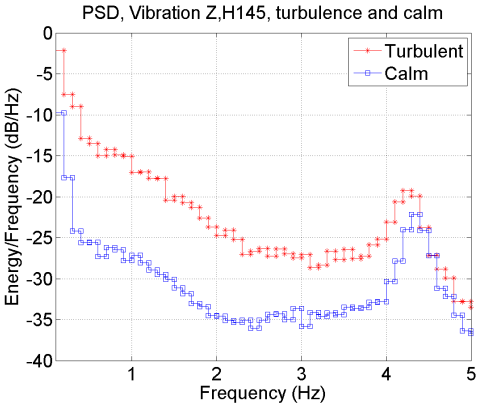

Figure 3.55: Power spectral density: Vibration Z, turbulence (Flight test data H145)

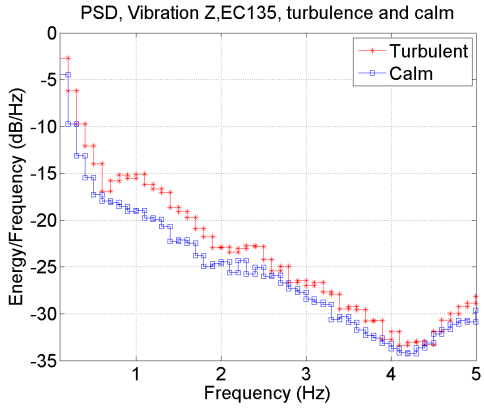

Figure 3.56: Power spectral density: Vibration Z, turbulence (Flight test data EC135)

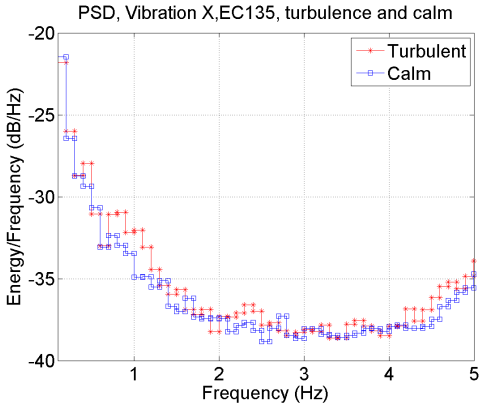

Figure 3.57: Power spectral density: Vibration X, turbulence (Flight test data EC135)

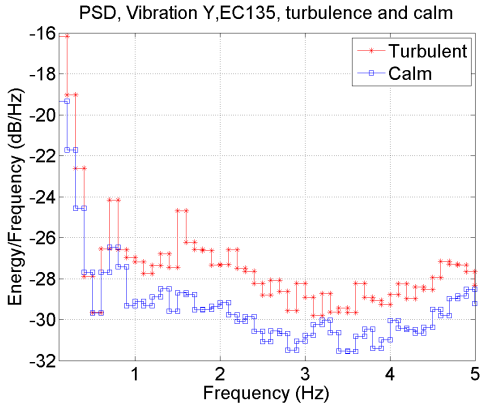

Figure 3.58: Power spectral density: Vibration Y, turbulence (Flight test data EC135)

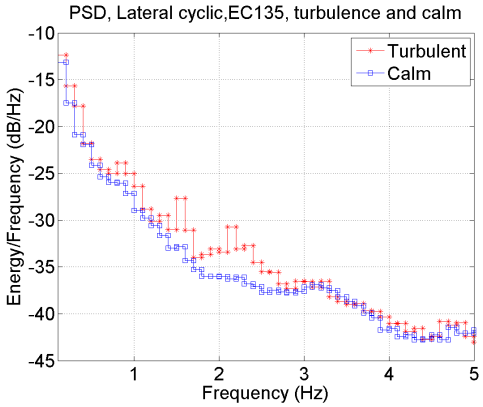

Figure 3.59: Power spectral density: Lateral cyclic, turbulence (Flight test data EC135)

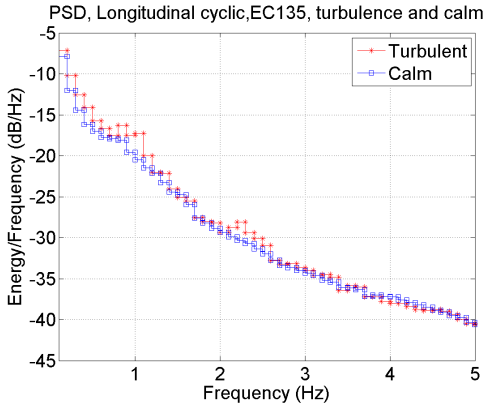

Figure 3.60: Power spectral density: Longitudinal cyclic, turbulence (Flight test data EC135)

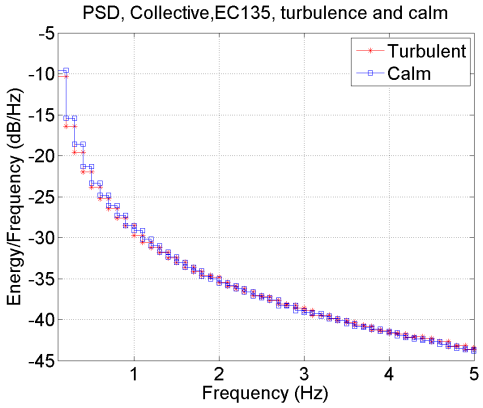

Figure 3.61: Power spectral density: Collective, turbulence (Flight test data EC135)

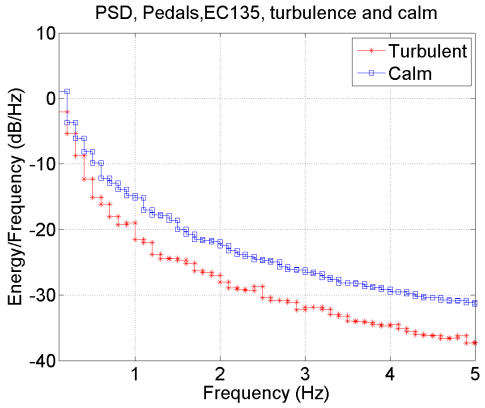

Figure 3.62: Power spectral density: Pedals, turbulence (Flight test data EC135)

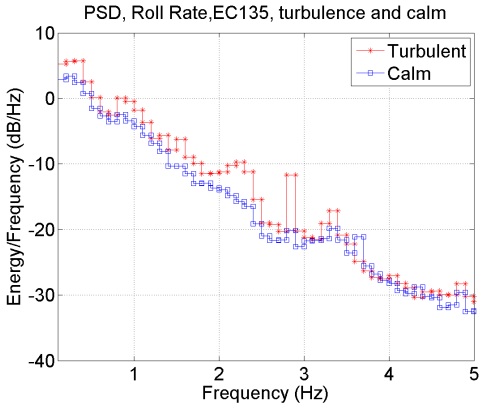

Figure 3.63: Power spectral density: Roll rate, turbulence (Flight test data EC135)

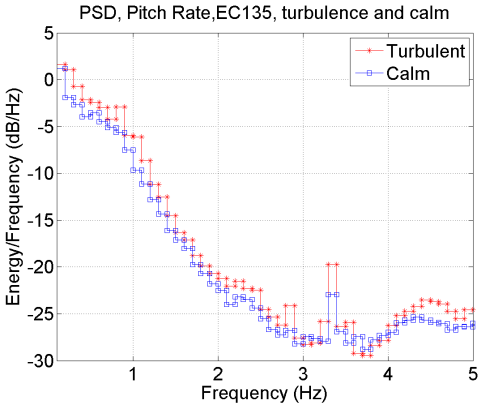

Figure 3.64: Power spectral density: Pitch rate, turbulence (Flight test data EC135)

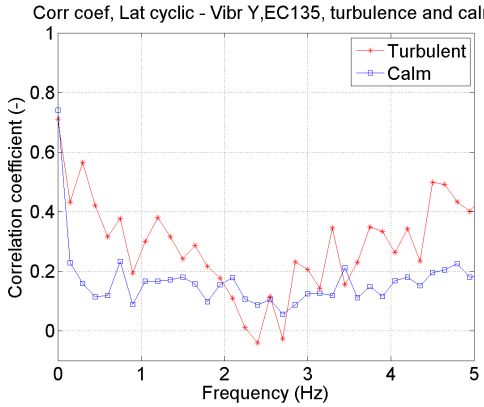

Figure 3.65: Correlation coefficient: Lateral cyclic - Vibration Y, turbulence (Flight test data EC135)

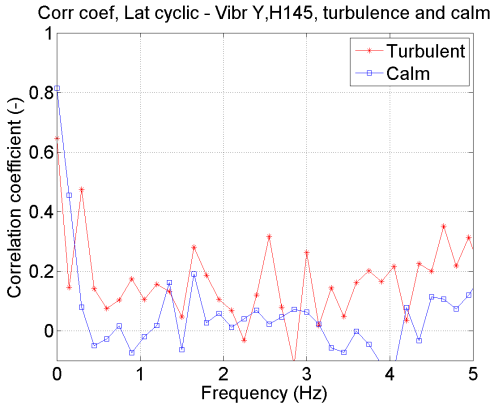

Figure 3.66: Correlation coefficient: Lateral cyclic - Vibration Y, turbulence (Flight test data H145)

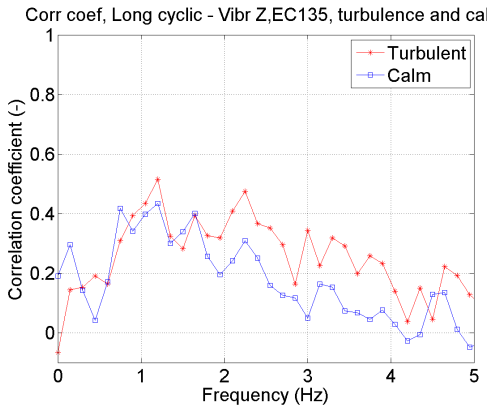

Figure 3.67: Correlation coefficient: Longitudinal cyclic - Vibration Z, turbulence (Flight test data EC135)

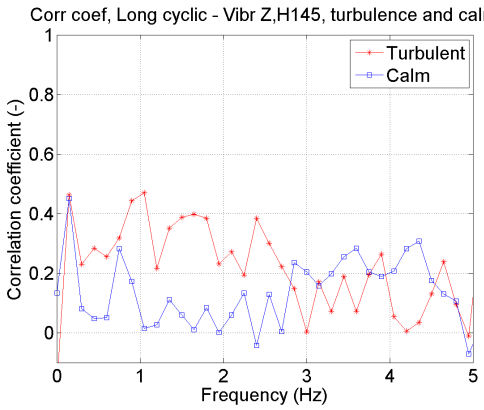

Figure 3.68: Correlation coefficient: Longitudinal cyclic - Vibration Z, turbulence (Flight test data H145)

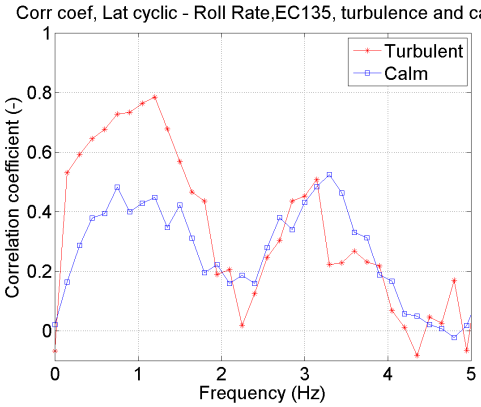

Figure 3.69: Correlation coefficient: Lateral cyclic - Roll rate, turbulence (Flight test data EC135)

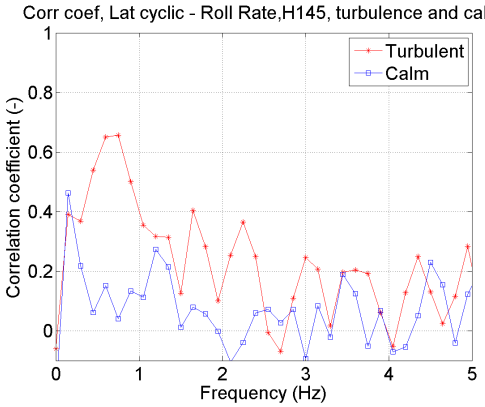

Figure 3.70: Correlation coefficient: Lateral cyclic - Roll rate, turbulence (Flight test data H145)

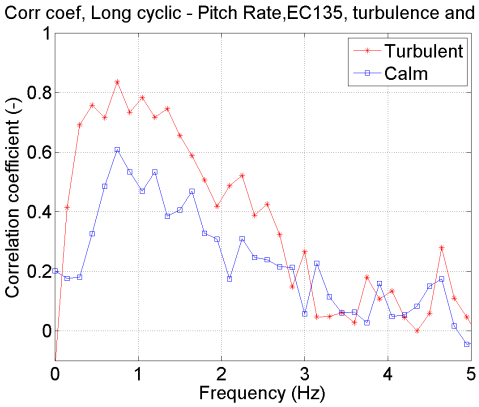

Figure 3.71: Correlation coefficient: longitudinal cyclic - Pitch rate, turbulence (Flight test data EC135)

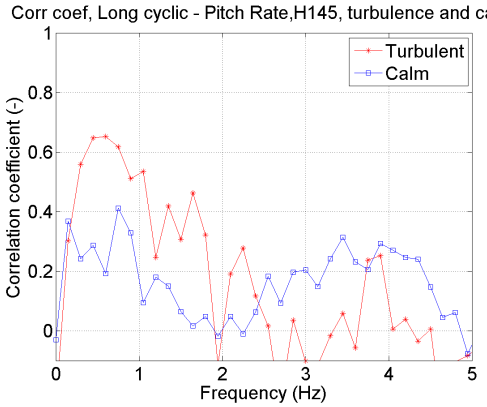

Figure 3.72: Correlation coefficient: Longitudinal cyclic - Pitch rate, turbulence (Flight test data H145)

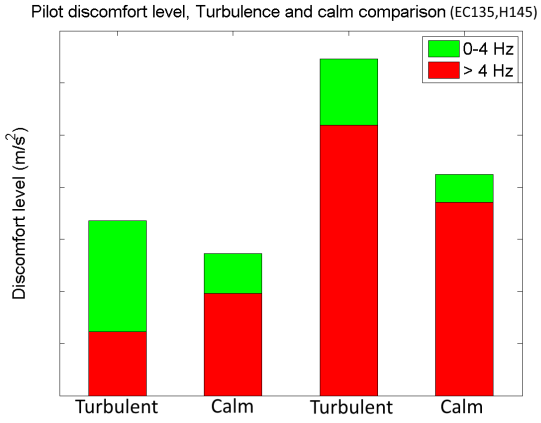

Figure 3.73: Pilot discomfort level for calm and turbulent conditions (Flight test data)

4

Flight simulation

The results of flight test data are complemented by related flight dynamics simulations in order to identify the relationship between control inputs and vibrations under laboratory and thus reproducible conditions. In this chapter, the tools and methods, which are used to evaluate the comfort of the pilot during a helicopter flight simulation, are explained. First, the used reference frame is described in Section 4.1. This is explained for both airframe and rotorblades coordinates. Afterwards, the equations of motion are discussed in Section 4.2. The stability analysis is explained in Section 4.3, which includes the trim process, the linearization, and the eigenvalues calculation. Section 4.4 elaborates on the used flight dynamics model, including the used flight control system and the gust model. The performed correlation analysis is discussed in Section 4.5, after which a conclusion is provided in Section 4.6.

4.1. Reference frame

In this section, the different body axes used throughout the model are defined, as well as the transformation matrices between the different frames [59]. All axes are based on the right handed orthogonal Cartesian coordinates, as illustrated in Figure 4.1.

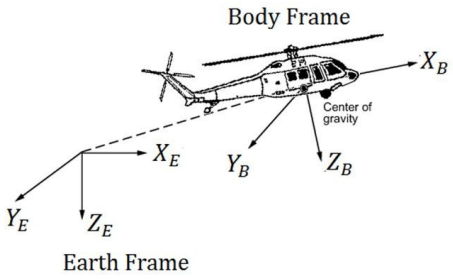

Figure 4.1: Right hand coordinate system [1]

Eulerian coordinates

The Eulerian coordinates refer to a fixed point on the earth (gravity axis x_G, y_G, z_G). The sequence of the Eulerian transformation angles is:

- Yawing (ψ_L): positive rotation about the Z_G-axis which is pointing to the center of earth
- Pitching (θ_L): positive rotation about a knot-line which is identical to the Y_G-axis, rotated with angle ψ_L
- Rolling (ϕ_L): positive rotation about the new x-axis which is already transformed by the angles ψ_L and θ_L

The transformation matrices used are shown in Equations 4.1, 4.2 and 4.3. They can be used as the rotation matrices for roll, pitch and yaw respectively. If one wants to go from earth fixed gravity axes to Eulerian coordinates, the rotation matrix for yaw should be used first, then the matrix for pitch and then the matrix for roll.

$$T_1(\alpha) = \begin{bmatrix} 1 & 0 & 0 \\ 0 & \cos(\alpha) & \sin(\alpha) \\ 0 & -\sin(\alpha) & \cos(\alpha) \end{bmatrix} \tag{4.1}$$

$$T_2(\alpha) = \begin{bmatrix} \cos(\alpha) & 0 & -\sin(\alpha) \\ 0 & 1 & 0 \\ \sin(\alpha) & 0 & \cos(\alpha) \end{bmatrix} \tag{4.2}$$

$$T_3(\alpha) = \begin{bmatrix} \cos(\alpha) & \sin(\alpha) & 0 \\ -\sin(\alpha) & \cos(\alpha) & 0 \\ 0 & 0 & 1 \end{bmatrix} \tag{4.3}$$

Fuselage coordinates

The body axes system (i_s, j_s, k_s) is moving and rotating with the helicopter. If all Euler angles are equal to zero, the i_s-axis, fixed to vehicle, is pointing forward. The k_s-axis is perpendicular to this axis and points positive towards the bottom of the vehicle. The j_s-axis is pointing positive to the right. In this coordinate system, the position of the center of mass and aerodynamic center of the fuselage are defined. This coordinate system is shown in Figure 4.2.

Coordinates of helicopter components

The coordinate systems of the horizontal stabilizer $(i_{s,HT}, j_{s,HT}, k_{s,HT})$ and vertical tail $(i_{s,VT}, j_{s,VT}, k_{s,VT})$ are defined with respect to the fuselage system using the position as displacement. The tail rotor coordinates $(i_{TRo}, j_{TRo}, k_{TRo})$ are placed at the body fixed coordinates, using the displacement and the tail rotor shaft angles. The main rotor hub coordinate system (i_{Ro}, j_{Ro}, k_{Ro}) is non-rotating with the rotor. The origin is in the center of the hub and is also placed in the body fixed coordinates. It includes the rotor shaft pitch and roll.

Rotor blade coordinates

The blade coordinates, which rotate with the rotor, depend on the number of blade degrees of freedom. For the definition of these coordinates, displacements and rotations to different coordinate systems are required. The blade degrees of freedom taken into account are flap, lead-lag, and blade torsion. The following individual coordinate systems are defined with respect to the just previously stated one. These are also shown in Figure 4.3.

- Rotating rotor hub coordinates (i_1, j_1, k_1): the origin is identical with the main rotor hub coordinate system. The azimuth angle of the main rotor $(\psi = \Omega t)$ rotates counter-clockwise if seen from above.
- Flap coning angle coordinates (i_i, j_i, k_i): the frame has a torque offset $(j_1 d_{PA})$. The flapwise coning angle (β_k) is also introduced.
- Control coordinates $(i_\theta, j_\theta, k_\theta)$: the pitching angle (θ) is valid here and puts together collective pitch, cyclic pitch, and feathering.
- Pre-sweep angle coordinates (i_2, j_2, k_2): it takes into account the inplane angle (ζ_k).
- Flap coordinates (i_p, j_p, k_p): this frame introduces the transformation with the flap angle β and the displacement $i_2(a_\beta - a_{GEOM})$, where a_β is the distance from the rotor hub center to fictive flapping hinge.
- Inplane coordinates (i_L, j_L, k_L): this frame introduces the inplane angle ζ and displacement $i_p(a_\zeta - a_\beta + j_p d_\zeta)$, where a_ζ is the distance from the rotor hub center to the fictive lead-lag hinge.
- Blade torsion coordinates (i_B, j_B, k_B): this frame introduces the blade torsion angle θ_B.

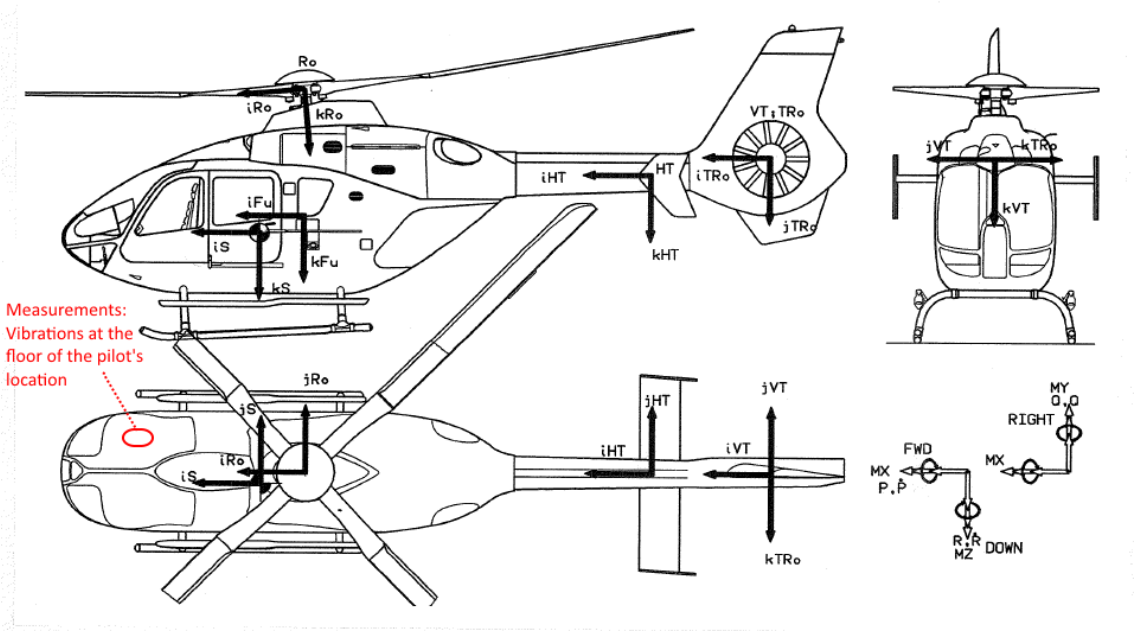

Figure 4.2: Reference frames of helicopter [59]

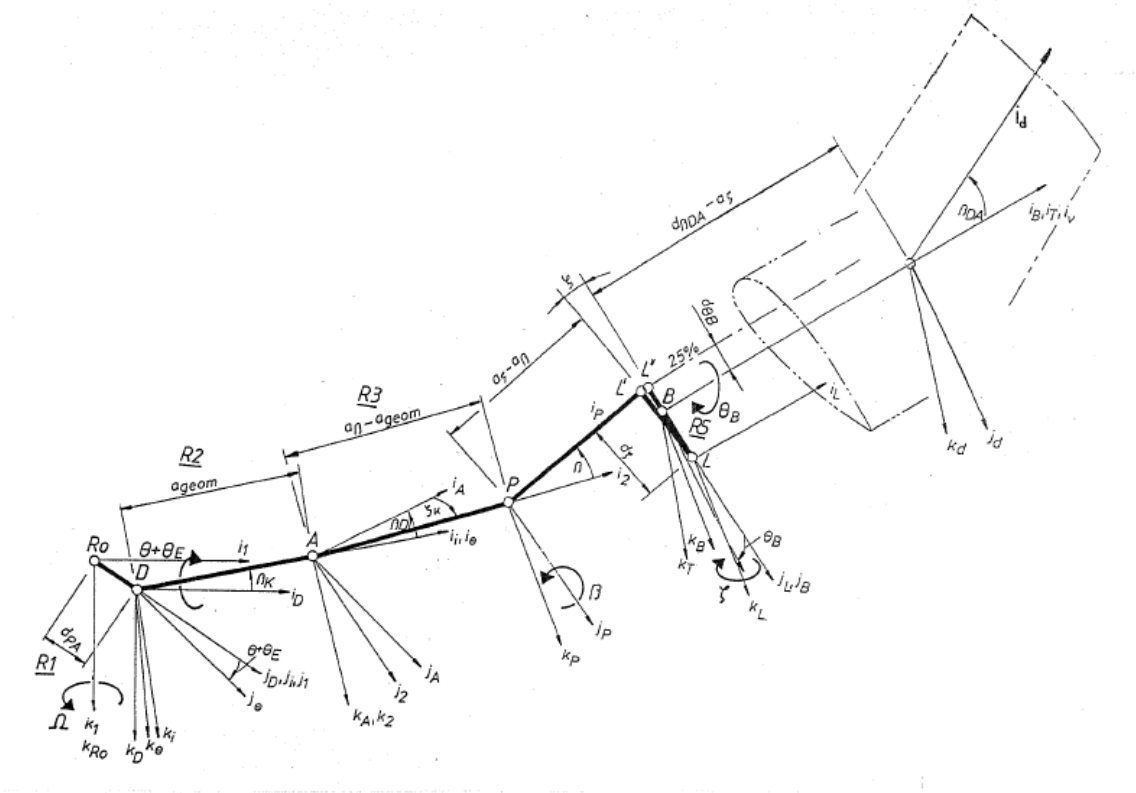

Figure 4.3: Reference frame of rotor blade [59]

4.2. Equations of motion

The behaviour of a helicopter in flight can be modelled as the combination of a large number of interacting subsystems. The components taken into account in the model provided by Airbus Helicopters are shown in Figure 4.4. In this section, the contribution of the main rotor, the fenestron, and the airframe will be discussed. The purpose of this section is not to derive the full equations of motion, but to provide a general

idea on what it taken into account and what it not. The assumptions used in this model will be discussed in Section 5.4.

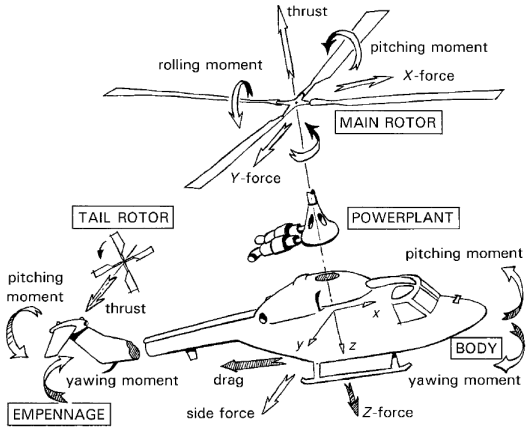

Figure 4.4: Helicopter components [47]

4.2.1. Main rotor

The model is able to take into account both hingeless and bearingless rotor blades. The degrees of freedom considered in this work are the flapping, lead-lag, and rigid blade torsion. Only the first natural eigenmodes are taken into account in the blade dynamics. The system is defined by the following physical quantities:

- Flapping and lagging hinge offsets: a_β, a_ζ
- Mass distribution of the blade and equivalent masses for flap and lead-lag: M_β, M_ζ
- First and second mass moments: I_β, I_ζ
- Springs and dampers: $k_{\theta B}, k_\beta, k_\zeta, c_{\theta B}, c_\beta, c_\zeta$

The aerodynamic calculation model is based on blade element theory, where the rotor blade is divided into a number of elements. The motion of a blade element is part of the motion of the blade. In general, there are three external forces acting on a blade element: aerodynamic, gravity and dynamic loads. An illustration of a blade element in forward flight is shown in Figure 4.5.

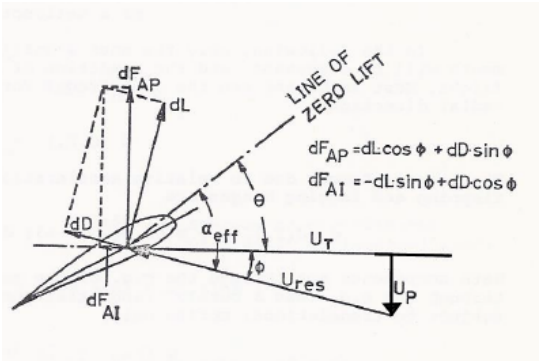

Figure 4.5: Blade element in forward flight [53]

From this figure, the external aerodynamic forces acting on the blade element can be determined. They are modelled as pressures distributed over the surface. The lift, drag and moment of a blade element are shown in Equations 4.4, 4.5 and 4.6 respectively. In these equations, U_T is the tangential and U_P is the perpendicular component of the tip speed (ΩR). The aerodynamic forces occur in a plane normal to the blade span. The aerodynamic moment is acting on the axis parallel to the span.

$$dL = \frac{1}{2}\rho c_l \Omega^2 R^2 (U_T^2 + U_P^2) c dr \tag{4.4}$$

$$dD = \frac{1}{2}\rho c_d \Omega^2 R^2 (U_T^2 + U_P^2) c dr \tag{4.5}$$

$$dM = \frac{1}{2}\rho c_m \Omega^2 R^2 (U_T^2 + U_P^2) c^2 dr \tag{4.6}$$

Gravity forces are represented by the weight of the blade element acting in its center of gravity. The dynamic forces and moments are dependent on the linear and rotational motion of the center of gravity of the blade element. Important forces are the centrifugal forces, inertia forces and the Coriolis force.

In general, for each of the elements, the resultant velocity vector due to rotor rotational speed, translational flight speeds, and rotor downwash is determined. The normal and tangential velocity components relative to the blade axis are considered for the airload calculation. Local angles of attack are obtained from cyclic and collective pitch angles, inflow angles, blade twist, and velocity components due to blade motion. This process will be shown in more detail in this section.

The purpose here is to obtain the blade equations of motions, which can be done by adding the mass, aerodynamic, spring and damper moments. This is shown in Equation 4.7.

$$M_{mass} + M_{spring} + M_{damp} = M_{aero} \tag{4.7}$$

First the mass forces and moments are determined. The acceleration vector of one blade element should be obtained first, for which Equation 4.8 can be used.

$$\vec{b_B} = \ddot{\vec{R}}_0 + \sum_{i=1}^{n} \ddot{\vec{\omega}}_i \times \vec{R}_i + 2^k \sum_{i=1}^{n} \sum_{j=1}^{n} \vec{\omega}_i \times (\vec{\omega}_j \times \vec{R}_j) \tag{4.8}$$

In this equation, $k = 0$ if $i = j$ and $k = 1$ if $i \neq j$, $\vec{\omega}_i$ are the angular velocity vectors of the rigid subsystem with index i relative to the system with index $i-1$. Then the mass force and mass moment about point B can be calculated with Equations 4.9 and 4.10 respectively. At point B the blade torsion is located and Q describes a blade point outside B.

$$\vec{F_B} = \int_{blade} (-\vec{b_B}) dm \tag{4.9}$$

$$\vec{M_B} = \int_{blade} \vec{BQ} \times (-\vec{b_B}) dm \tag{4.10}$$

With this method, all the mass forces and moments can be determined. From the mass forces and the spring and damping terms, the differential equations of angular blade motions are obtained. Equations 4.11, 4.12 and 4.13 are derived for the blade torsion, lead-lag motion, and flap motion respectively.

$$\int_{blade} (z_B b_{yB} - y_B b_{zB}) dm + c_{\dot{\theta}B}\dot{\theta_B} + k_{\theta B}\theta_B = M_{aero_B} \tag{4.11}$$

$$\int_{blade} ((d_{\theta B} - d_\zeta + y_B) b_{xL} - x_B b_{yL}) dm + c_{\dot{\zeta}}\dot{\zeta} + k_\zeta \zeta = M_{aero_\zeta} \tag{4.12}$$

$$\int_{blade} (x_p b_{zp} - z_p b_{xp}) dm + c_{\dot{\beta}}\dot{\beta} + k_\beta \beta = M_{aero_\beta} \tag{4.13}$$

The calculation of the aerodynamic motions will be explained next. This starts with the calculation of the velocity vector of one blade element, as shown in Equation 4.14.

$$\vec{v} = \dot{\vec{R}}_0 + \sum_{i=1}^{n} (\vec{\omega}_i \times \vec{r}_i) + \vec{w}_i \tag{4.14}$$

In this equation $\vec{w}_i$ is the inflow velocity and the local vector $\vec{r}_i$ points to the local aerodynamic center. Knowing the velocity of the blade, the section angle of incidence can be determined with Equation 4.15. This is an addition of the inflow angle, the twist angle, the elastic blade control angle, and the blade pitch control angle.

$$\alpha_{eff} = \phi_i + \theta_v + \theta_B + \theta \tag{4.15}$$

The inflow angle can be determined with Equation 4.16, where U_P is the normal velocity component and U_T is the tangential velocity component. The rotor flow is modelled by the dynamic inflow model of Pitt&Peters [58]. Their model is based on the derivation of relationships from an unsteady, actuator-disc theory. With this approach, transient rotor loads are related to the total transient response, which is determined by the rotor-induced flow field. The blade pitch control angle can be calculated with Equation 4.17, which is the addition of the collective and cyclic controls.

$$\phi_i = \arctan(\frac{U_P}{U_T}) \tag{4.16}$$

$$\theta = \theta_0 + \theta_\beta \cos(\psi) + \theta_\alpha \sin(\psi) \tag{4.17}$$

Knowing the flow condition (Mach number and local angle of attack), the aerodynamic forces and moments are calculated using airfoil characteristics from empirical data tables with Equations 4.4, 4.5 and 4.6. The loss of rotor blade thrust near the tip due to tip-vortex is also taken into account. Further derivation of the equations of motion is outside the scope of this thesis. The final form of the equations of motion can be integrated by application of the Runge Kutta method.

After integrating the differential equations of motion of the blade, the blade forces $\vec{P}_B$ and moments $\vec{M}_B$ are calculated in the blade coordinate system. These can then be transformed to the rotor hub system for adding all blade contributions. This composition of all rotor blade loads is shown in Equations 4.18 - 4.23, where DA_{hub} is the drag area of the rotor hub, DA_{ba} is the drag area of the blade attachment, z_N is the number of blade and n_j is a counter. The contribution of each blade is added up for the total forces at hub center. The equivalent system technique applied for blade/hub modelling is representing the first Eigenmode for each blade DOF.

$$F_{x_{Ro,z_N}} = \sum_{n_j=0}^{z_N-1} F_{x_{Ro}}(\psi + \frac{2\pi n_j}{z_N}) - \frac{1}{2}\rho V_{x_{Ro}}^2 DA_{hub} - \frac{1}{2}\rho (a_{GEOM}\Omega)^2 DA_{ba} \sin(\psi + \frac{2\pi n_j}{z_N}) \tag{4.18}$$

$$F_{y_{Ro,z_N}} = \sum_{n_j=0}^{z_N-1} F_{y_{Ro}}(\psi + \frac{2\pi n_j}{z_N}) - \frac{1}{2}\rho V_{x_{Ro}}^2 DA_{hub} - \frac{1}{2}\rho (a_{GEOM}\Omega)^2 DA_{ba} \cos(\psi + \frac{2\pi n_j}{z_N}) \tag{4.19}$$

$$F_{z_{Ro,z_N}} = \sum_{n_j=0}^{z_N-1} F_{z_{Ro}}(\psi + \frac{2\pi n_j}{z_N}) \tag{4.20}$$

$$M_{x_{Ro,z_N}} = \sum_{n_j=0}^{z_N-1} M_{x_{Ro}}(\psi + \frac{2\pi n_j}{z_N}) \tag{4.21}$$

$$M_{y_{Ro,z_N}} = \sum_{n_j=0}^{z_N-1} M_{y_{Ro}}(\psi + \frac{2\pi n_j}{z_N}) \tag{4.22}$$

$$M_{z_{Ro,z_N}} = \sum_{n_j=0}^{z_N-1} M_{z_{Ro}}(\psi + \frac{2\pi n_j}{z_N}) - \frac{1}{2}\rho z_N (a_{GEOM}\Omega)^2 DA_{ba} a_{GEOM} \tag{4.23}$$

4.2.2. Fenestron

The model for the Fenestron is developed at Eurocopter France [59] and only a short discussion can be provided on this. The theoretical model yields thrust, drag, and torque of the fenestron and includes the determination of the induced velocity. If the sideslip is at zero degrees, the drag to thrust ratio will be approximately 0.5 for a wide range of control angles. It also has approximately constant torque at minimum level. When the sideslip angle is not zero, there can be a destabilising effect on directional stability proportional to advance ratio, which need to be considered when dimensioning the vertical tail. Two empirical constants are used

within the model. The first constant is the lift curve slope of the blade airfoil; the other constant defines the effect of sideslip angle on fenestron thrust. This semi-empirical model was validated with flight test data and wind tunnel tests.

4.2.3. Airframe

When considering the airframe, every aerodynamic surface is considered separately, such as the fuselage and the empennage. The force and moment coefficients are determined as a function of angle of attack and angle of sideslip, which determined by wind tunnel tests with a helicopter model. Interference with rotor downwash on the components is taken into account by empirical factors during the calculation of the local angle of attack and sideslip angle. The forces can be calculated with Newton's theory, where the forces will be integrated over the entire fuselage mass. In this model, the fuselage is treated as a rigid body, which means that elasticities are neglected. This means that the tailboom modes are not visible in the results, which will not have a big effect on the considering frequency area.

4.2.4. Total aircraft formulation

The differential equation of the whole aircraft in the fuselage coordinate system (x_s, y_s, z_s) can be established by adding all the aerodynamic forces and moments of the individual components. These components are shown in Equations 4.24 and 4.25 respectively.

$$\vec{F_s} = \vec{F_{main\ rotor}} + \vec{F_{fuselage}} + \vec{F_{tail\ rotor}} + \vec{F_{empennage}} + ... = 0 \tag{4.24}$$

$$\vec{M_s} = \vec{M_{main\ rotor}} + \vec{M_{fuselage}} + \vec{M_{tail\ rotor}} + \vec{M_{empennage}} + ... = 0 \tag{4.25}$$

These can be used to define six equilibrium conditions in Equation 4.26. Here, the vectors in the left matrix are the masses and mass moment of first and second order. The states are the three translational and three rotational motions. The elements of vector $\vec{G}$ are terms with $p, q, r, \dot{x_s}, \dot{y_s}, \dot{z_s}$ and force and moment contributions from the different components. This equation can be solved by the Runge Kutta approach for time simulations, after the equation is rearranged in new order by Gaussian elimination. The equations of motion are defined in general form, as shown in Equations 3.3 and 3.4.

$$\begin{bmatrix} \vec{A} & \vec{B} & \vec{C} & \vec{D} & \vec{E} & \vec{F} \end{bmatrix} \cdot \begin{bmatrix} \ddot{x_s} \\ \ddot{y_s} \\ \ddot{z_s} \\ \dot{p} \\ \dot{q} \\ \dot{r} \end{bmatrix} = -\vec{G} \tag{4.26}$$

4.3. Stability analysis

Instability can be characterized by some of the outputs or internal states that is growing with no boundaries. Not all systems are either stable or unstable, as systems can also be marginally stable. Dynamic stability refers to the response of the system over time. After a certain response, as the system is reaching equilibrium, the forces or moments that move it there also generate momentum which causes it to overshoot or go beyond the equilibrium condition. After this, the system tends to move back to the equilibrium; it is oscillating. If the system is unstable, the overshoot will keep growing. If it is stable, the system will move closer to the equilibrium. Shock absorbers and springs can help making the system more stable.

An eigenmode is a natural vibration of a system, such that various parts all move together at the same frequency. The frequency for a particular mode is called the eigenfrequency. In order to determine the eigenfrequencies, one can use the defined equations of motion from Section 4.2. After this, Fourier transformation should be implemented on the individual blade coordinates (IBC). Next, linearization is performed about the trim solution, after which a state space matrix can be formulated. Finally, the eigenfrequencies can be determined. This process is also shown in Figure 4.6. The results of this analysis will be discussed in Section 5.1.3.

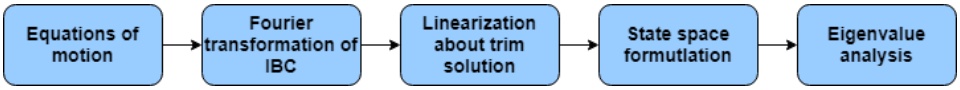

Figure 4.6: Flow chart for stability analysis

4.3.1. Trim

The purpose of trimming is to free the pilot from having to exert a constant pressure on the controls. To fulfil a constrained flight condition, one should find the correct control settings and state variables. The previously mentioned six degrees of freedom equilibrium condition is solved in the earth fixed system by iterative approximation (Newton-Raphson approach) of a subset of six parameters. These can be selected from the following degrees of freedom:

- Main rotor control angles: $\theta_\theta, \theta_\alpha, \theta_\beta$
- Tail rotor collective pitch: θ_δ
- Angles of attitude: ψ_L, θ_L, ϕ_L
- Translational speeds: v_x, v_y, v_z
- Translational accelerations: $\dot{v_x}, \dot{v_y}, \dot{v_z}$
- Angular speeds: r, p, q
- Angular accelerations: $\dot{r}, \dot{p}, \dot{q}$
- Angular speed of main rotor: Ω

4.3.2. Linearization

From the equilibrium condition obtained during the trim procedure, a perturbation analysis can be performed. This will provide the derivatives required for the calculation of the first order stability equations. A first order formulation of linearization for a function $f(x,y)$ at a point $p(a,b)$ is given in Equation 4.27. The general formulation is shown in Equation 4.28. These formulations are based on the Taylor expansion.

$$f(x,y) \approx f(a,b) + \frac{\delta f(x,y)}{dx}\bigg|_{a,b}(x-a) + \frac{\delta f(x,y)}{dy}\bigg|_{a,b}(y-b) \tag{4.27}$$

$$f(\vec{x}) \approx f(\vec{p}) + \Delta f\big|_{\vec{p}}(\vec{x}-\vec{p}) \tag{4.28}$$

The full 6 DOF helicopter equations are ninth order, arranged as $u, w, q, \theta, v, p, \phi, r, \psi$, but the heading angle appears only in the kinematic equation relating the rate of change of Euler angle ψ to the fuselage rates. Therefore, the heading angle is usually omitted in the stability analysis. Note that, for the ninth-order system including the yaw angle, the additional eigenvalue is zero, as there is no aerodynamic or gravitational reaction to a change in heading [47]. The stability matrix will be an 8×8 matrix. This can only be done if frequencies of the rotor dynamic modes are separated from the fuselage modes. By evaluating the changes in the helicopter forces and moments from their trim value, caused by successive perturbations of the elements of the state variable vector, the control input vector and the first derivative of the state variable vector, the quasi-static derivatives can be obtained. The used state variable vector is shown in Equation 4.29. The control input vector is shown in Equation 4.30

$$\vec{x_1} = \begin{bmatrix} u & v & w & p & q & r & \phi & \theta \end{bmatrix} \tag{4.29}$$

$$\vec{u} = \begin{bmatrix} \theta_\theta & \theta_\beta & \theta_\alpha & \theta_\delta \end{bmatrix} \tag{4.30}$$

This will lead to the expression shown in Equation 4.31.

$$\dot{\vec{x_1}} = \left(\frac{\delta \dot{\vec{x_1}}}{\delta \vec{x_1}}\right)\vec{x_1} + \left(\frac{\delta \dot{\vec{x_1}}}{\delta \vec{u}}\right)\vec{u} = A_1\vec{x_1} + B_1\vec{u} \tag{4.31}$$

In order to have a more profound stability analysis, the dynamic coupling of rotor and fuselage has to be taken into account. The rotor state variables will be added to the previously mentioned matrix. By adding the rotor degrees of freedom (flapping, lead-lag, and blade torsion), a 26 × 26 state-matrix of stability derivatives can be obtained.

The individual coordinates should be transformed to the multiblade coordinates, which is also called Fourier transformation. There are three advantages for this formulation. First it means that the variables can be defined in the nonrotating reference frame. Secondly, the blade motions are isolated and actually couple with the supporting-structure. Finally, the procedure is relatively independent of the number of rotor blades. The general purpose of the multiblade coordinates is to represent each of the many different motions of any individual blade as the sum of two basic components. The first component (a_0) is shared by all blades and is therefore referred to as the collective responses, which is in general a low-frequency motion. The second component (a_1, b_1) can be compared to an amplitude modulated signal whose carrier frequency is the rotor rotational velocity and whose Fourier component amplitudes are the generalized multiblade coordinates. These latter motions are called the cyclic responses. These motions can also be seen in Figure 4.7.

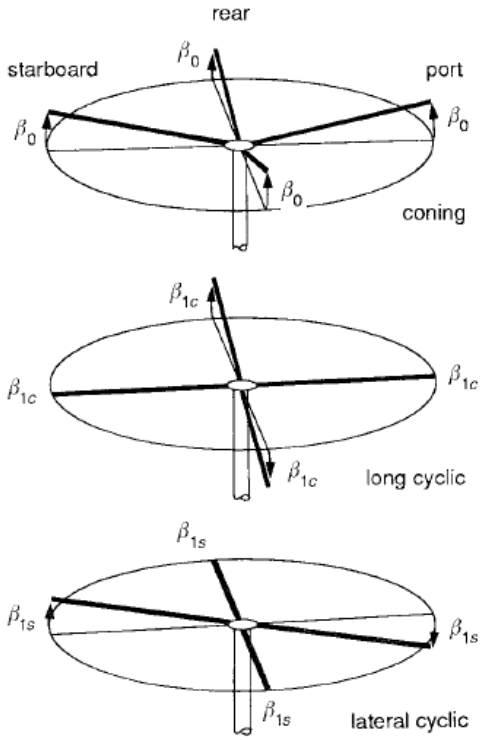

Figure 4.7: The rotor disc in multi-blade coordinates [47]

For the flap, lead-lag, and blade torsion motion, this is described in Equations 4.32, 4.33 and 4.34 respectively. The flight mechanics are mainly influenced by the zeroth and first harmonics. The other terms are omitted in this model.

$$\beta(\psi) = a_{0\beta} + a_{1\beta}\cos(\psi) + b_{1\beta}\sin(\psi) \tag{4.32}$$

$$\zeta(\psi) = a_{0\zeta} + a_{1\zeta}\cos(\psi) + b_{1\zeta}\sin(\psi) \tag{4.33}$$

$$\theta_B(\psi) = a_{0\theta_B} + a_{1\theta_B}\cos(\psi) + b_{1\theta_B}\sin(\psi) \tag{4.34}$$

The derivatives are also required for linearization. For the flapping motion, these are shown in Equations 4.35 and 4.36. The state variable vector for the flapping motion is then shown in Equation 4.37.

$$\dot{\beta}(\psi) = \dot{a_{0\beta}} + \dot{a_{1\beta}}\cos(\psi) + \dot{b_{1\beta}}\sin(\psi) - \Omega a_{1\beta}\sin(\psi) + \Omega b_{1\beta}\cos(\psi) \tag{4.35}$$

$$\ddot{\beta}(\psi) = \ddot{a_{0\beta}} + \ddot{a_{1\beta}}\cos(\psi) + \ddot{b_{1\beta}}\sin(\psi) - 2\Omega a_{1\beta}\sin(\psi) + 2\Omega b_{1\beta}\cos(\psi) - \Omega^2 a_{1\beta}\cos(\psi) - \Omega^2 b_{1\beta}\sin(\psi) \tag{4.36}$$

$$\vec{x_2} = \begin{bmatrix} \dot{a_{0\beta}} & \dot{a_{1\beta}} & \dot{b_{1\beta}} & \dot{a_{0\beta}} & \dot{a_{1\beta}} & \dot{b_{1\beta}} \end{bmatrix} \tag{4.37}$$

In this equation, the first three Fourier coefficients and their derivatives are added. Then, the linearized first order stability equation can be deduced, as shown in Equation 4.38.

$$\dot{\vec{x}} = \begin{bmatrix} \dot{\vec{x}_1} \\ \dot{\vec{x}_2} \end{bmatrix} = \underbrace{\begin{bmatrix} A_{11} & A_{12} \\ A_{21} & A_{22} \end{bmatrix}}_{A} \cdot \begin{bmatrix} \vec{x}_1 \\ \vec{x}_2 \end{bmatrix} + \underbrace{\begin{bmatrix} B_1 \\ B_2 \end{bmatrix}}_{B} \cdot \vec{u} \tag{4.38}$$

The blade torsion and lead-lag can be added with the same approach.

4.3.3. Eigenvalues analysis

With the state space representation, one can use matrix A to calculate the eigenvalues. It is assumed that the response of the system is as shown in Equation 4.39. This response can be diverging, damped or neutral, and periodic or aperiodic. In this equation, $\hat{\vec{x}}$ represents the eigenvector, and the eigenvalue is defined as $\lambda = \sigma \pm i\omega$. In general, the period can be calculated with $2\pi/\omega$ and the double or half amplitude time can be approximated with $ln(2)/\sigma$. With this assumption, the state space-space system can be written as in Equation 4.40.

$$\vec{x} = \hat{\vec{x}}e^{\lambda t} \tag{4.39}$$

$$([A] - \lambda[I])\hat{\vec{x}} = \vec{0} \tag{4.40}$$

When the non-trivial solution $\hat{\vec{x}} = 0$ is neglected, the characteristic Equation 4.41 can be derived.

$$det([A] - \lambda[I]) = \vec{0} \tag{4.41}$$

The solutions of this characteristic equation are the eigenvalues. The amount of eigenvalues are equal to the amount of entries in the state vector $\vec{x}$.The system is asymptotically stable (damped), if all the real parts, σ, of the eigenvalues are negative. If even one real part of the eigenvalue is positive, the system becomes unstable. The system is neutrally stable if one or more eigenvalues are located on the imaginary axis, while the other eigenvalues are on the left side of this axis. Most helicopters are dynamically unstable. Dynamic stability is not essential, but it is in general desirable. The eight natural modes are described as linearly independent, which means that no single mode can be made up of a linear combination of the other. The eigenvalues and eigenvectors can be complex numbers, which means that the mode has an oscillatory behaviour. Such a mode will be described by two eigenvalues. The important modes of this analysis are listed below:

- Dutch roll
- Phugoid
- Spiral mode
- Short period
- Roll subsidence mode
- Flapping modes (collective, progressive and regressive)
- lead-lag modes (collective, progressive and regressive)
- Blade torsion modes (collective, progressive and regressive)

A graphical representation of the eigenvalues of the flapping motion is shown in Figure 4.8 in the complex plane. The frequency of the collective mode is equal to that of the rotating system. The progressive mode is approximately one rotating blade frequency higher and the regressive mode is one rotating blade frequency lower than the collective mode. Furthermore, after solving the coefficients of rotor motions, it can be noticed that the eigenvalues are largely dependent on the Lock number. This non-dimensional scaling coefficient provides the ratio of aerodynamic to inertia forces acting on a rotor blade. This is shown in Equation 4.42, where a_{L0} is the main rotor blade lift curve slope and I_β is the flap moment of inertia.

$$\gamma = \frac{\rho c a_{L0} R^4}{I_\beta} \tag{4.42}$$

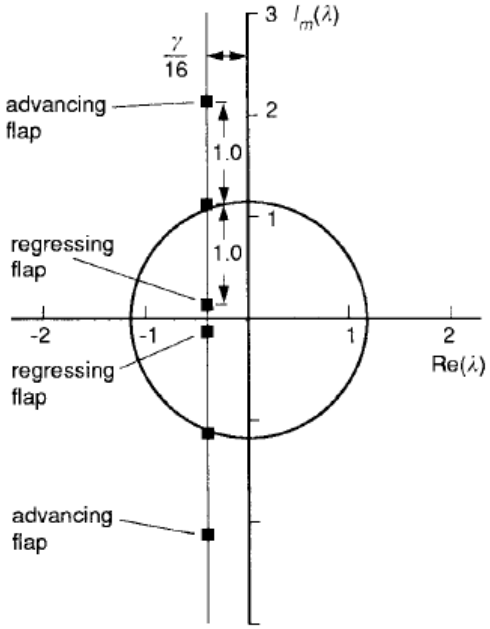

Figure 4.8: Flapping eigenvalues of a multi-blade coordinate rotor system [47]

The eigenvalues can be calculated as shown in Table 4.1. An elaborate discussion on the influence of the eigenmotions is provided in Section 5.1.3.

Table 4.1: Frequencies of the rotor modes that result from the MBC transformation

Frequency	Rotor mode
ω_{IBC}	Collective
$\omega_{IBC} + \Omega$	Progressive
$\lvert\omega_{IBC} - \Omega\rvert$	Regressive

4.4. Flight model settings and gust model

At Airbus Helicopters, the model GenSim [21] is used for flight simulations, including a helicopter model, based on the theory discussed before, a flight control system and a gust model. It is a 6 DOF rigid body model with 3 DOF blade model. Advantages of using a simulation model are that the results are reproducible. The flight conditions and helicopter configurations are not set, which means that a parametric study can be performed. For example, different turbulence levels can for example be implemented. Additionally, there is a certainty on the rotorcraft parameters, such as moment of inertia, and the measurements from the sensors.

As it is a simulation model, it will include some assumptions. It contains a rigid body frame, which means that no elasticities are taken into account, which will not have a big effect on the considered frequency area. This

will mean that the tailboom modes are not visible in the results. The rotor model only takes into account the first rotor Eigenmodes of lead-lag, flapping and torsion. This also will not cause big deficiency in the results, as only the first rotor Eigenmodes occur in the lower frequency domain. There are no drive train dynamics. A discussion on the model assumptions and methodology will be provided in Section 5.3.

The outputs of the model are the accelerations/vibrations in the center of gravity. The full model is shown in Figure 4.9. In the flight simulation application, the user can choose a pilot model, or, as in the studied case, the autopilot. The reason to choose the autopilot is that the pilot input given by an inexperienced steerer will never be comparable to the one given in a real flight test. The available options in the 3-axes flight control system are the Stability Augmentation System (SAS) and the attitude mode (ATT). This control system reacts instantaneously to the simulated helicopter conditions by a feedback loop to correct the flight control parameters. Atmospheric turbulence is generated as disturbance by an implemented gust model. The helicopter dynamic model block calculates the state-characterizing quantities using the analytical and mathematical techniques discussed in the previous sections.

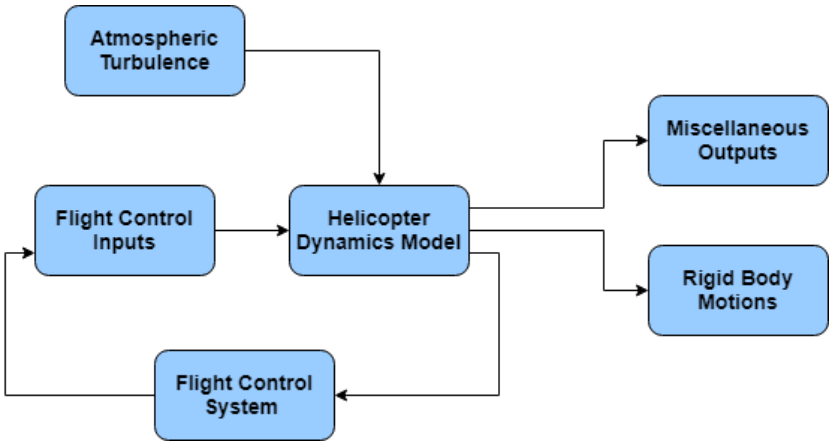

Figure 4.9: Structure of the non-linear helicopter model with model input, disturbance and output

The Dryden wind turbulence model [25] is used to generate turbulence within the helicopter flight simulation. It generates a time-invariant, spatial varying gust field, through which the aircraft is flying at a certain flight speed V. The Dryden model describes turbulence as a stochastic process specified by velocity spectra. Their definitions are provided by the Military Specification MIL-F-8785C [43], and are discussed in Section 2.3.2. Within this model, gusts are generated by passing band-limited noise through appropriate forming filters. For this thesis, only the translational wind speed components will be used. The reason is that the Dryden gust model is initially designed for aircraft application and that the rotational wind speed components are not yet validated for rotorcraft applications.

As mentioned in Section 2.3.2, the gust model has been adapated in previous works to match the characteristics of a flight-test validated turbulence model developed by Seher-weiss and Gruenhagen [64]. Three turbulence levels 'low', 'medium' and 'high', are specified according to the turbulence levels in the performed flight tests. These levels and their representative velocities are listed in Table 4.2.

Table 4.2: Turbulence levels for gust modelling [64]

Turbulence level	Wind (Mean)	Wind (Standard Deviation)
Low	8.7 kts	3.3 kts
Medium	11.1 kts	3.9 kts
High	15.4 kts	5.1 kts

Based on these turbulence levels (L_{Tu}), the appropriate turbulence intensity (σ) and turbulence scale lengths (l) of the Dryden model are defined for three different altitudes (291 ft, 3000 ft and 5000 ft). These turbulence parameters as well as the inflow velocity (V_i) define the transfer functions of the Dryden model. The outputs of the gust model are the three gust speed components (u_G, v_G, w_G), which are added in the body

coordinate system.

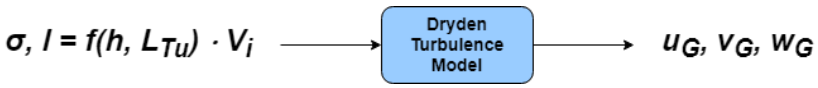

Figure 4.10: Input and output of the Dryden turbulence model

The output of the non-linear helicopter are the rigid body accelerations in the center of gravity. For the pilot comfort assessment, the accelerations at the position of the pilot are required. The model provides the translational acceleration $\vec{a_{CG}}$, the angular acceleration $\dot{\vec{\omega_{CG}}}$, and the angular rates $\vec{\omega_{CG}}$. For the conversion of the acceleration from the center of gravity to another reference point, in this case the position of the pilot, Equation 4.43 can be used. In general, the rigid body motions at the considered position can be found by summing up the translational accelerations at the center of gravity, the centripetal acceleration caused by the position outside of the center of gravity, and the translational acceleration due to rotational accelerations. The vector $\vec{r_{CG-PIL}}$ is the distance from the center of gravity to the position of the pilot.

$$\vec{a_{PIL}} = \vec{a_{CG}} + \underbrace{\vec{\omega_{CG}} \times (\vec{\omega_{CG}} \times \vec{r_{CG-PIL}})}_{Centripetal\ Acceleration} + \underbrace{\dot{\vec{\omega_{CG}}} \times \vec{r_{CG-PIL}}}_{Translational\ Acceleration\ due\ to\ Rotation} \tag{4.43}$$

4.5. Correlation analysis and pilot comfort assessment

After converting the vibration measurements from the center of gravity to the position of the pilot, these values can be used in the correlation analysis. The flight controls are measured just before the helicopter dynamics block. The same methodology as described in Section 3.3 is used here. First the signal are converted to the frequency domain. This is done with the Discrete Fourier Transform approach using the Fast Fourier Transform algorithm. After this, the power of the vibration and flight control input signals is determined with Power Spectral Density. As mentioned before, these powers cannot be compared one on one as the unit is different. A parametric study is performed to investigate how both signals behave under different circumstances. The advantage of using the simulation model, is that certain conditions can be modified, while the rest stays equal. Another advantage is that some helicopter or blade parameters, such as the stability gains or blade inertia, can now be modified, which was impossible during the flight test data analysis. The different considered conditions and configurations are listed below:

- Rotorcraft configuration (for example weight and center of gravity)
- Rotor blade parameters
- Flight control system gains
- Velocity
- Atmospheric conditions (calm or turbulent flight)
- Rotorcraft mission (level flight or manoeuvre)
- Rotor rotational speed

The correlation coefficient between the vibrations and control inputs can then be calculated. One should keep in mind that the collective control input is omitted in this analysis. The reason is that the simulation model is using a 3-axes flight control system, which means that no input is given to the collective. Finally, the pilot discomfort is calculated for both the lower frequencies as well as over the whole frequency domain. With the lack of rotor blade harmonic loads and tail boom induced loads, it is expected that the latter value is lower.

4.5.1. Rotorcraft configuration

The baseline simulation is the EC135 helicopter and the parameters are shown in Table 4.3. The pilot location is defined from the center of gravity in the body reference frame. An algorithm is implemented in the attitude controller to keep the path and altitude as constant as possible. This means that the reference roll angle will

be slightly positive if a correction to the left is required and a negative reference value for the case the other way around. This is also done for the reference pitch angle to keep the altitude constant. This makes it more valuable to compare with the level flights of the flight test data. This is not the same as an altitude controller, as a new reference value is not calculated. For the baseline simulations, low turbulence is implemented. This is probably higher than the turbulence level during most flight tests, but still more realistic than a perfect flight with no disturbances. Furthermore, the influence of turbulence is an important topic in this thesis.

Table 4.3: Baseline configuration

Parameter	Input
Mass	2980 kg
Pilot Location (x/y)	1.7/0.39 m
Pressure altitude	3000 ft
Ambient temperature	9.06° C
Initial speed	120 kts
Turbulence intensity (low/medium/high)	2.44/2.89/4.42 (low is default)
Turbulence wavelength scale	533.4

For this baseline flight, the spectral analysis graphs are shown in Figures 4.11 - 4.18. If the spectral analysis graphs of the vibrations are compared with the ones from the flight tests, one can indeed notice the lack of vibrations due to the tail boom shake and the harmonic loads, which is due to the assumptions made in the model. Because of this, most of the vibrations occur in the lower frequency domain. One can indeed notice that the vibration level is higher in the lower frequency domain and has a small peak around 12 Hz. This is due an eigenmode and will be discussed in Sections 5.1.3 and 5.2. Furthermore, the vibrations in z-direction are higher. It can also be seen that most of the control inputs occur in the region from zero till four hertz. It can also be noticed that roll and pitch rate have their peaks values at a lower frequency, when compared to the flight test data. Therefore, it can be expected that the respective correlation coefficients are already higher at a lower frequency. This is indeed the case as can be seen in the correlation coefficient between the lateral cyclic and the roll rate as shown in Figure 4.20.

One can notice some similarities and differences between the correlation coefficients of the EC135 and the H145 shown in figures 4.19 and 4.20. In general, most of the peaks occur at the same frequencies, but with different magnitudes. The EC135 has slightly higher lateral correlation coefficients in general. This could also be seen with the flight tests, which can be due to a difference in helicopter configuration or blade parameter, which will be investigated next.

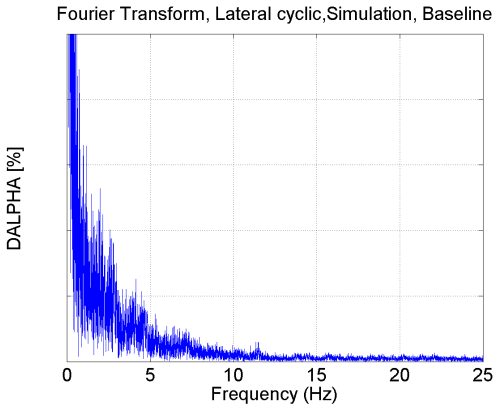

Figure 4.11: Frequency spectrum of lateral cyclic (Flight simulation EC135)

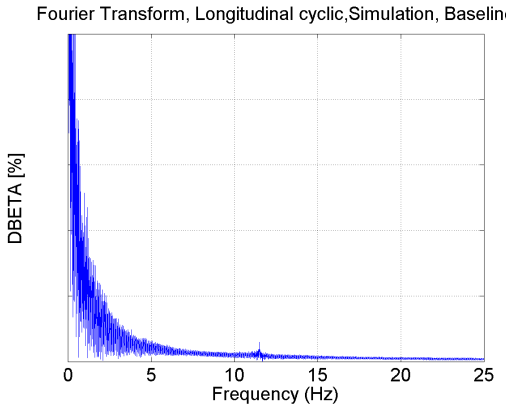

Figure 4.12: Frequency spectrum of longitudinal cyclic (Flight simulation EC135)

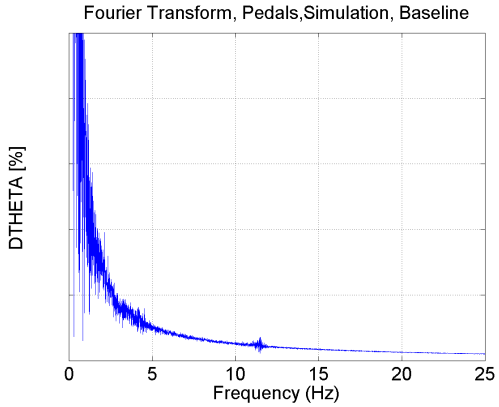

Figure 4.13: Frequency spectrum of pedals (Flight simulation EC135)

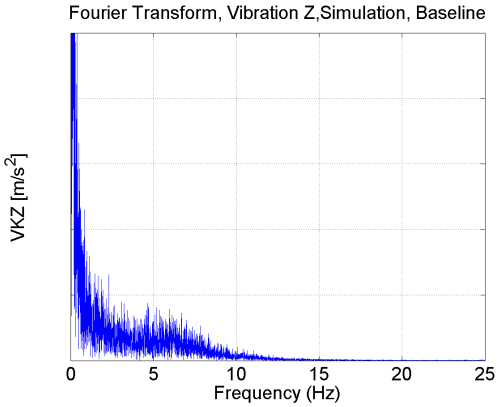

Figure 4.14: Frequency spectrum of vibration in z-direction (Flight simulation EC135)

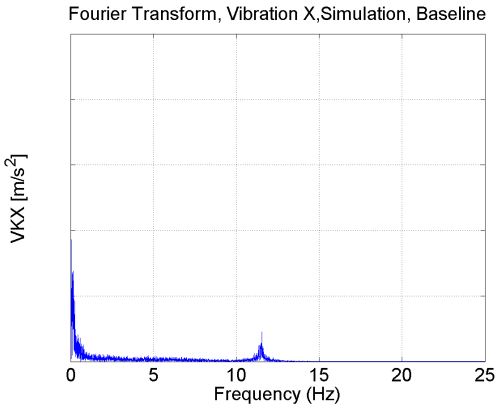

Figure 4.15: Frequency spectrum of vibration in x-direction (Flight simulation EC135)

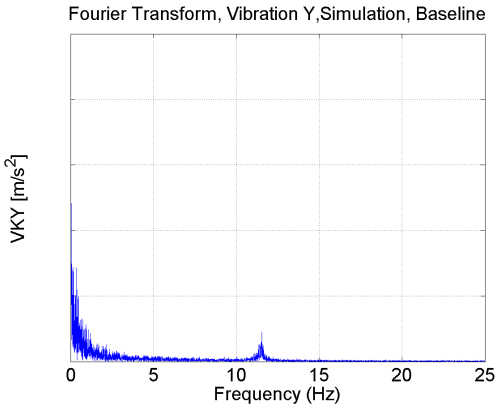

Figure 4.16: Frequency spectrum of vibration in y-direction (Flight simulation EC135)

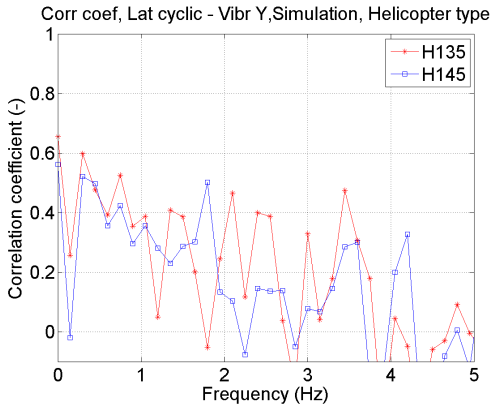

Figure 4.19: Correlation coefficient: Lateral cyclic - Vibration Y (Flight simulation EC135/H145)

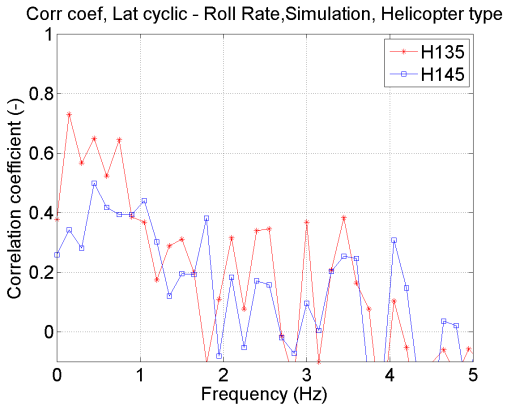

Figure 4.20: Correlation coefficient: Lateral cyclic - Roll rate (Flight simulation EC135/H145)

4.5.2. Sensor location

In this section, the influence of the sensor location on the results will be discussed. This aspect has already been verified for the vibration spectra by Martin [38] and Bernaschek [6] and is also included in the model verification [59]. An important conclusion is that the pilot comfort per directions changes a bit, but that the combined pilot discomfort value is almost the same. Therefore, the focus here is on the correlation coefficients. The vibrations during the flight tests are measured at the location of the pilot, while the vibrations of the simulation are calculated initially for the center of gravity. Using Equation 4.43, the location of the

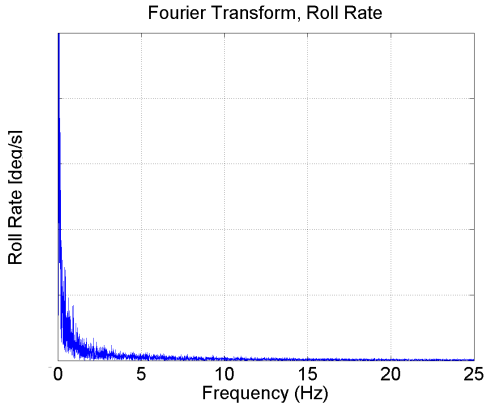

Figure 4.17: Frequency spectrum of roll rate (Flight simulation EC135)

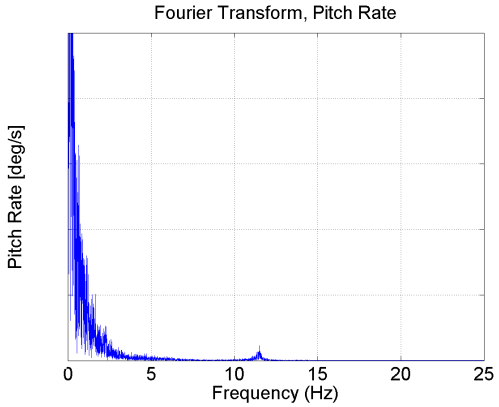

Figure 4.18: Frequency spectrum of pitch rate (Flight simulation EC135)

vibrations of the flight simulations is translated to the location of the pilot. Therefore it would be interesting to compare the coefficients at the center of gravity and at the pilot location. They are shown in Figures 4.21 and 4.22. It can be concluded that although the magnitude changes slightly, the influence on the correlation coefficients is negligible. Unfortunately, the yaw rate is not measured during the flight tests, which means that the same comparison cannot be made for the flight test data, as Equation 4.43 is not applicable.

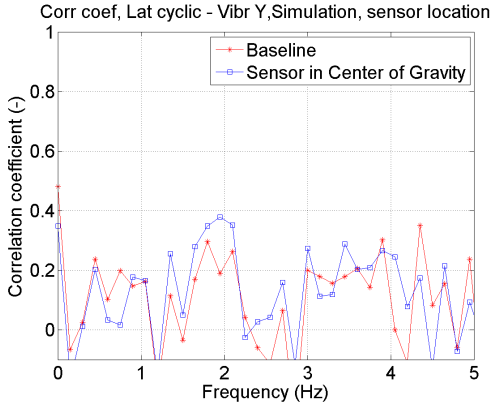

Figure 4.21: Sensor location verification: Correlation coefficient, Lateral cyclic - Vibration Y (Flight simulation EC135)

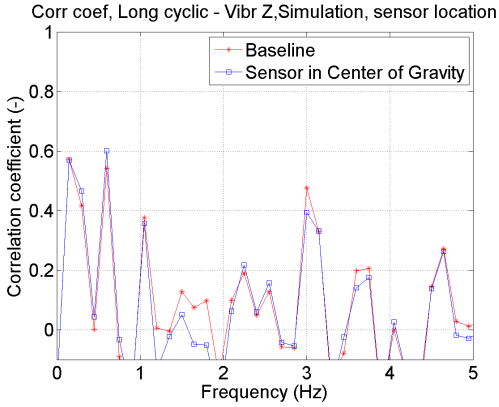

Figure 4.22: Sensor location verification: Correlation coefficient, Longitudinal cyclic - Vibration Z (Flight simulation EC135)

4.5.3. Sensor noise

In this section, the influence of the sensor noise on the results will be discussed. As discussed in Section 3.3.3, the correlation coefficient can be subjective to noise correlation. To investigate the influence of noise on the correlation coefficients, several simulations are performed with different levels of white noise added to the control inputs. The results are illustrated in Figures 4.23 and 4.24. It can be noticed that most of the peak values remain in the same frequencies. The magnitude of the peaks differs slightly at the locations of the expected peaks, and more considerably outside the region of expected correlation. This is expected, as the latter region is more subjective to noise correlation. A discussion on the area of expected correlation is provided in Section 5.1.

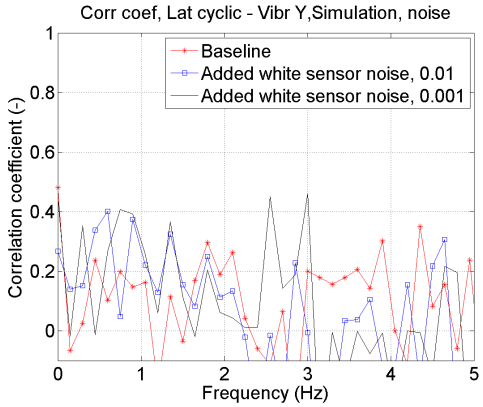

Figure 4.23: Sensor noise verification: Correlation coefficient, Lateral cyclic - Vibration Y (Flight simulation EC135)

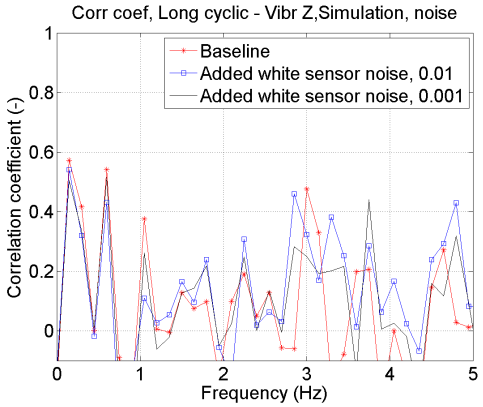

Figure 4.24: Sensor noise verification: Correlation coefficient, Longitudinal cyclic - Vibration Z (Flight simulation EC135)

4.5.4. Center of gravity

As concluded before, the more the center of gravity is forward, the more stable the helicopter is. This means that less control inputs and vibrations are expected for the case in which the center of gravity is more forward. This is indeed the case, although the differences in the simulation are very small. This can also be seen in the discomfort level, shown in Figure 4.27. One can notice that the discomfort in the lower frequency region is slightly lower. It is also interesting to point out that some of the peaks are shifted in the correlation coefficients. The reasoning for this is provided in Section 5.1.3.

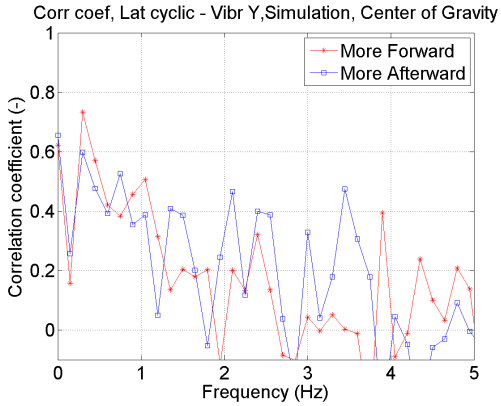

Figure 4.25: Correlation coefficient: Lateral cyclic - Vibration Y, center of gravity (Flight simulation EC135)

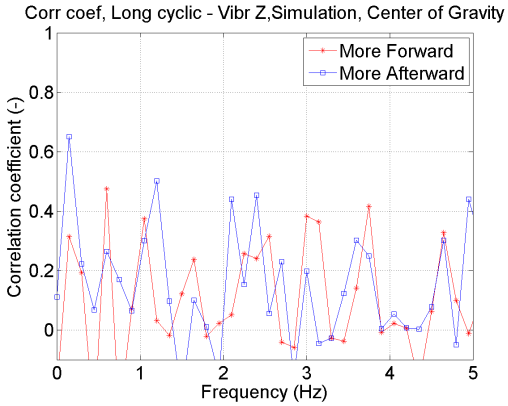

Figure 4.26: Correlation coefficient: Longitudinal cyclic - Vibration Z, center of gravity (Flight simulation EC135)

4.5.5. Weight

In general, lower weight helicopters are more susceptible to forces. This explains the higher vibration level in Figure 4.29. Furthermore, the lower the weight of the helicopter, the more manoeuvrable it is [32]. This means that in some cases lower control inputs are required for the same flying path. This explains the lower amount of control inputs for a lower weight rotorcraft in Figure 4.28. The correlation coefficients are in this case also higher, as can be seen in Figure 4.30, showing the higher correlation between the control inputs and the weight. With other words, the correlation coefficient can potentially measure the higher sensitivity of the lower weight helicopter to vibrations. From the pilot discomfort shown in Figure 4.31 it can be seen that the pilot discomfort is much higher for a lower weight helicopter in both frequency regions.

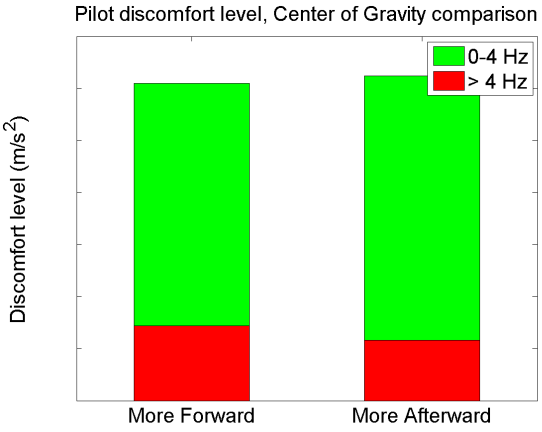

Figure 4.27: Pilot discomfort level for shifts in center of gravity (Flight simulation EC135)

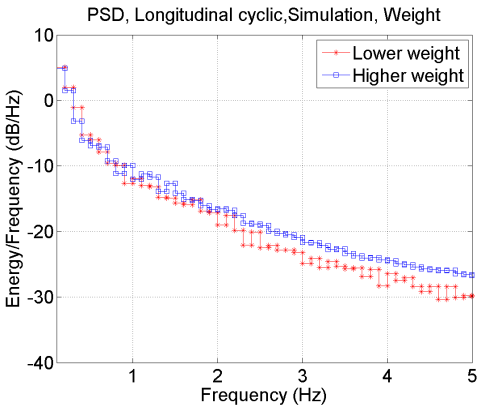

Figure 4.28: Power spectral density: Longitudinal cyclic, weight (Flight simulation EC135)

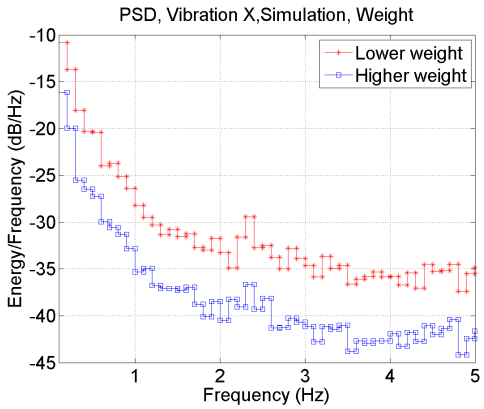

Figure 4.29: Power spectral density: Vibration X, weight (Flight simulation EC135)

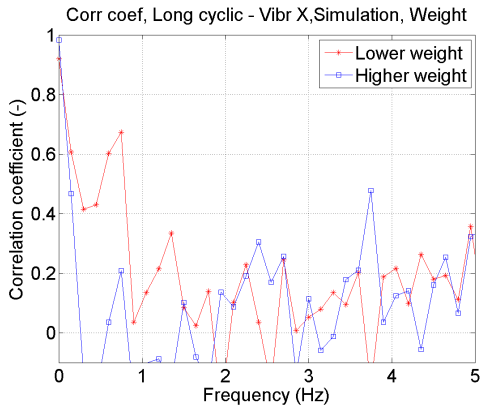

Figure 4.30: Correlation coefficient: Longitudinal cyclic - Vibration X, weight (Flight simulation EC135)

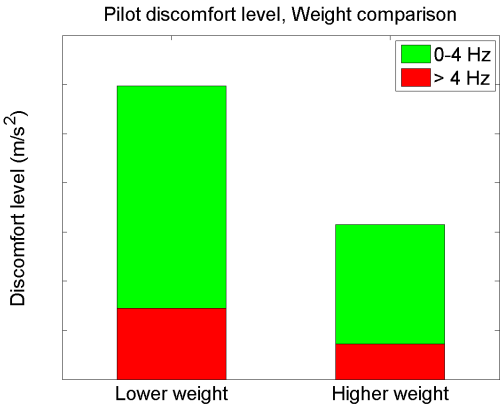

Figure 4.31: Pilot discomfort level for different weights (Flight simulation EC135)

4.5.6. Rotor blade parameters

Several blade parameters are modified to investigate the effect on the correlations. Some of these parameters include the blade mass, blade inertia, flapping / lead-lag damping, spring stiffness and effective flap and lead-lag hinges. A 10% increase and decrease is implemented on the listed parameters. The distance of the hinges from the hub centre is a critical parameter in determining the magnitude of the hub moment induced by

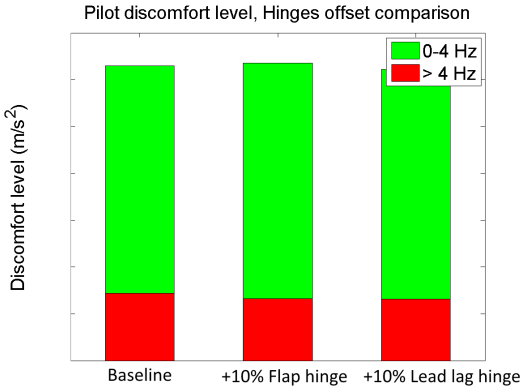

Figure 4.34: Pilot discomfort for modifications in flap and lead-lag hinges (Flight simulation EC135)

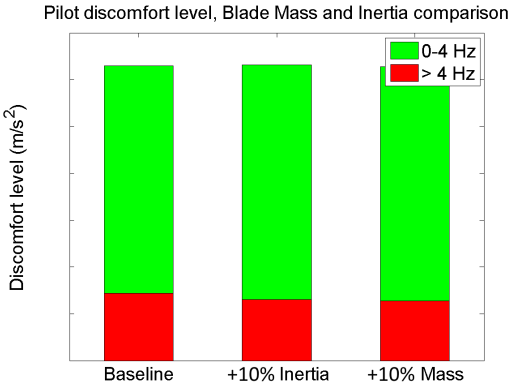

Figure 4.35: Pilot discomfort level for modifications in blade mass and inertia (Flight simulation EC135)

blade flapping and lagging. Rigid rotors, as in the studied case, do not have any hinges, and are considered to have an "effective hinge offset". This offset is larger than the hinge offset found in helicopters with articulated rotors, which will lead to a higher hub moment and more manoeuvrability. With severe modification in the blade parameters, the peaks of the correlation coefficients can be shifted and the pilot discomfort will be affected. This happens for example for the lead-lag damping and blade inertia. However, with more minor changes, which are feasible and logical within the design space, the pilot discomfort is barely affected. The correlation coefficients are shown in Figures 4.32 and 4.33. The discomfort assessment can be seen in Figures 4.34 and 4.35. The flapping hinge offset seems to have negligible effect on the ride quality, while it is expected to have some effects on the loads and therefore on the vibrations. Further research on this aspect in the simulation model is necessary during future investigations.

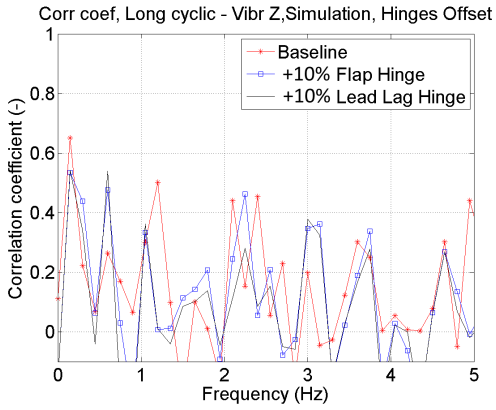

Figure 4.32: Correlation coefficient: Longitudinal cyclic - Vibration Z, Hinge offset (Flight simulation EC135)

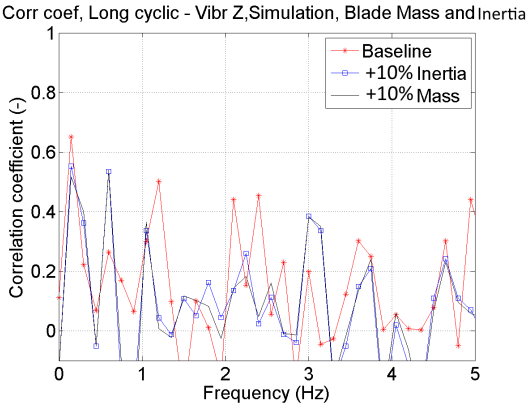

Figure 4.33: Correlation coefficient: Longitudinal cyclic - Vibration Z, Blade mass and inertia (Flight simulation EC135)

4.5.7. Velocity

For medium and high speeds, the results are the same as during the flight test analysis. For higher speeds, the vibrations and control inputs are higher. This can be seen in Figures 4.36 and 4.37. As explained before, at higher speeds the aerodynamic disturbances are higher and the occurrence of blade stall is also higher. However, for the low speed case, the vibrations and control inputs are almost equal as the medium speed case. This can be explained by the fact that during low speeds, more control inputs are required to fly a certain path, resulting in more vibrations. Furthermore, the correlation coefficients are in general higher for higher speeds, as shown in Figure 4.38. These observations can also be seen in the pilot comfort comparison in Figure 4.39.

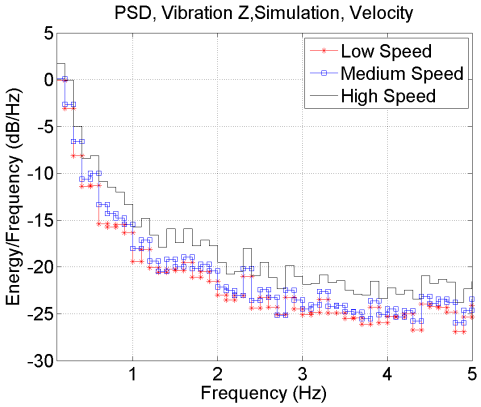

Figure 4.36: Power spectral density: Vibration Z, speed (Flight simulation EC135)

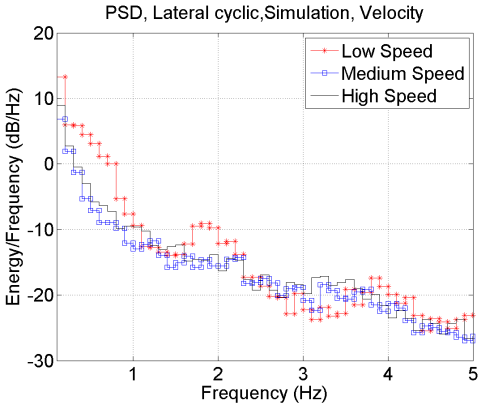

Figure 4.37: Power spectral density: Lateral cyclic, speed (Flight simulation EC135)

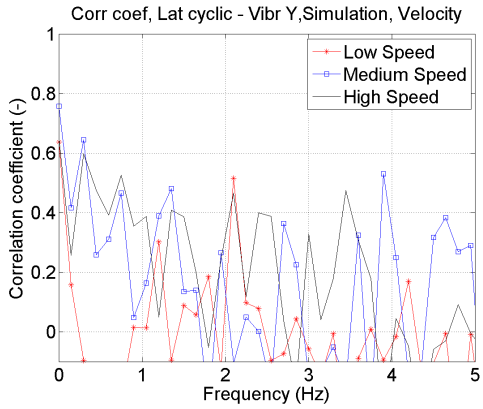

Figure 4.38: Correlation coefficient: Lateral cyclic - Vibration Y, speed (Flight simulation EC135)

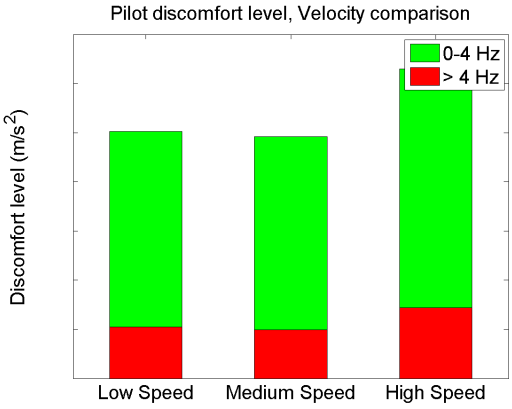

Figure 4.39: Pilot discomfort level for different flight speeds (Flight simulation EC135)

4.5.8. Rotorcraft Mission

During a simulation where more lateral control inputs are required, it is expected that there will also be more vibrations. Figures 4.42, 4.40 and 4.41 show an increase in correlation coefficient, lateral cyclic input and vibration in y-direction. This also means that the pilot discomfort value is higher, as can be seen in Figure 4.43. It is also interesting to point that the vibrations are higher up to around 2.5 Hz, where there is also an increase in lateral cyclic control input.

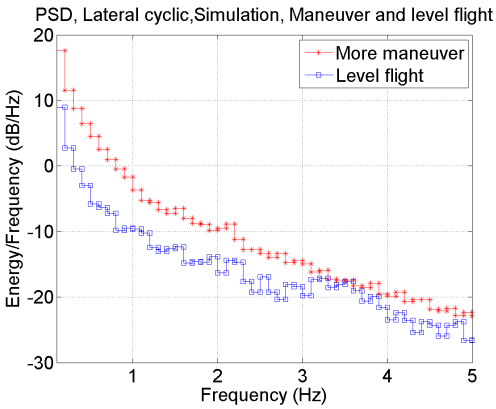

Figure 4.40: Power spectral density: Lateral cyclic, mission (Flight simulation EC135)

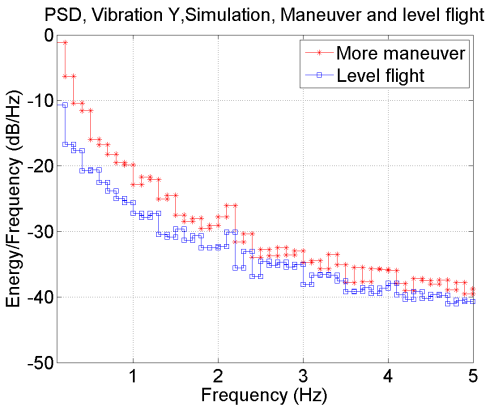

Figure 4.41: Power spectral density: Vibration Y, mission (Flight simulation EC135)

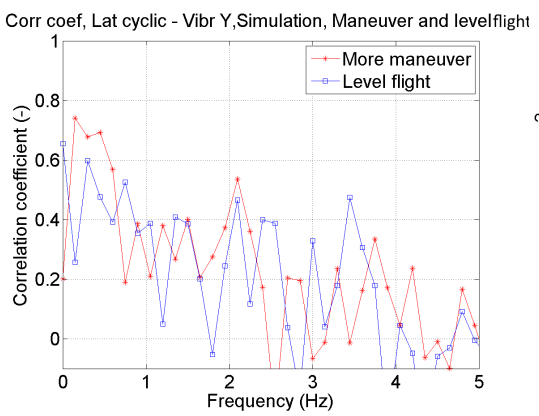

Figure 4.42: Correlation coefficient: Lateral cyclic - Vibration Y, mission (Flight simulation EC135)

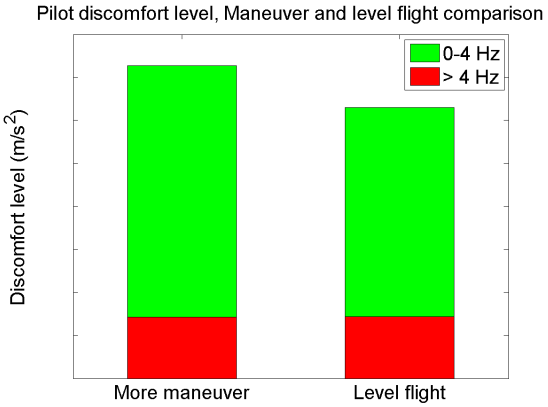

Figure 4.43: Pilot discomfort level for different flight missions (Flight simulation EC135)

4.5.9. Flight Control System Gains

In the investigation of the influence of the flight control system, the effects of the control gain are measured. The values of the PID gains are amplified by a factor three, each separately as well as all together. The purpose of this is not to determine the control and stability characteristics, but to know whether the gains have influence on the pilot discomfort level. If yes, it provides an interesting starting point for a potential solution for pilot comfort enhancement, especially if there is a relationship between the amount of control inputs, vibration level and the correlation coefficient. This seems indeed the case.

The tuning of the gains can have a large influence on the control inputs, which is expected, and can be seen in Figure 4.48 and 4.49. One can notice that the increase due to the amplification of the P-gain or all three PID-gains is the highest. The change in I-gain barely has influence. The tuning of the gains influences how the helicopter model corrects for a disturbance. The proportional component depends only on the difference between the reference value and the process variable. This difference is presented as the error term. The proportional gain determines the ratio of output response to the error signal. The integral component sums the error term over time. The results that even a small error term will cause the integral component to increase slowly. Unless the error is zero, the integral response will continually increase over time. The effect is to drive the Steady-State error to zero. The derivative component causes the output to decrease, if the process variable is increasing rapidly. The derivative response is proportional to the rate of change of the process variable. Increasing the derivative time parameter will cause the control system to react more strongly to changes in the error term and will increase the speed of the overall control system response. Therefore, it can be expected that the proportional component has the most influence in this case, as it now reacts more to the error term. The integral component is a slowly increasing term based on the error. With only an increased integral term, the error is not necessarily larger. The derivative reacts to the changes in the error, which means that more input will be given in each simulation step [47].

What a PID controller can also do, is to modify the eigenvalues of the eigenmodes. This means that some of the peaks can be more or less damped. It can be noticed in the Power Spectral Densities of the cyclic inputs, that there is a huge peak around 2 Hz. This can also be seen in the correlation coefficients shown in Figures 4.44 and 4.45. Here one can also notice an increase in correlation coefficient for the cases where the proportional or derivative gains are amplified. More elaborations on the peak around 2 Hz will be provided in Section 5.1.3. The pilot discomfort value is shown in Figure 4.51.

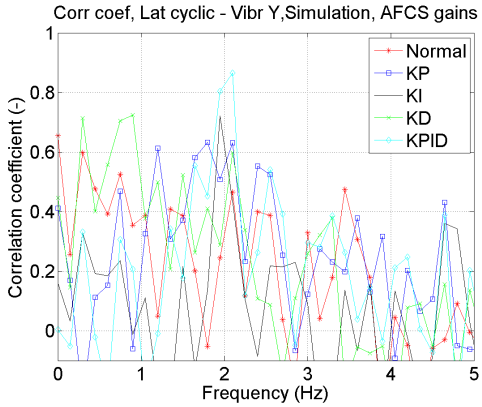

Figure 4.44: Correlation coefficient: Lateral cyclic - Vibration Y, AFCS gains (Flight simulation EC135)

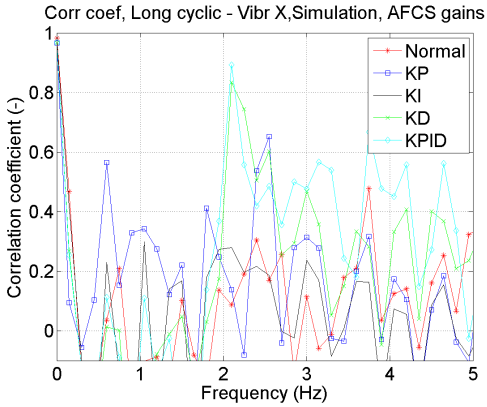

Figure 4.45: Correlation coefficient: Longitudinal cyclic - Vibration X, AFCS gains (Flight simulation EC135)

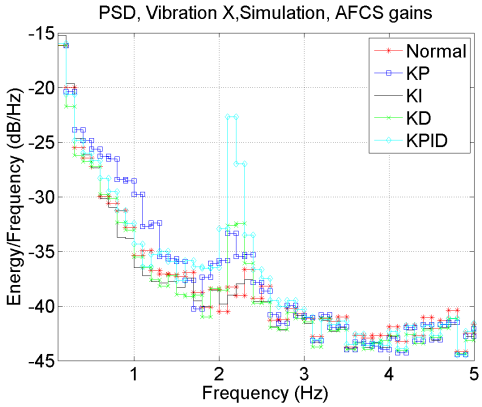

Figure 4.46: Power spectral density: Vibration X, AFCS gains (Flight simulation EC135)

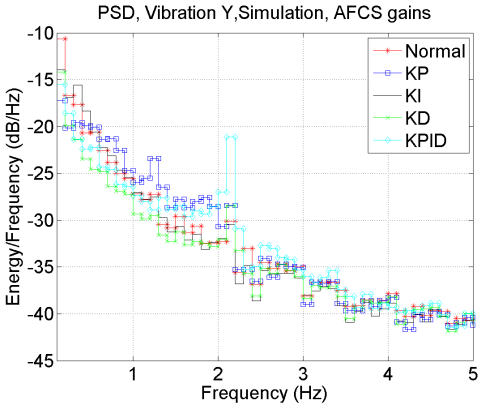

Figure 4.47: Power spectral density: Vibration Y, AFCS gains (Flight simulation EC135)

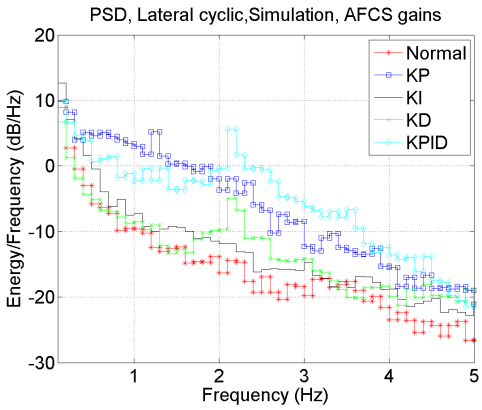

Figure 4.48: Power spectral density: Lateral cyclic, AFCS gains (Flight simulation EC135)

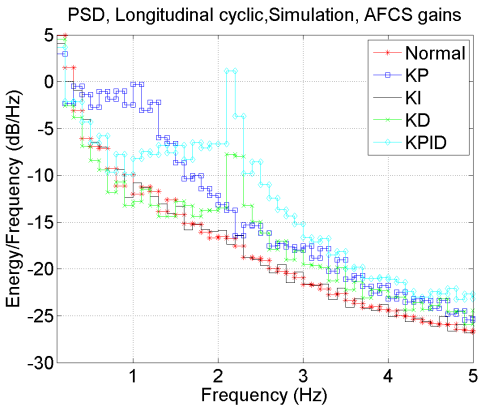

Figure 4.49: Power spectral density: Longitudinal cyclic, AFCS gains (Flight simulation EC135)

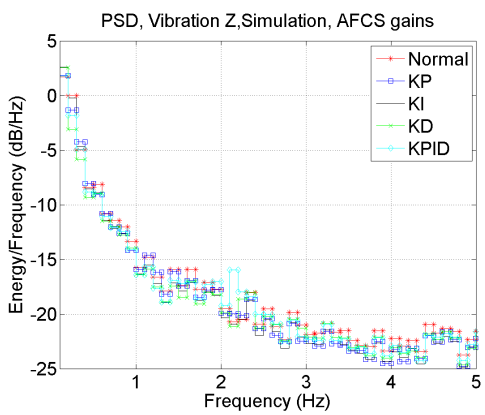

Figure 4.50: Power spectral density: Vibration Z, AFCS gains (Flight simulation EC135)

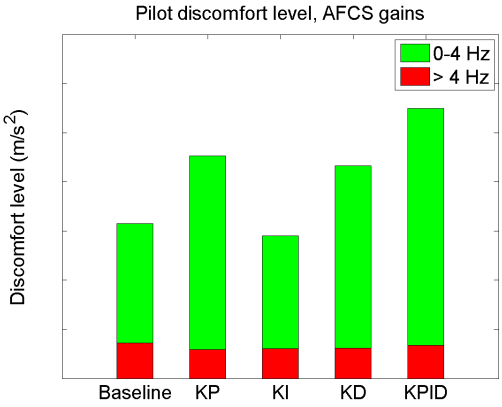

Figure 4.51: Pilot discomfort level for different AFCS gain tunings (Flight simulation EC135)

4.5.10. Atmospheric conditions

Three different turbulent levels are investigated and described in Table 4.2. Three possible ways about how the turbulence level can influence the control inputs were mentioned during the analysis of the flight test data. As there is no pilot input given, the control inputs are fully caused by the flight control system. This system tries to correct the disturbances caused by the gust model. One can notice that the control inputs increase slightly for higher turbulence levels, up to around 2 Hz, as shown in Figures 4.52, 4.53 and 4.54. One could also notice an increase the translational vibrations and angular rates as shown in Figures 4.56 - 4.59. As expected, there is an increase in all these values. The pilot discomfort is shown in Figure 4.64. It can be noticed that the higher the turbulence level, the higher the discomfort in the lower frequency region. Furthermore, when investigating the correlation coefficients, the values at higher turbuelnce levels are in general higher up to around 2 Hz.

4.6. Conclusions on flight simulation analysis

From the flight simulation analysis, one can determine in which frequency area there is a correlation between the control inputs and the vibrations. This is done by comparing the power and the pattern between the signals. The vibrations were calculated with a non-linear helicopter model, a gust model and flight control system model. After converting the vibrations from the center of gravity to the pilot location, spectral analysis is performed. It can be seen that most of the control inputs occur in the region of 0-4 Hz, with a small peak around 12 Hz. More elaborations on this will provided in Chapter 5. Most of the vibrations also occur in the lower frequency region, due to the lack of the rotor harmonic loads and tailboom induced loads.

In most cases, when one compares two simulations with only one varying parameter, the simulation with higher correlation coefficients has higher pilot discomfort, even with the same amount of control inputs. This is most visible in the case of varying weight. Here, both simulations have comparable amount of control inputs, while the case with lower weight has higher correlations coefficients. Therefore the correlation coefficient can potentially be used as a tool to indicate the sensitivity of the helicopter model to vibrations.

The parametric studies of the center of gravity and rotor mission show comparable results as with the flight test data analysis. It can further be concluded that the rotor blade parameters barely influence the pilot discomfort. The velocity investigation provided comparable results with the flight test data analysis, except for the lower speed case. Here, an increase in the lateral cyclic can be noticed, with also an increase in the vibration level.

The study of the gains of the flight control system show some interesting results. From the results it can be concluded that the proportional and derivative gains influence the pilot discomfort rating. This means that the amount of input given is linked with the vibrations of the helicopter. Furthermore, it can provide an interesting topic for future study about the solution to lower the pilot discomfort level.

And finally, it can be concluded that in case of turbulence, the non-rotor induced vibrations tend to dominate

the pilot discomfort. An increase in control inputs up to 2 Hz can be noticed, as well as an increase in the translational vibrations and angular rates. This does happen along the whole lower frequency range up to 5 Hz. An increase up to around 1.5 Hz can be noticed in the correlation coefficients. The results of the flight simulations and flight test data will be compared in Section 5.2 and the proposed methodology and assumptions will be discussed in Section 5.4.

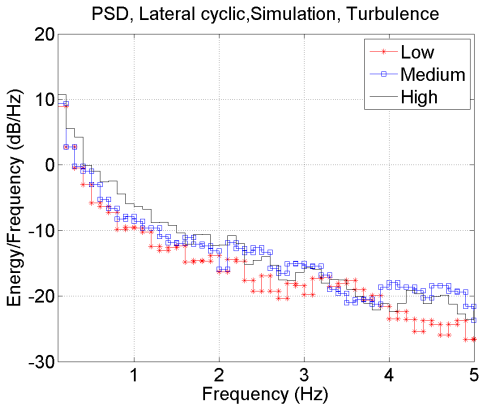

Figure 4.52: Power spectral density: Lateral cyclic, turbulence (Flight simulation EC135)

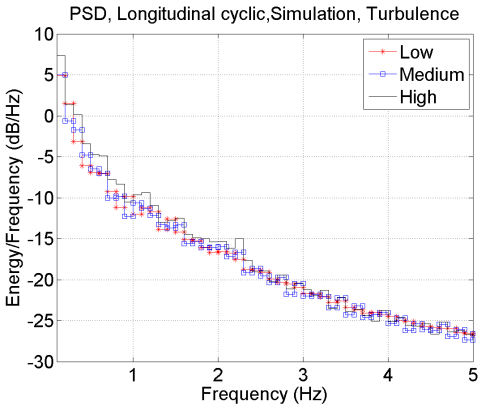

Figure 4.53: Power spectral density: Longitudinal cyclic, turbulence (Flight simulation EC135)

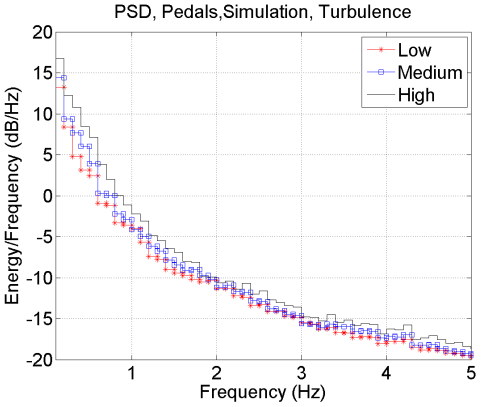

Figure 4.54: Power spectral density: Pedals, turbulence (Flight simulation EC135)

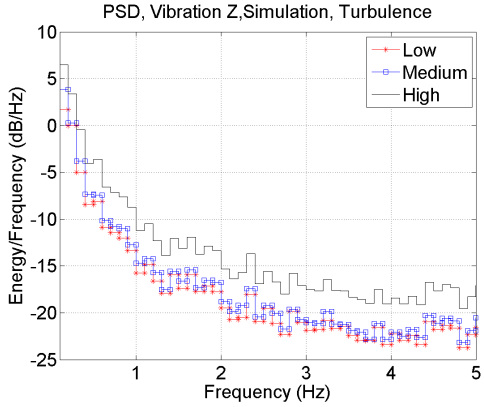

Figure 4.55: Power spectral density: Vibration Z, turbulence (Flight simulation EC135)

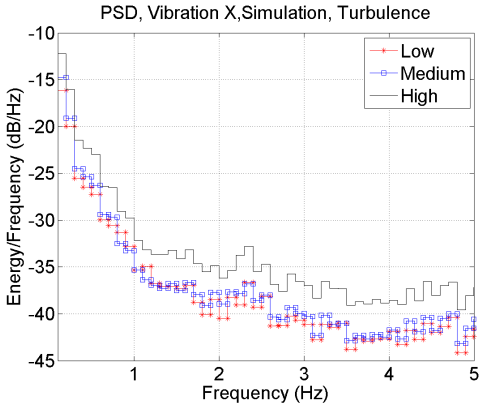

Figure 4.56: Power spectral density: Vibration X, turbulence (Flight simulation EC135)

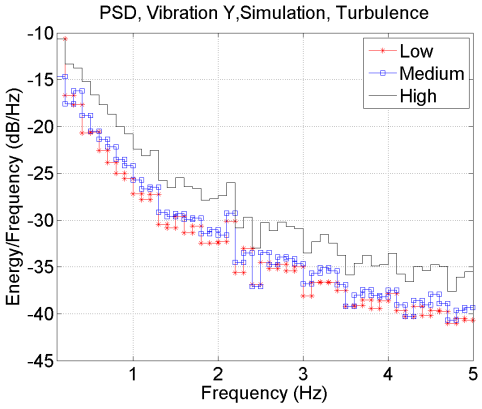

Figure 4.57: Power spectral density: Vibration Y, turbulence (Flight simulation EC135)

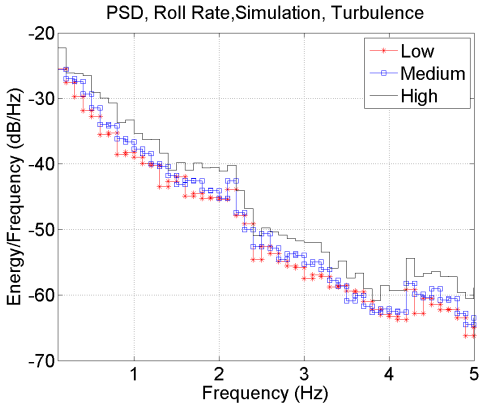

Figure 4.58: Power spectral density: Roll rate, turbulence (Flight simulation EC135)

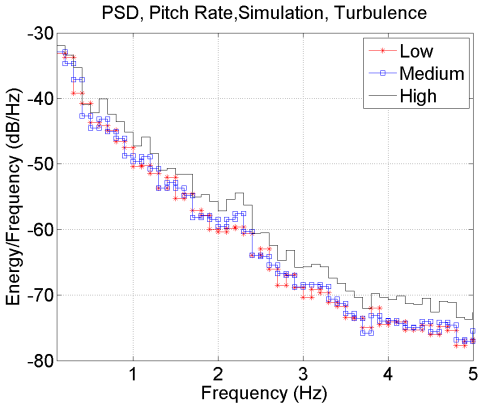

Figure 4.59: Power spectral density: Pitch rate, turbulence (Flight simulation EC135)

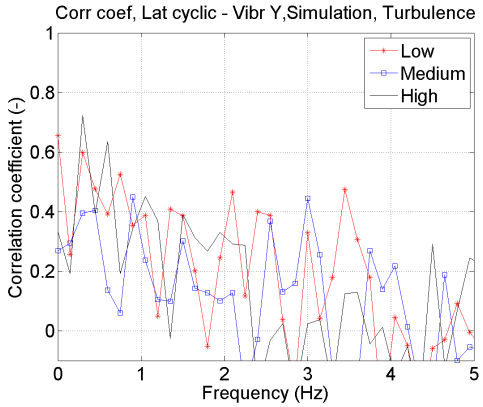

Figure 4.60: Correlation coefficient: Lateral cyclic - Vibration Y, turbulence (Flight simulation EC135)

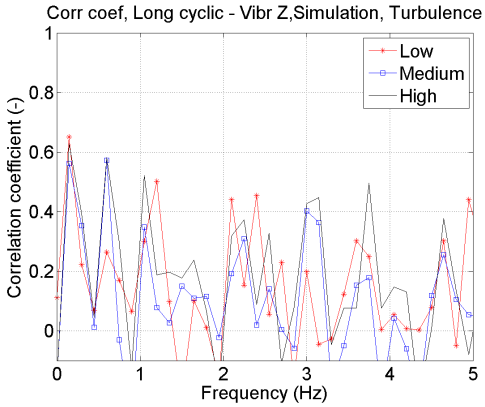

Figure 4.61: Correlation coefficient: Longitudinal cyclic - Vibration Z, turbulence (Flight simulation EC135)

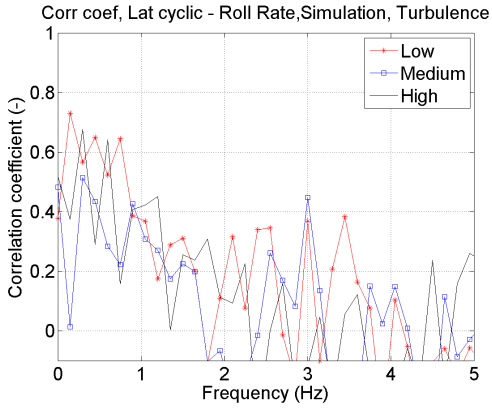

Figure 4.62: Correlation coefficient: Lateral cyclic - Roll rate, turbulence (Flight simulation EC135)

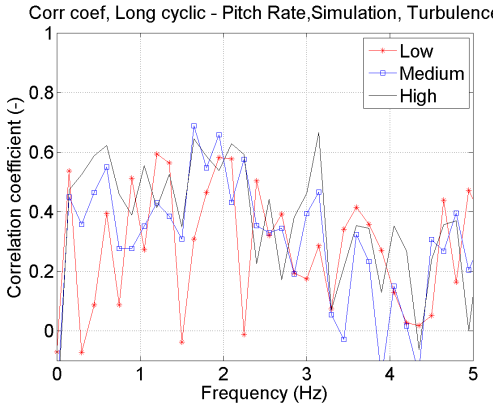

Figure 4.63: Correlation coefficient: Longitudinal cyclic - Pitch rate, turbulence (Flight simulation EC135)

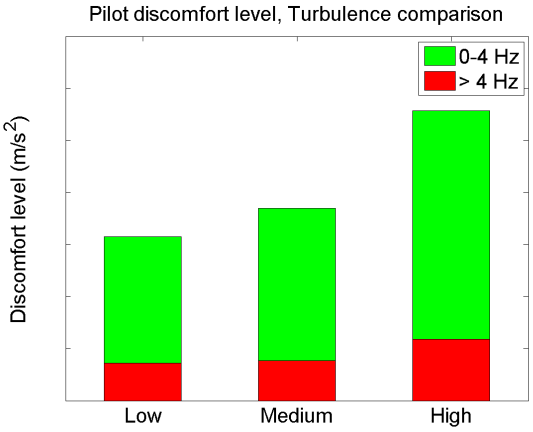

Figure 4.64: Pilot discomfort level for calm and turbulent conditions (Flight simulation EC135)

5

Results: analysis

The focus of the previous chapters has been mainly on identifying at which frequencies there is a correlation between the flight control inputs and vibrations, and how the different flight conditions and helicopter configurations influence this correlation. The purpose of this chapter is to investigate the causes of the correlations and discuss how the obtained knowledge can be used to improve ride quality.

One of the main focus points is therefore on combining the results of the flight test data analysis in Chapter 3 and the flight simulations in Chapter 4. Based on these results, the causes for high correlation are analyzed. The focus is on investigating whether the methods used in the correlation analysis are leading to logical and expected results. This process is discussed in Section 5.1. After this, the results of the flight dynamics simulations are validated with the results of the flight test data. The parametric studies are compared and some focus is put on the validation of the gust model. This is treated in Section 5.2. A final evaluation on the pilot comfort and some recommendations are provided in Section 5.3. In this section, it is explained how the obtained knowledge can be used to improve the pilot comfort. A discussion on the assumptions, methodology and the added value of this thesis is provided in Section 5.4.

5.1. Causes for correlations between control inputs and vibrations

This section investigates whether the methods used are providing logical and expected results. This thesis only focuses on vibrations up to 4 Hz, as this is the region where the pilot comfort is affected the most by the actively provided control inputs. The flight dynamics simulation model is already verified and validated by Airbus Helicopter [59]. Up to around 4 Hz the model should be valid. Above this frequency, the assumption of rigid body motion will not hold anymore. This is further discussed in Section 5.4. Furthermore, the influence of the sensor location and sensor noise are already verified in Section 4.5.

Examples of the PSD and correlation coefficient based on flight test data at 120 kts for a EC135 helicopter are shown in Figures 5.1 and 5.2. These figures are averaged for 5 flights with different flight conditions. Only correlation coefficients larger than 0.3 are shown, as it was previously determined in Section 3.3.3 that the correlation coefficients lower than 0.3 should not be taken into account. The causes for the peak until 15 Hz will be discussed, even though most of the control inputs occur in the 0-4 Hz frequency domain. This is done to verify the method in general, as there are some expected correlations at certain frequencies. The peaks that will be discussed are numbered.
The control inputs can be provided by:

- Intentional pilot inputs
- Unintentional pilot inputs
- Flight control system

The first two sources for added control inputs are assessed by previous researches and literature. The third point is mainly investigated with the simulation model. The latter is also used to determine the Eigenmodes. This is done by linearising the helicopter model. Some unidentifiable correlation peaks are investigated in Section 5.4.

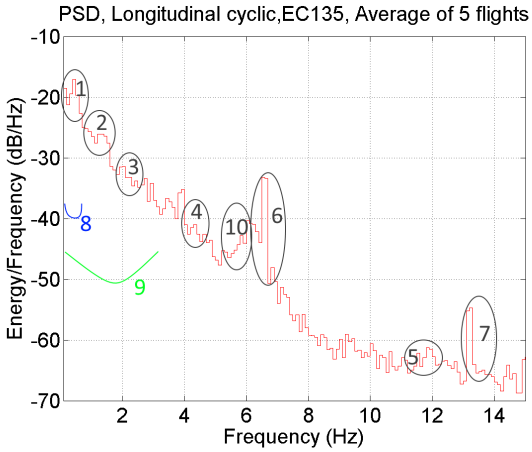

Figure 5.1: Interesting peaks in Power Spectral Density (Flight test data EC135)

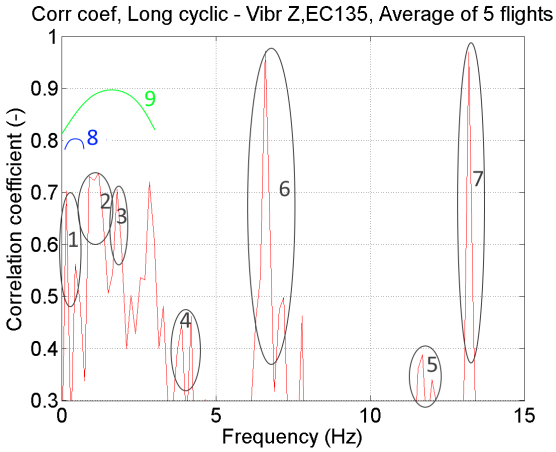

Figure 5.2: Interesting peaks in Correlation coefficient (Flight test data EC135)

5.1.1. (Auto)-pilot input

In this section, first the pilot model is discussed, and then the autopilot. It is interesting to know in which frequency area both types of inputs have influence.

The purposes of the pilot models are to summarize behavioural data, provide a basis for rationalization and understand pilot control actions. Furthermore, it can be used in conjunction with vehicle dynamics to form predictions or to explain the behaviour of pilot-vehicle systems. The most important class of situations for which pilot vehicle models are useful are closed-loop compensatory tracking tasks in which the pilot acts on the displayed error between a desired command input and the comparable vehicle output motion to produce a control action. For this, McRuer [42] has proposed the crossover model.

From the crossover model, it is expected that most of the intentional pilot control inputs are below approximately 0.5 Hz in closed loop situations. Control inputs at higher frequencies could be possible during open loop situations, which is not expected during level flights. This model can explain the higher correlations in the frequency region of number **8** in Figures 5.1 and 5.2. The same can also be seen in the results when investigating the flight control system during the flight test data analysis. An increase in the region of 0-0.5 Hz exists in the power spectral densities when the flight control system is switched off, as shown in Figures 3.41 and 3.42. One can notice that the pilot tend to use more control inputs with a lower frequency than the flight control system. Moreover, the correlation coefficients in Figures 3.39 and 3.40 are higher in this frequency range.

As no pilot model is used during the flight dynamics simulations, the control inputs during simulations are based on the inputs provided by the attitude controller of the flight control system. A discussion on the spectral analysis of these results was already provided in Section 4.5. In general, the flight control system is able to provide inputs at higher frequencies than the pilot, although most of the inputs occur in the 0-4 Hz frequency domain.

5.1.2. Biodynamic feedthrough

Biodynamic feedthrough occurs when the vibrations of a vehicle are fed through the pilot's body and cause unintentional motions of limbs, which results in unintentional control inputs. This phenomenon is initiated by whole body vibrations and can further reduce the pilot comfort. Several studies have been performed in order to develop a biodynamic feedthrough model, most notably by Mayo [40]. He developed a model that is able to describe unintentional control inputs as a function of accelerations.

In the experiment of Mayo, the collective stick motion was recorded while the pilot was being perturbed using vertical, sinusoidal acceleration disturbances of discrete single frequencies. These disturbances range from 1 to 5 Hz, in 0.5 Hz increments. The duration of each disturbance signal was approximately 3 minutes. The results of this experiment are the transfer functions, describing the acceleration of the hand holding the col-

lective as a function of the vertical acceleration of the seat. Mayo's model takes into account mesomorphics (athletic bone structure and muscle build) and ectomorphics (slim bone structure and muscle build).

This model was extended by Venrooij [71]. Most significantly, he added within-subject variability, meaning the model parameters are a function of the pilot's neuromuscular adaptation to different tasks. Next to this, the model's frequency range is increased. He also added the subject group endomorphics (smaller and rounder body type). The results of his research are shown in Figure 5.3. Different transfer function are shown for different subject groups and tasks.

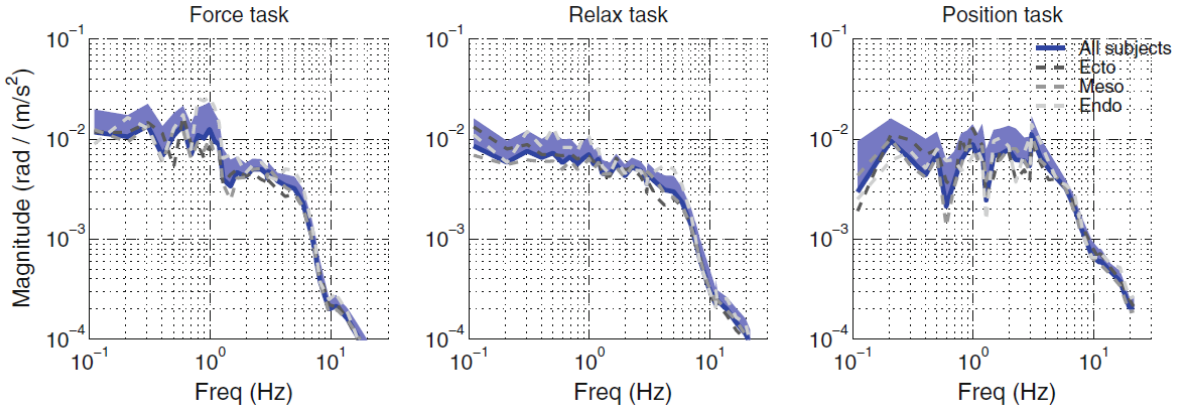

Figure 5.3: The BDFT dynamics measured for different somatotypes (Collective) [71]

Most experiments regarding biodynamic feedthrough are focused on the collective stick. In one research [39], the influence of the lateral vibration on the cyclic stick is measured. Here the frequency response of the lateral acceleration of the pilot limbs relative to the flight simulator reference frame was measured under lateral accelerations of motion-base. The results are shown in Figure 5.4 for the acceleration at the wrist and the shoulder. One can observe that the amplification of vibrations is mainly between zero and three Hz, although small amplifications at higher frequencies can still occur.

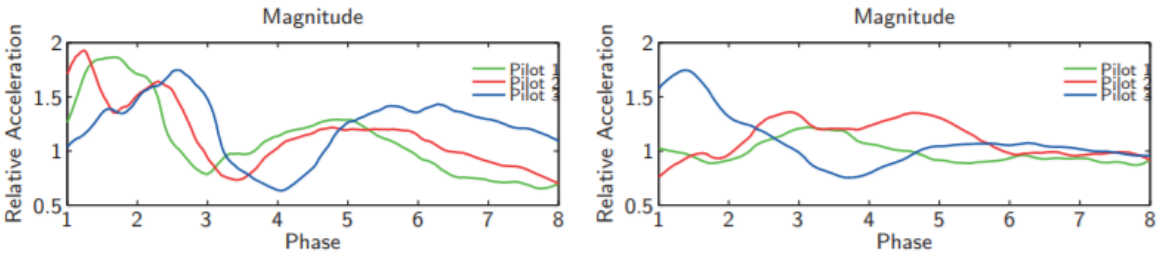

Figure 5.4: The BDFT dynamics measured for three different pilots (Cyclic) [39]

Although this is a simplified model and only consists of input vibrations in the vertical and lateral axes, it does provide an indication at which frequency range biodynamic feedthrough could have an influence, which is useful for this thesis. It should be noted that there is a considerable difference in the results of the lateral case between the different pilots. From these results the conclusion is made that pilot inputs, although unintentional, can be provided up to around 3 Hz. As there are many sources for higher control inputs in this frequency domain, it is hard to identify which part of the vibration spectra is caused by biodynamic feedthrough in the PSDs of the control inputs. However, the correlation coefficients do provide higher value in the region numbered with **9** in Figure 5.2.

5.1.3. Eigenmodes

In order to investigate the influences of the eigenmodes, the helicopter model is linearized using Equation 4.28. Both the body eigenmodes and the rotor eigenmodes are taken into account. These derivatives are represented in a state-space matrix, after which the eigenvalues are calculated using Equation 4.41. First, the body eigenmodes are discussed, followed by the rotor eigenmodes.

It is determined that the short period and spiral mode do not have oscillatory parts in their eigenvalues, which means that their effect on the pilot discomfort is negligible. The main natural eigenmodes affecting the oscillations are the phugoid and the dutch roll. The frequency and damping describing these motions are shown in Table 5.1 for the baseline configuration, which was shown in Table 4.3.

Table 5.1: Frequencies of the natural eigenmodes (Flight simulation: calculated for EC135 baseline configuration)

Natural Eigenmodes	Frequency [Hz]	Damping [$-$]
Phugoid	0.07	-0.3985
Dutch roll	0.27	0.0471

Both eigenmodes are marked as number **1** in Figures 5.1 and 5.2, which was previously also marked as the frequency domain for higher correlation due to pilot inputs. Still, sharp peaks can be found in many cases around this area, which are expected to be caused by the eigenmotions. By comparing Figures 4.60 and 4.61, it can be observed that the peak at $0.27Hz$ in the correlation coefficient of the lateral cyclic control with the corresponding vibrations is in general higher than of the longitudinal cyclic control with the corresponding vibrations. This is expected, as the Dutch roll is more a lateral movement.

Table 5.2: Frequencies of the rotor eigenmodes (Flight simulation: calculated for EC135 baseline configuration)

Rotor Eigenmodes	Frequency [Hz]	Damping [$-$]
Regressive flapping mode	0.17	0.9885
Roll subsidence mode	1.08	0.7929
Regressive lead-lag mode	2.23	0.0455
Collective lead-lag mode	4.67	0.0446
Collective flapping mode	6.82	0.3001
Progressive lead-lag mode	11.6	0.0143
Progressive flapping mode	13.3	0.1621
Regressive torsion mode	28	0.0622
Collective torsion mode	31.5	0.0505
Progressive torsion mode	35	0.0420

The eigenmodes of the rotors are shown in Table 5.2. The torsion eigenmodes of the rotor are all at frequencies higher than the relevant human sensitivity domain, and their influence on the pilot discomfort is negligible. In general, the eigenmodes up to 5 Hz are interesting to look at. This frequency domain includes some of the flapping and lead-lag eigenmodes. In many cases, at the same frequency as the first harmonic rotor load, the collective flapping mode can be found and the progressive flapping mode is close to the second harmonic rotor load. These are marked as numbers **6** and **7**. The regressive flapping mode occurs close to the phugoid and Dutch roll, which is marked as number **1**. A large peak can often be found around 1 Hz, as marked with number **2**, which is the eigenfrequency of the roll subsidence mode. In most Power Spectral Density plots and correlation coefficient graphs, the regressive, collective and progressive lead-lag modes can be found, which are marked as numbers **3**, **4** and **5** respectively. In general, not all eigenmodes can always be found in the power spectral density of vibrations, as they can be either be not initiated or largely damped. However, as the correlation coefficient is independent on the magnitude of the control inputs and vibrations, the eigenmodes can almost always be identified here.

The influence of damping values on the results of the correlation analysis is investigated. The damping values are stated in Tables 5.1 and 5.2. It can be concluded that the phugoid mode is unstable, which is a common characteristic of helicopters [47]. Furthermore, a low positive damping value means that the mode is largely underdamped, which means that it should appear less in the Power Spectral Density graphs of the vibrations.

For example, the peak of the roll subsidence mode, which has a damping value closer to 1, is in general large. However, the lower frequency eigenmodes are also easier to be initiated by an input or gust. The peak of the regressive lead-lag mode is for example larger than the peak of the progressive lead-lag mode, while both modes have comparable damping values. Therefore, one can conclude that although more damping of the eigenmodes is beneficial in decreasing the total amount of vibrations, it cannot be used to determine which eigenmode will have more influence on the helicopter ride quality.

It was stated in Section 3.5 that a more forward center of gravity leads to better stability, which means that it can be expected that there is more damping in the symmetric eigenmodes. This is indeed the case as can be seen in the damping of the phugoid, which is shown in Table 5.3. Furthermore, the conclusion was made that the correlation coefficients shape differs per configuration. As a change in configuration can change the eigenmodes, the peaks can indeed be shifted, damped or amplified. One can notice that the change in center of gravity only changes the eigenmodes slightly. The influence on the rotor modes is negligible and the natural body eigenmodes are shifted slightly. In Figure 4.26 for example, it can be seen that the peak of the roll subsidence mode shifts slightly, which coincides with the shift in eigenfrequency. The same holds for the eigenfrequencies of the lower weight configuration, which are shown in Table 5.3. Figure 4.30 for example shows a high peak at 0.8 Hz, which coincides with the eigenfrequency of the roll subsidence mode.

This shift in eigenfrequency does not necessarily have to be attributed only to the change in configuration, as this is also dependent on the thrust level, as shown by Equations 5.1 and 5.2. The hub moment (M_β) about the center of mass is approximated here as an addition of the moments due to thrust vector tilt and hub stiffness. In this equation K_β is the hub stiffness, h_R is the length of the hub, N_b is the number of blades and T is the thrust. The thrust can be varying during the flight path. This could explain the small shift in the roll subsidence eigenfrequency (ω_ϕ).

Table 5.3: Influence of configuration changes w.r.t. baseline configuration in eigenfrequencies

Eigenmodes	Frequency [Hz]	Damping [-]	Frequency [Hz]	Damping [-]
	Center of Gravity 20 cm more forward		*Lower weight: 1600 kg*	
Phugoid	0.07	-0.0757	0.06	-0.2065
Regressive flapping mode	0.17	0.9785	0.25	0.9815
Dutch roll	0.34	0.0977	0.37	0.0971
roll subsidence mode	1.02	0.7856	0.80	0.8679
Regressive lead-lag mode	2.22	0.0489	2.24	0.0488
Collective lead-lag mode	4.68	0.0459	4.67	0.0438
Collective flapping mode	6.83	0.2979	6.92	0.3010
Progressive lead-lag mode	11.6	0.0136	11.8	0.0136
Progressive flapping mode	13.3	0.1606	13.31	0.1667

$$\omega_\phi = \sqrt{\frac{M_\beta}{I_{xx}}} \tag{5.1}$$

$$M_\beta = \frac{N_b K_\beta}{h_R T} \tag{5.2}$$

In general, the peaks shown are not straight line peaks, but rather peaks with small bandwidths. This is because, as mentioned earlier, the thrust can be variable. Even though the rotor speed will be kept close to a constant value, small discrepancies can still occur. This leads to slightly varying eigenfrequencies during a flight. This can be seen in Figures 5.5 and 5.6, where the engine torque and rotor speed are plotted based on the results from the baseline simulation. Furthermore, another cause for this occurrence can be spectral leakage.

5.1.4. Turbulence

A literature review on turbulence was provided in Section 2.3.2. As turbulence is a random phenomenon, it is hard to define in which frequency exactly it occurs. In this research, the calm and turbulent flight cases

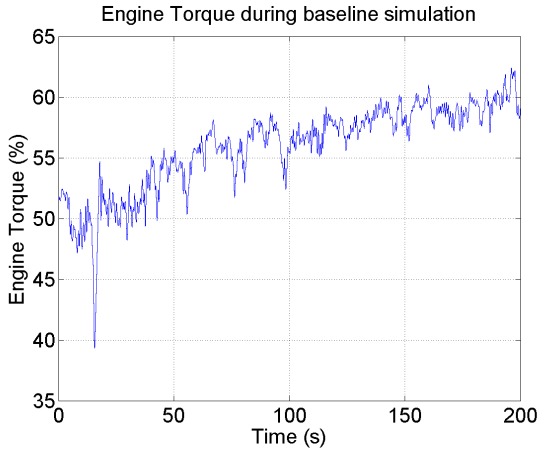

Figure 5.5: Engine torque

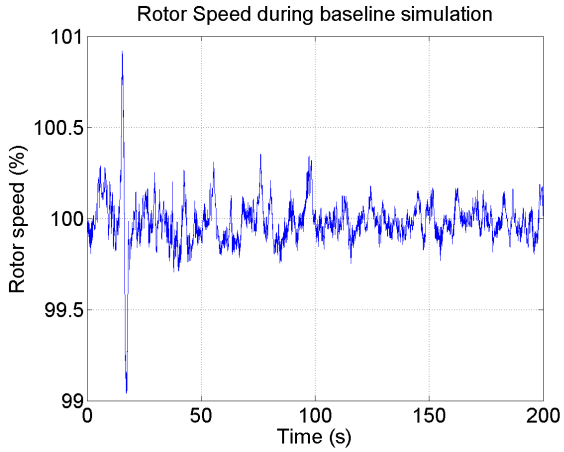

Figure 5.6: Rotor speed

were compared with each other in Sections 4.5 and 3.5. In general, the turbulent cases saw increased vibrations, angular rates and control inputs up to around 2.5 Hz. In some cases, it can happen that some of the eigenmodes will be initiated more in case of turbulence, as can be seen in Figure 3.59 around 2.3 Hz.

5.1.5. Rotor harmonic loads

The rotor induced vibrations are caused by the periodic air loads on the rotor blades and the imbalance and tracking errors of the main rotor, as discussed in Section 2.2. It is expected that the pilot is not able to provide an input at such a high frequency. The causes for increased control inputs can be due to the flight control system or biodynamic feedthrough. These added inputs can be seen in Figure 5.1. Here peaks can be noticed at numbers **6** and **7**, which belongs to the 1/rev and 2/rev loads. The correlation coeffcient graph in Figure 5.2 show some correlation peaks as well at the same frequencies.

5.1.6. Tailboom induced vibrations

The tailboom induced vibrations can influence the biodynamic feedthrough and can be seen as a disturbance by the flight control system, although the amplitudes of these vibrations are much lower compared with the rotor harmonic loads. A Finite Element Model of the helicopter is used by Bernaschek [6] to realize the determination of elastic motion, which has been validated by an on-ground shake test. The frequencies of these tailboom modes are listed in Table 3.1.

It can be seen that around these frequencies, some increase in control inputs can be found. This is marked with as number **10** in Figure 5.1. Important to know is that there are also a lot of flights, which do not show peaks around these frequencies. As the bandwidth of these structural modes are relatively large, some of the tailboom induced vibrations can occur around the peaks of the collective lead-lag mode and in few cases even the collective flapping mode. Furthermore, there are no large peaks at the calculated frequencies of the tailboom modes in the correlation coefficients, which means that the increase in control inputs does not does directly translate into vibrations at the same frequencies. Knowledge on elastic motions is required to investigate this phenomenon.

5.1.7. Conclusion on causes for correlation

In this section, the causes for high correlations are investigated. This has been done for two reason. First of all, the correlation analysis between the control inputs and the vibrations has not been performed yet. Therefore it was necessary to verify that the methods used are showing logical and expected results, especially the results based on the correlation coefficient, which is an uncommonly used tool to analyse vibrations. Secondly, knowing the causes for correlation will help in the process of defining solutions. The following conclusions were made:

- Using literature on the crossover model, it was determined that the intentionally provided pilots inputs are mainly in the 0-0.5 Hz frequency domain.

- The flight control system will provide most of the control inputs up to 4 Hz, although higher frequency inputs are possible.
- Biodynamic feedthrough occurs mostly in the region until 3 Hz, although amplifications at higher frequencies are possible.
- The eigenfreqencies are determined with a non-linear model and most peaks are identified in the correlation coefficient graphs and PSDs. Up till 4 Hz, the phugoid, Dutch roll, roll subsidence mode, regressive flapping mode and regressive lead-lag mode are identified.
- The exact range of turbulence is hard to define, although most of it will occur below the 2.5 Hz. Turbulence is also a cause for initiating eigenmodes.
- Peaks can be observed round the rotor harmonic loads. This can be caused by the flight control system or biodynamic feedthrough. Furthermore, the tailboom induced vibrations can have some influence on the control inputs as well. However, as most control input occur in the frequency domain 0-4 Hz, the influence of added control inputs due to these two aspects on the ride quality is negligible.

5.2. Validation simulation model with flight test data

In this section, first the vibration and control inputs frequency spectrum of the flight dynamic simulations and flight test data will be compared with each other. After that, the correlation coefficients and the gust model will be validated. Finally, an elaboration will be provided on the results of the parametric studies of both analyses.

5.2.1. Vibrations and control inputs spectra

The fourier transformed signals from the flight test data, shown in Figures 3.6 - 3.14, are compared with the results from the flight simulations shown in Figures 4.11 - 4.16. In order to investigate the differences more closely, the frequency spectrum of the baseline simulation is compared with one set of flight test result in Figures 5.7 and 5.8. As the conditions cannot be simulated exactly the same, and the fact that the simulation model contains some assumptions, it is expected that there are some discrepancies. The following observations can be made:

- The signals of the flight test data contain more noise, it can be noticed that these signals fluctuate more, especially at higher frequencies. This is expected as the sensor in the simulations are assumed to be perfect. Furthermore, most of the higher order dynamics were not modelled, such as the influence of elastic motions.
- The amplitude of the progressive lead-lag mode is higher in the spectra of the flight simulations. A reason for this could be that this eigenmode is less damped in the flight model.
- High amplitude vibrations at the rotor speed frequencies cannot be noticed in the flight simulation model due to the assumption of perfect rotor blades and balance.
- The vibrations caused by the tail boom cannot be noticed in the flight model due to the implementation of rigid body motion only.
- In both cases, most of the control inputs occur till around 4 Hz.
- Comparable looking vibrations and control inputs spectra can be found till around 4 Hz.
- The vibrations in z-direction are in both cases higher than the vibrations in x,y-directions.

Based on this, it can be concluded that the flight simulation model is valid for the considered low frequency range till around 4 Hz. For higher frequencies, the tailboom modes and rotor harmonic loads occur and the vibration spectra specifically is not as accurately anymore. As it is hard for a flight simulation to perfectly match the helicopter configuration and flight conditions of the flight test data, discrepancies in the amplitude of signals will certainly occur. However, the model will mainly be used for relative comparison between different configurations and conditions. Therefore, the mentioned discrepancy in the amplitude should not be a problem.

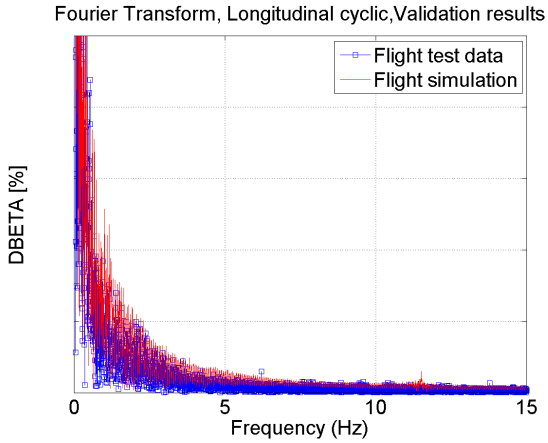

Figure 5.7: Validation: Frequency spectrum Longitudinal Cyclic

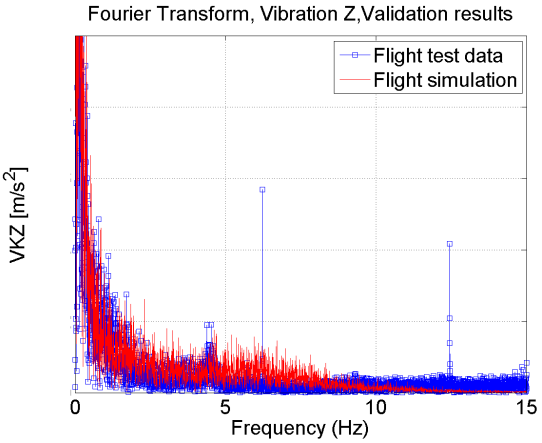

Figure 5.8: Validation: Frequency spectrum Vibration in Z-direction

5.2.2. Correlation coefficients

Next, the correlation coefficients will be compared up to 4 Hz. These are shown for the baseline simulation and a flight tests at the same speed in Figures 5.9 and 5.10. Here again, there seems to be quite a discrepancy on the magnitude of coefficient, although most of the peaks occur at the same frequency point or range. The following observations can be made:

- In both cases the peaks occur at comparable locations, most notably at around 1 Hz (roll subsidence mode) and around 2.3 Hz (regressive lead-lag mode).
- The shape of the coefficients outside the frequency area of the expected peaks differ more, probably due to noise correlation, which was discussed in Section 4.5.3. Also, at higher frequencies, the coefficients differ more, probably due to elastic motions, which are ignored in flight simulations.
- At low frequencies up to 1 Hz, the coefficients of the flight test data analysis are in general slightly higher. This can be due to more disturbances during the flight test. Furthermore, this is the area at which the pilot inputs occur.
- The peaks around the eigenmodes in general contain a larger bandwidth, which can be due to the more fluctuating torque or rotor speed.

Based on this, it can be said that it is hard to compare the correlation coefficients of the flight simulations directly with the ones from the flight test data. The magnitude of the coefficients is in many cases different, as the coefficients are quite sensitive to the flight condition or helicopter configuration. Still, the shape is quite comparable till 1 Hz and at the expected peaks. This means that the correlation coefficients are still reliable for relative comparison with only one varying parameter, but not for absolute comparison with several varying parameters. It can be concluded that the exact same flight conditions and helicopter configurations are hard to model.

5.2.3. Gust model

The used gust model is based on the Dryden model as discussed in Sections 2.3.2 and 4.4. This model was optimized by Martin [38] based on the validated DLR gust model. It was concluded that the tuning of the Dryden Gust Model based on the DLR gust model, gives a better coherence between dynamic analysis and realistic flight data for hover and cruise flight. Some discrepancies were also described in his report during the validation with flight test data. It was stated that the low turbulence model overestimates the pilot discomfort with 10% when compared with a flight test rated as low turbulent. The main difficulty with this validation process is that it is hard to know what exactly 'low' turbulent means for the assessing pilot and whether it corresponds with what is modelled as low turbulent. As a verification and validation process has already been applied on the gust model [59], this is not necessary anymore. However, it is still required to validate the effect of the gust model on the correlation coefficients. In order to do this, the following method has been applied:

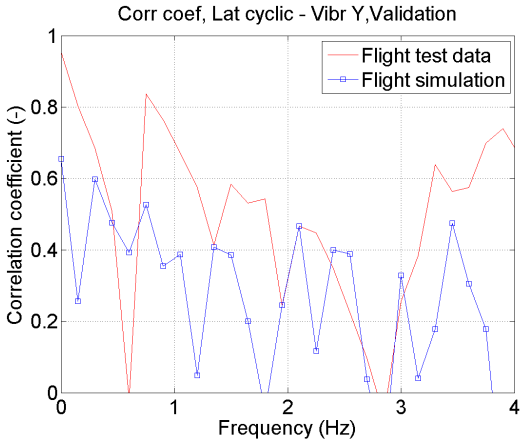

Figure 5.9: Validation: Correlation coefficient, Lateral cyclic - Vibration Y

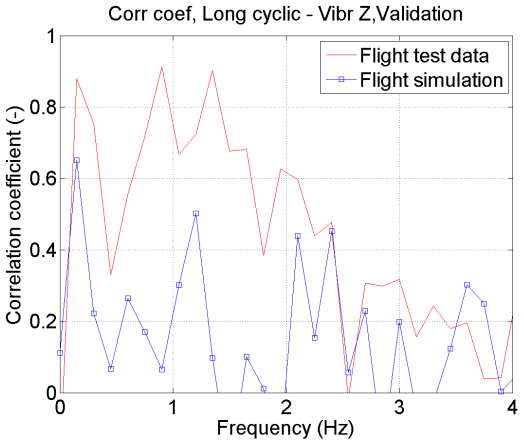

Figure 5.10: Validation: Correlation coefficient, Longitudinal cyclic - Vibration Z

1. The differences between each correlation coefficient of a low turbulent flight test and the flight simulation are calculated per bin. This is done with the Root Mean Square Error (Equation 2.6). Higher weighting factors are used for the frequencies up to 1 Hz and at the expected peaks.

2. The differences per bin will be summed. Afterwards, the differences of all correlation coefficients will be summed. To normalize the differences caused by other parameters (different flight conditions or configurations), this total amount of difference is set to one between the correlation coefficients of the flight test and flight simulation.

3. The wavelength scale and the turbulence intensity will now be tuned, and it will be determined whether the error has increased or decreased.

This process has been repeated for several low turbulent flight tests. The results of one such validation process is shown in Figures 5.11 and 5.12. The value used in the Dryden model is marked with a cross.

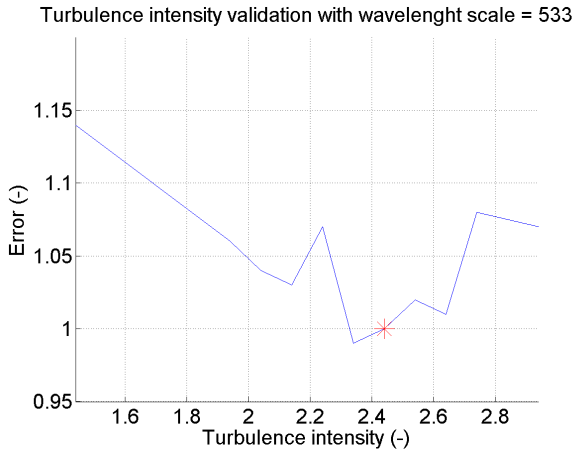

Figure 5.11: Turbulence intensity factor validation

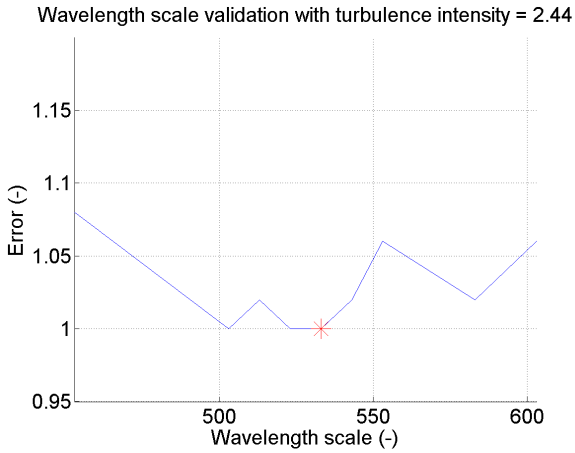

Figure 5.12: Turbulence wavelength scale validation

The validation results of the different flight tests cannot be averaged together, as the normalized value is different. This normalized value is based on the error due to a different flight condition or configuration. It can be noted from the results that if one tries to change the turbulence intensity or wavelength scale to much higher or lower values, the error increases significantly. In that case the gust model in the simulation would reflect the actual gust conditions less accurately. It can be concluded that the optimum values for turbulence intensity and wavelength scale are determined to be within the range of 15 % of the used values. These results are not unexpected, as Martin [38] has explained in his research that there were still some discrepancies in

the validation process when comparing the flight simulations including the gust model with the real flight tests.

5.2.4. Results parametric studies

In this section, the results of the parametric studies are compared. This is done for the correlation coefficients, the Power Spectral Densities and the pilot discomfort values. The conclusions of this section are important for Section 5.3, where a final evaluation on pilot discomfort will be performed and some recommendations for ride quality improvement will be provided. To make all the different points more clear, the discussion per parameter is listed below. Physical explanations were already provided in Sections 3.5 and 4.5 for the flight test data and flight simulations respectively.

- **Control inputs** - The vibrations are more correlated with the cyclic control inputs than with the collective and the pedal inputs. This was observed from the higher correlation coefficients between lateral cyclic & vibration in y-direction, and longitudinal cyclic & vibrations in x,z-direction. Furthermore, from the flight test analysis it can be concluded that the vibrations and the cyclic control inputs have a positive relationship in case of flight condition or confuration changes, while the relationship with the collective and the pedals were more random. Unfortunately, the flight control system of the simulation model was not able to simulate the collective input. But it can be concluded that the correlation with the pedals remains low.

- **Center of gravity** - A more forward center of gravity will lead to less vibration and less control inputs in both simulation and flight test data. The pilot discomfort value decrease slightly in this case. Some shifts in the peaks can be noticed in the correlation coefficients, but the magnitude remains the same.

- **Weight** - In both simulation and flight test data, it was concluded that the vibrations along the whole frequency range are larger for a lower weight helicopter. The amount of control inputs remains equal (flight test data) or decreases in power (simulation). The correlation coefficients are in general higher for a lower weight helicopter. It was suggested here that the correlation coefficient could possibly be used to measure the sensitivity of a helicopter to vibrations.

- **Velocity** - The vibrations are higher for a higher velocity due to the higher amount of aerodynamic disturbances. In general it can be said that the control inputs are also increasing in power for higher velocities. However, for low speeds, the amount of control inputs in the simulation increases. The correlation coefficients are increasing slightly with higher velocities, although the relationship is less clear than with other parameters.

- **Rotorcraft mission** - During flights where more lateral manoeuvre is required, the lateral control input increases, as well as the vibrations. The correlation coefficients are also higher. Peaks in these values can be observed between zero and 1 hertz. During the calculation of the pilot discomfort value, only the vibrations are taken into account, even though the pilot might feel less uncomfortable if he expects the lateral movement. However, if one considers that the peak increase is mainly below one hertz, a region where the pilot is less sensitive to vibrations, it is actually indirectly taken into account.

- **Sensor location** - The location of the sensor influences the measured pilot discomfort and the correlation coefficients minimally. A slightly different ratio between the vibrations in the different directions can be noticed.

- **Blade parameters** - The blade parameters modifications seems to have small influence the correlation coefficients. A small shift can in some cases be noticed. A lower blade inertia for example can lead to a lower hub moment, which can lead to a higher eigenfrequency of the roll subsidence mode, as can be seen in Equation 5.1. Furthermore, some blade parameters such as the flapping hinges do influence the damping of the eigenmodes and therefore the vibrations slightly. With huge changes in these blade parameters, the ride quality can be affected. However, with changes around the 5% w.r.t. the actual design parameters, the influence on the ride quality is almost negligible. This conclusion is solely based on the flight simulations. It should also be noted that the flight control system was not adapted to blade parameters variations. The tuning of the control system will influence the vibrations, which are discussed next.

- **Flight control system** - During the flight test data analysis, it was concluded that the level of vibrations and control inputs is higher if the flight control system is not used. In general, the correlation coefficients are higher as well. However, there was one case with higher control inputs, lower correlation coefficients and also lower vibrations. In general, the more automation is used, the lower the pilot discomfort value. During the flight simulation analysis, the gains were tuned and the effects on the pilot discomfort were measured. It can be concluded that the gains will influence either the correlation coefficients or the amount of control inputs or both. This will lead to different results for the pilot discomfort value.
- **Atmospheric conditions** - The statement that in case of turbulence, the non-rotor induced vibrations will dominate the pilot discomfort, can be confirmed. In general, an increase in the cyclic controls up to 2.5 Hz can be noticed, which can be due to counter steering by the pilot, autopilot or biodynamic feedthrough. In some cases, the eigenmodes are initiated more in case of turbulence. As the increase in control inputs is more in the flight tests than the flight simulations, the increase can most probably be attributed to the pilot. The correlation coefficients are in general also higher, with the highest increase generally up to 2.5 Hz.

5.3. Final evaluation on pilot discomfort and recommendations

Up to this point, the focus was on the correlation analysis between the vibrations and the control inputs. It was investigated where in the frequency spectrum a high correlation could be found and what the causes of the peak correlations were. Now it would be interesting to know how this knowledge can be used for ride quality improvements. Based on the results of the flight test data and flight dynamics simulation analyses, a final evaluation on pilot discomfort is provided here. The focus is on providing the stepping stones in finding solutions on how to optimize the pilot comfort, as well as the comfort of other occupants.

It was suggested before that either high correlation coefficients or high control inputs can lead to high vibrations in the lower frequency domain. One of the examples mentioned for this was during the weight comparison in the flight simulation analysis. Here it was determined that for a lower weight helicopter, the vibrations are higher, while the control inputs are slightly lower. Next to this, it was determined that the correlation coefficients were in general higher. It was suggested that the correlation coefficient could be used as an indicator for measuring the sensitivity of a helicopter to vibrations. In addition, this hypothesis is illustrated more clearly in Figure 5.13.

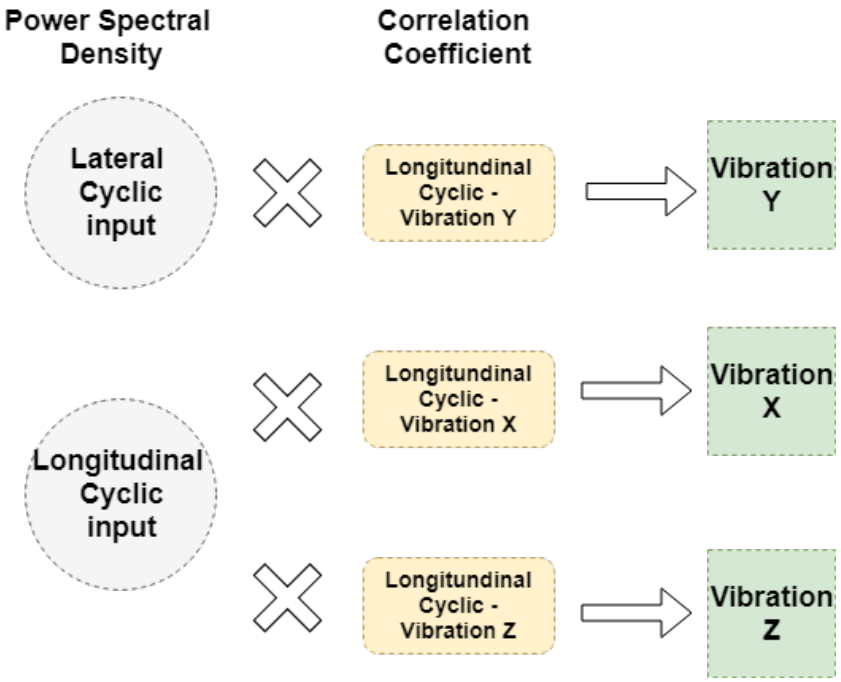

Figure 5.13: Pilot comfort assessment approach

It was suggested before that either high correlation coefficients or high control inputs can lead to high vibrations in the lower frequency domain. To investigate this further, the following sensitivity analysis is proposed and applied to the results of the parametric study:

1. The **correlation coefficients** taken into account are shown in Figure 5.13. After they are calculated, the coefficients larger than 0.3 are summed and divided by the amount of bins. This value can be seen as an average value for the correlation coefficient.
2. The following calculation is applied on the **Power Spectral Density** of the lateral and longitudinal cyclic.
   (a) The Power Spectral Density of the lateral and longitudinal cyclic inputs are calculated in small bins.
   (b) The increase/decrease between each of the cases, as stated in the parametric study, is calculated with respect to the baseline case. This is done per bin. For example: the increase/decrease is calculated in the frequency range 0-0.1 Hz in the first iteration, until it reaches the bin 3.9-4 Hz in the final iteration.
   (c) These increases/decreases are summed and divided by the amount of bins. This is the average value of increase/decrease in the PSDs of the cyclic controls. With the normalization, it is avoided that the values in the first bins dominate the final value.
3. The ratio of the vibration levels between the investigated cases is estimated. This is done by multiplying the correlation coefficient with the power of the respective control input. This will be referred to as **'estimated vibration'**.
4. These estimated ratios are compared with the ratio's of the **measured vibration** levels. The latter are also estimated by determining the change between each of the cases with respect to the baseline case per bin, which is summed together.

The idea of this approach is not to try to estimate the actual vibrations value, but rather to determine whether the power of the control inputs and the correlation coefficients can be used to determine which helicopter configuration or flight condition will be better in terms of ride quality. As the vibrations will be compared relatively, the frequency scaling according to ISO2631-I could unfortunately not be used. The reason is that this scaling will affect the absolute value of the vibrations but not the ratio between the different cases due to normalization. The upper frequency limit of this is taken to be 4 Hz, which is the area where most of the control inputs occur. It also includes the area of maximum human sensitivity. As the occurrence of large negative correlation coefficients was almost non-existent as discussed in Section 3.5.1, these coefficients are not taken into account.

This approach is now applied for the different flight speed cases of the flight simulation. The summations of the correlation coefficients and Power Spectral Densities are shown in Table 5.4. It can be noted that the correlation coefficients for higher speeds are higher. This can be true as it was previously determined that at higher speeds there are more aerodynamic disturbances. It was further determined that the control inputs for the low speed case are higher, as discussed in Sections 3.5.4 and 4.5.7. This can also be seen in this table.

Table 5.4: Velocity comparison: summations of correlation coefficients and Power Spectral Densities (Flight simulation EC135)

Case	**Correlation Coefficient**			**Power Spectral Densities**	
	Lateral cyclic - Vibration Y	Longitudinal cyclic - Vibration X	Longitudinal cyclic - Vibration Z	Lateral Cyclic	Longitudinal Cyclic
High Speed	0.2425	0.0827	0.0981	1.0000	1.0000
Medium Speed	0.1735	0.0625	0.0720	0.8619	1.0685
Low Speed	0.0539	0.0877	0.0463	1.9104	1.2836

It was already determined in Figure 4.39 that the pilot comfort was higher for the high speed case and lower for the medium/low speed case. The latter two also have a comparable discomfort value. The estimated ratio of the vibration levels between the different cases are compared to the measured ratio in Table 5.5. Here it can be seen that in both the estimated as well as in the measured case, the vibrations in y,z-directions are highest

for the high speed case, followed by the medium speed case and then the low speed case. For the vibration in x-direction, the low speed case indeed has higher vibrations than the medium speed case, shown both in the estimated and measured value. However, a small discrepancy occurs when comparing it with the high speed case. It can be observed that the estimated and measured ratio's between the different velocity cases are not the same. This was also not expected, as the multiplication of the power and the correlation coefficient is just to determine the weights of both factors on the vibrations, rather than a method to determine the actual vibration. To conclude, the vibration level is indeed dependent on both the amount of control inputs, as well as the correlation coefficient. Although the correlation coefficients are lower for the low speed case, higher pilot discomfort can still occur due to higher amount of control inputs. And although the amount of the control inputs are lower for the high speed case than for the low speed case, the higher correlation coefficients can still lead to higher pilot discomfort.

Table 5.5: Velocity comparison: estimated vs measured vibrations (Flight simulation EC135)

Case	**Vibration X**		**Vibration Y**		**Vibration Z**	
	Estimated	Measured	Estimated	Measured	Estimated	Measured
High Speed	1.0000	1.0000	1.0000	1.0000	1.0000	1.0000
Medium Speed	0.8077	0.6955	0.6165	0.4128	0.7839	0.5884
Low Speed	1.3615	0.9140	0.4243	0.3858	0.3435	0.4960

This sensitivity analysis can now be applied to the parametric studies of the flight control system tuning in order to test whether it can be used as a potential solution for ride quality improvement. It should be noted that the focus is solely on the vibrations and that the influence on other control and stability characteristics is not further analyzed. During the parametric study, it was concluded that increasing the PID gains by three will affect the correlation coefficients and the amount of control inputs, as shown in Table 5.6, and the pilot discomfort value. Ranking the different cases from highest discomfort: increasing all three PID gains, followed by the proportional gain, then the derivative gain and finally the integral gain. This also coincides with the ratio of the measured vibrations in Table 5.7. Based on the observations made from Tables 5.6 and 5.7, the following conclusions can be made:

- The case with increased PID gains has the highest correlation coefficients and amount of control inputs, which also results in the highest amount of vibrations.
- The amount of longitudinal control inputs of the baseline case and the case with increased I (integral) gain is comparable. However, the case with increased I (integral) gain has lower correlation coefficients between the longitudinal cyclic controls and vibrations in x-direction, which leads to relatively lower vibrations in x-direction.
- The correlation coefficients between the lateral cyclic and the vibrations in y-direction are almost equal for the baseline case and the case with higher P (proportional) gains. However, the case with higher P (proportional) gains has higher amount of lateral cyclic inputs, which leads to higher vibrations in y-direction.

These three conclusion strengthens the theory that the vibration level is dependent on both the amount of control inputs, as well as the correlation coefficients. There are also some observations which do not follow this rule. These are marked in red. For example, the weighting of the baseline case in the ratio of the vibrations in z-direction are estimated too low. The reliability of this method will be further discussed in Section 5.4.

Table 5.6: Control gains comparison: summations of correlation coefficients and Power Spectral Densities (Flight simulation EC135)

Case	Correlation Coefficient			Power Spectral Densities	
	Lateral cyclic - Vibration Y	Longitudinal cyclic - Vibration X	Longitudinal cyclic - Vibration Z	Lateral Cyclic	Longitudinal Cyclic
Baseline gain	0.2425	0.0827	0.0981	1.0000	1.0000
P gain (× 3)	0.2453	0.1643	0.0941	12.8597	3.0840
I gain (× 3)	0.0550	0.0516	0.0899	2.0190	1.0495
D gain (× 3)	0.2591	0.1782	0.1675	2.2486	1.6965
PID gain (× 3)	0.1843	0.2694	0.1393	17.9920	5.2858

Table 5.7: Control gains comparison: estimated vs measured vibrations (Flight simulation EC135)

Case	Vibration X		Vibration Y		Vibration Z	
	Estimated	Measured	Estimated	Measured	Estimated	Measured
Baseline gain	1.0000	1.0000	1.0000	1.0000	1.0000	1.0000
P gain (× 3)	6.1256	1.4207	13.0064	1.2199	2.9597	0.9893
I gain (× 3)	0.6548	0.9067	0.4582	0.9688	0.9617	0.9508
D gain (× 3)	3.6542	1.1414	2.4022	0.9547	2.8974	0.9828
PID gain × 3)	17.2163	2.3898	13.6718	1.3419	7.5046	1.0640

From these results it can indeed be concluded that the flight control system can be used as a potential solution for ride quality improvements. Both measurements on the power of the control inputs as well as the correlation coefficients can be used for this purpose. One can for example notice in this sensitivity analysis that increasing the P gain will lead to higher amount of control inputs, while increasing the D gain will mainly influence the correlation coefficients. Both parameters affect the pilot comfort significantly. Of course, a trade-off with the other design criteria should be made, which means that further investigations are required.

How a change in helicopter configuration can influence the pilot discomfort is discussed next. During the parametric studies, different weights of the helicopter have been compared. It can be seen in Table 5.8 that the amount of control inputs are lower for a lower weight helicopter, but that the correlation coefficients are higher. This results that the vibration levels are estimated higher, as can be seen in Table 5.9, which is also the case. This means that by increasing the weight, the vibration level can be lowered. However, this is in some cases not desirable as it reduces the possible payload. These arguments should be taken into account during the design process.

Table 5.8: Weight comparison: summations of correlation coefficients and Power Spectral Densities (Flight simulation EC135)

Case	Correlation Coefficient			Power Spectral Densities	
	Lateral cyclic - Vibration Y	Longitudinal cyclic - Vibration X	Longitudinal cyclic - Vibration Z	Lateral Cyclic	Longitudinal Cyclic
Baseline	0.2425	0.0827	0.0981	1.0000	1.0000
Lower weight	0.2955	0.1475	0.2723	0.8224	0.7654

Table 5.9: Weight comparison: estimated vs measured vibrations (Flight simulation EC135)

Case	Vibration X		Vibration Y		Vibration Z	
	Estimated	Measured	Estimated	Measured	Estimated	Measured
Baseline	1.000	1.0000	1.000	1.0000	1.000	1.0000
Lower weight	1.3652	4.3726	1.0021	3.7193	2.1254	2.9270

Finally, the sensitivity analysis is applied to the parametric study of the atmospheric conditions, which were discussed in Sections 3.5.7 and 4.5.10. The division is made between vibrations due to a high amount of control inputs and vibrations due to a higher correlation coefficient. The results are shown in Tables 5.10 and 5.11. At first sight, there seems to be no strong relationship between the correlation coefficients and the

increasing turbulence level. The average power of the control inputs does increase. Also a discrepancy in the ratio division occurs when estimating the vibration in x-direction for medium turbulence. The conclusions that can be made are:

- In general, the correlation coefficients with the vibration in z-direction increases with increasing turbulence, while the control inputs are only increasing a bit in this case. This results in a high value of estimated vibration. There is also a huge increase for high turbulence in the vibration in z-direction.
- When comparing vibrations in y-direction, it can be noted that the decrease in correlation coefficients is lower than the increase in the average power of control inputs, which will lead to higher estimated vibrations. This coincides with the ratio between the actual vibrations.

Table 5.10: Turbulence comparison: summations of correlation coefficients and Power Spectral Densities (Flight simulation EC135)

Case	**Correlation Coefficient**			**Power Spectral Densities**	
	Lateral cyclic - Vibration Y	Longitudinal cyclic - Vibration X	Longitudinal cyclic - Vibration Z	Lateral Cyclic	Longitudinal Cyclic
Low turbulence	0.2425	0.0827	0.0981	1.0000	1.0000
Medium turbulence	0.1474	0.0471	0.1079	1.7433	1.0125
High turbulence	0.1586	0.1142	0.1671	1.9603	1.2307

Table 5.11: Turbulence comparison: estimated vs measured vibrations (Flight simulation EC135)

Case	**Vibration X**		**Vibration Y**		**Vibration Z**	
	Estimated	Measured	Estimated	Measured	Estimated	Measured
Low turbulence	1.0000	1.0000	1.0000	1.0000	1.0000	1.0000
Medium turbulence	0.5768	1.1392	1.0598	1.2040	1.1142	1.1683
High turbulence	1.6989	2.4467	1.2825	2.6940	2.0968	2.6062

The same approach is applied to the results of the flight test data. Here, the turbulence level was assessed by a rating provided from the pilot. The power spectral densities and the correlations coefficients are calculated for several turbulent and calm flights. These flights were then averaged per category (calm and turbulent). The results of the sensitivity analysis for the H145 helicopter are shown in Tables 5.12 and 5.13. For the EC135, they are shown in Tables 5.14 and 5.15. It can be seen that the power of both control inputs increases. Furthermore, all correlation coefficients increase as well. This results that the estimated vibration level is higher in each direction in case of turbulence, which match with the actual vibrations.

Table 5.12: Turbulence comparison: summations of correlation coefficients and Power Spectral Densities (Flight test data H145)

Case	**Correlation Coefficient**			**Power Spectral Densities**	
	Lateral cyclic - Vibration Y	Longitudinal cyclic - Vibration X	Longitudinal cyclic - Vibration Z	Lateral Cyclic	Longitudinal Cyclic
Calm	0.0470	0.0360	0.0167	1.0000	1.0000
Turbulent	0.0533	0.0738	0.1333	3.5805	2.4027

Table 5.13: Turbulence comparison: estimated vs measured vibrations (Flight test data H145)

Case	**Vibration X**		**Vibration Y**		**Vibration Z**	
	Estimated	Measured	Estimated	Measured	Estimated	Measured
Calm	1.0000	1.0000	1.0000	1.0000	1.0000	1.0000
Turbulent	4.9250	2.4092	4.0596	6.8907	6.8170	9.2905

Table 5.14: Turbulence comparison: summations of correlation coefficients and Power Spectral Densities (Flight test data EC135)

Case	Correlation Coefficient			Power Spectral Densities	
	Lateral cyclic - Vibration Y	Longitudinal cyclic - Vibration X	Longitudinal cyclic - Vibration Z	Lateral Cyclic	Longitudinal Cyclic
Calm	0.0274	0.0846	0.1090	1.0000	1.0000
Turbulent	0.1684	0.0889	0.1955	1.4716	1.1777

Table 5.15: Turbulence comparison: estimated vs measured vibrations (Flight test data EC135)

Case	Vibration X		Vibration Y		Vibration Z	
	Estimated	Measured	Estimated	Measured	Estimated	Measured
Calm	1.0000	1.0000	1.0000	1.0000	1.0000	1.0000
Turbulent	1.2364	1.1147	9.0438	1.5828	2.1128	1.6655

The advantage of using this approach over solely basing the pilot comfort on the discomfort value calculated with ISO2631-I is that the sources of discomfort here are based on the amount of control inputs given and the sensitivity of helicopter to low frequency vibrations, quantified with the correlation coefficients. So far, investigations were mainly based on calculating the total discomfort value under different conditions or for different configurations. However, now it would also provide more insights to why there is or there is not an increase in pilot discomfort. For example, the derivative gain tuning does not necessarily provide more control inputs than the baseline simulation, but due to the higher correlation coefficients, it does lead to in higher vibrations. The added value of this approach is that the amount of control inputs, as well as the correlations coefficients, can be used to measure the sensitivity of the helicopter to lower frequency vibrations.

The correlation coefficient is based on helicopter configuration or flight condition. More explanation is provided on this. In general, the correlation coefficient measures how big the chance is that more control inputs will lead to more vibrations. Configuration-wise, a low weight helicopter is in general more sensitive to vibrations, therefore extra force inputs, caused by the control inputs, will easily cause more vibrations. Another example is the increase in derivative gain. This means that the flight control system will react stronger to the changes in the error. With the SAS mode, this means that in case of a disturbance, the derivative gain will directly sense a change in error and react to it quickly. The higher the gain, the higher the reaction will be. This means that the helicopter is more sensitive to vibrations. This discussion not only holds for different design parameters, but also for different flight conditions. In general, the aerodynamic forces (lift, drag) are dependent on the square of the velocity. This means that at high speeds, a change in helicopter orientation caused by a control input, will lead to changes in the different velocity components, which leads to extra vibrations. Therefore, at high speeds, the helicopter is more sensitive to vibrations. Another example is the occurrence of turbulence. Turbulence is able to perturb the incident flow of the rotor blades. This itself will already lead to more vibrations, however this also means that if one adds more control inputs in this case, it will cause more disturbances. The reason why the correlation coefficient of the vibration in z-direction increases the most in case of turbulence, is that the lift force is probably affected the most. This means that the vertical movement is the most sensitive to vibrations. The latter point can be investigated in a future study, as it requires detailed knowledge about the aerodynamic workings of a rotor blade in case of turbulence.

Based on the findings of this section, conclusions can be provided on the ride quality. The potential causes for higher correlations were discussed in Section 5.1 and can be used when designing a solution to improve ride quality. It was stated in the research objectives that a (mechanical) solution was outside the scope of this thesis. Still, some suggestion will be provided on how the ride quality can be improved, which can be used for future works. This require a trade off with other design parameters, such as stability, fuel efficiency et cetera.

- The multiplication of the Power Spectral Density of the control inputs and the correlation coefficients can be used to approximate which helicopter design can have a lower vibration level between 0-4 Hz. This is also the frequency area in which the maximum human sensitivity lies.
  - The correlation coefficient can be used to indicate the sensitivity of a helicopter to vibrations. A lower correlation coefficient will improve the helicopter ride quality.

- ◇ This tool can for example compare different designs with each other during flight simulations. With this, the helicopter configuration with lower vibrations can be determined. Potential solutions provided in this research are for example the tuning of the control system or the modification of the weight of the helicopter.
- ◇ Some mechanical devices can be hard to model, but can be implemented during flights tests. Examples are seat vibration isolators [74] and biodynamic resistant control stick [55]. The correlation coefficient can measure the sensitivity to vibrations for flights with and without these devices.

– By lowering the amount of control inputs provided over the frequency range 0-4 Hz, the ride quality can be improved.

- ◇ The amount of pilot inputs can for example be limited by providing extra training on this to pilots. An analysis between experienced and inexperienced pilots was not performed in this research, but could be interesting to investigate.
- ◇ Seat dampers can be used to limit whole body vibrations, which results in less biodynamic feedthrough. Seat vibration isolation devices have been discussed in Section 2.4 and can be a useful tool as well. Another type of solution can be to restrain and immobilize body parts. Efforts have also been devoted to build a model-based cancellation approach, where the biodynamic feedthrough model is used to obtain a cancelling signal [70].
- ◇ It was determined that in general using the autopilot will result in a lower amount of control inputs. The tuning of the flight control systems will also affect the control inputs provided by the system and therefore the ride quality, as investigated in this chapter.
- ◇ It was determined that shifting the center of gravity forward will increase the stability and decrease the amount of control inputs required.

Most of these suggested solutions will influence both the correlation coefficients and the amount of control inputs. Therefore, it should be checked whether both parameters will decrease with the suggested change. A discussion on the reliability of this newly introduced method is provided in the next section.

5.4. Discussion on the proposed methodology

In this section, a discussion is provided on the used methodology and assumptions. It provides a more critical look on the results, and investigates what improvements can be made on this topic in the future work.

Within this investigation, a non-linear helicopter model is used to determines helicopter fuselage vibrations, which appear for example due to excitation forces and moments at main and tail rotor hub. These vibrations are rated by a comfort evaluation method according to ISO 2631-I at the pilot's seat. With this, the influence of the control inputs (collective, longitudinal/lateral cyclic and pedals) in the lower frequency domain is determined. This is done by comparing the Power Spectral Densities of the control inputs and vibrations, as well as by calculating the correlation coefficient between these two variables. This investigation is complemented by analyzing flight test data from the EC135 and H145.

From the flight test data, measurements at the seat of the pilot and several other locations for the vibrations and at the actuators for the control inputs are analyzed. In general, as discussed in Section 5.1, the results did show correlation at the expected frequency regions. However, the measured values at the actuators can be caused by the pilot or autopilot. Furthermore, the actuators could have been vibrated due to other high amplitude vibrations, which is outside the scope of this thesis and therefore not investigated. Some investigation has already been performed on flight tests where the flight control system was switched off to measure the input of the pilot more clearly. In order to provide a more specific solution for each of these sources, more investigation should be done on each of these sources separately. In this way, the solution to improve pilot comfort can be more pilot-centered or flight control system centered. This can be done by using a position sensor on the pilot sticks and pedals, and by saving the values outputted by the flight control system.

Another issue with using the flight test data is that it is hard to have exact the same flight tests with only one parameter different. The parametric study of the atmospheric conditions takes into account flights with varying flight speeds for example, as there were not two approximately equal flight tests performed. This could of course have an influence on the results. Some others, such as the parametric study of the flight speed, is

investigated with an approximately equal helicopter configuration and flight conditions. Furthermore, not all flight tests are performed with the same pilot. This could have an influence as well. Therefore, it is tried to have either the same pilot within the same parametric study, or if that is not possible, take into account several cases with different pilots before drawing conclusions, in order to minimize its effect. Finally, except for the parametric study of the flight mission, the conclusions of the other parametric studies are based on level flights. This means that the correlation coefficient between the lateral cyclic and the vibrations in z-direction, which was ignored for level flights, can be important in lateral movements. Furthermore, the correlation coefficients with the pedals and collective can become more important as well.

The flight dynamics simulation model contains some assumptions. These assumptions and the influence on the results are now discussed. One of the assumptions is that within this analysis, the blade dynamics are represented by the first natural modes and frequencies. It is expected that the higher order natural modes occur at higher frequencies than the considered frequency area and that this assumption is expected to have a low impact on the conclusions. This should of course be investigated. Another assumption was to neglect the elastic motions. This means that the matrix of inertia is constant if the vehicle does not deform and aeroelastic effects are assumed to be small and can be ignored. This assumption reduces the parameters that describe the configuration of the system to the translation and rotation of reference frames attached to each body. This means that a change in control input will lead to a change in translational or rotational motion. However, for higher frequencies, elastic motions can occur. Studies [60, 65] have been performed on the fuselage bending modes and higher order flapping modes for different types of helicopters and rotor speeds. While the higher order flapping modes occur in higher frequencies than the first order flapping mode, the first order fuselage bending can occur in lower frequencies. This topic was discussed in Sections 2.3.1 and 3.1.1 for the investigated helicopter. In general, this phenomenon occurs above 4 Hz. For low frequency motions, this should therefore not be the cause for much discrepancies. Both the modelling of the elastic motions and the rotor harmonic loads can provide more insides on why there is a high correlation coefficient at certain frequencies. However, they will not provide a significant decrease in pilot discomfort due to control inputs, as the power of the control is already quite low at those frequencies, as discussed in Section 5.1. What is interesting to take into account in the flight simulation for future research, are pilot models. They are one of the main contributors to a higher amount of control inputs, and it can therefore be investigated how this amount can be lowered.

The gust model used in the helicopter model only takes into account the translational gust velocities. The reason for this is that only these components are validated for rotorcraft applications. The effect of this assumption on the results has yet to be investigated. The used gust model has been tuned by Martin [38] as explained in Section 2.3.2. This was done by optimizing the gust intensity and wavelength scales with a validated model. However, it was stated by Martin, that there are still some discrepancies, mainly in yaw rate. As can be noticed when comparing the results of the flight test data and flight simulations, there are some discrepancies in the correlation coefficients. This was discussed in Section 5.2. The influence of turbulence on the correlation coefficient with the angular rates is different for flight simulations and flight tests. Furthermore, the increases of the correlation coefficients for higher turbulence levels are more subtle than expected. Therefore, the gust model should be optimized, for example by including the rotational gust components to obtain more accurate results.

The pattern comparison in the frequency spectrum between the control inputs and the vibrations is performed with the correlation coefficient. The main advantage of this tool is that it is able to compare the control inputs and vibration directly with each other, even if the units of both variables are different. This is not a commonly used tool in rotorcraft applications, therefore it is investigated whether results shown are as expected. As this statistical parameter is susceptible to noise correlation, only the coefficients higher than 0.3 were taken into account. However, noise can still be a nuisance factor, which can either prevent some high correlation peaks from other sources or cause some small correlation peaks itself. Therefore, several simulations and flight tests were taken into account before making a conclusion. From Section 5.1, it can be concluded that most peaks are identifiable with a reasoning. The unidentifiable peaks are discussed later. Spectral leakage can be another nuisance factor, which was assumed to insignificant during relative comparisons. However, the exact influence is not determined and can be interesting for future work.

The average bin size used in the correlation coefficient and the Power Spectral Density is also investigated.

If the bin size of the correlation coefficient is too small, noise correlation will become larger, and if the bin size is too large, some peak correlations with small bandwidth will become unidentifiable. In general, the bin size of the correlation coefficients is dependent on the amount of minimum amount of data points required, as calculated with Equation 3.10. For the Power Spectral Densities, a trade off has to be made between the identifiability of small bandwidth peaks and avoidance of huge oscillations due to noise in the pattern. The used bin size was therefore determined based on trial and error.

It can be concluded from Section 5.1, that there were still some unidentifiable peaks left. Most notable are the peaks around 3.5 Hz and around 8.5 Hz, both in the simulation results as well as in the flight test data. The latter is in the region of decreased sensitivity, while the first one is still within the considered frequency area. One of the possibilities for the peak around 3.5 Hz are the interharmonic or subsynchronus inter-harmonic vibrations described in Section 2.2, the drive train modes or the engine eigenmodes. However, the rotor is modelled without imperfections and no drive train dynamics are taken into account in the simulation model, which means that these two reason are not valid. The engine eigenmodes occur generally in higher frequency domains as well [69]. Furthermore, it is too deterministic for random gusts to happen repeatedly at the same frequency area. Therefore, this peak is possibly caused by the flight control system. The exact reason needs still to be investigated. It should also be noted that the expected peaks can be seen in most of the cases, but not always. For example, there are cases where one of the eigenmodes are for example not initiated, or that the correlation peak is prevented due to the occurrence of too much noise.

It is determined that the correlation coefficient could be used to indicate the sensitivity of a helicopter to vibrations. Moreover, this coefficient and the amount of control inputs together can roughly approximate the vibration level of a helicopter. The statistical tool cannot be used to estimate the absolute value of the vibration level, but can be used to provide more insights during relative comparison. For example to check whether a certain change in the design is better than another. Of course, as this is a statistical tool, it can be affected by for example noise and could produce some false conclusions. Therefore, several tests and analyses are required before making a conclusion. However, it does provide people more insights into the causes of the low frequency vibrations and a direction on how the pilot comfort can be improved. It should be noted that the approach to estimate the vibration level was simply a multiplication between the average increase in the power spectral densities of the control inputs and the correlation coefficients higher than 0.3. Other mathematical approaches can be investigated as well. Furthermore, this approach estimates the vibrations level close around the area of maximum sensitivity, and makes no use of the weighting functions described in ISO2631-I. This could be taken into account in future work.

6

Conclusions

The purpose of this thesis was to investigate the influence of (auto-)pilot control inputs on the vibrations in the lower frequency area and on the pilot comfort. This was relatively unknown so far, as the focus in previous work was mainly on higher order vibrations. The reason to investigate this area is because it was stated that the vibrations in this low frequency area tend to dominate the pilot discomfort, which means that more investigations are necessary to improve the helicopter ride quality.

The main goals stated in the beginning of this thesis were:

1. Based on the flight test data and flight simulations, determine where in the frequency domain the correlation between the control inputs and vibrations are, during both calm and turbulent flights.
2. Investigate the causes of the correlations between the control inputs and vibrations.
3. Use the obtained knowledge to provide recommendations on pilot comfort improvement.

The influence of (auto)-pilot control inputs on the helicopter ride quality was determined in two steps. First the vibrations in helicopters was correlated with pilot comfort. Afterwards, the pattern and the power of these control inputs and vibration signals were compared with each other. For the first point, several pilot assessment methods were reviewed and the chosen method was to use the weighting functions defined by ISO by ISO2631-I. This was based on the fact that it was able to take into account vibrations in all three translational vibrations, was based on r.m.s. values instead of peak values and it takes a larger frequency range in consideration. It was shown that the peak sensitivity for the x,y-directions is around 1 Hz and for the z-direction slightly higher.

The important parameters for the second point were the flight control inputs (collective, lateral cyclic, longitudinal cyclic and the pedals) and the vibrations in x,y,z-directions. The correlation between the flight control inputs and the vibrations/angular rates was determined by comparing both the magnitude of the signals in frequency domain as well as the pattern. This was succeeded using the power spectral density and the correlation coefficient. A parametric study was performed in order to determine the correlation and discomfort value for different flight conditions and helicopter configurations. For each case, the increase in power of the control inputs, correlation coefficient and the pilot discomfort value was determined. With this, it became clear at which frequency ranges the correlation between control inputs and vibrations is high. This has been determined for two helicopters types under different flight conditions. It can be concluded that the cyclic control inputs and the vibrations are mainly correlated between 0-4 Hz. This is also the frequency domain where most of the control inputs occur. Peaks were observed at the rotor harmonics as well. The vibrations in y-direction are mainly influenced by the lateral cyclic. The vibrations in x,z-direction are mainly influenced by the longitudinal cyclic. The correlation between the pedal and collective inputs and the vibrations is negligible. The correlation coefficient is influenced by a change in rotorcraft configuration and flight condition. The following parameters negatively influenced the ride quality: A more aft center of gravity, a lower-weight helicopter, higher flight speeds, a manoeuvring flight, no use of flight control system. Finally, it was determined that in case of turbulence, the non-rotor induced vibrations are higher. It was also approximated in

which area these increases are. Interestingly, there seems to be a relationship between the helicopter configuration, the amount of control inputs, the shape of the correlation coefficient graphs and the pilot discomfort.

As the flight test data still has uncertainties and limitations, reproducible flight dynamics simulations were used. A non-linear helicopter model was used with a flight control system and gust model. In general, equivalent conclusions were obtained in most cases from the correlation analysis during relative comparisons.

The peak correlations were investigated next. This was done by performing research on the inputs provided by the pilot and autopilot. The pilot inputs can be caused intentionally and unintentionally. Both types were investigated using literature on pilot models and biodynamic feedthrough models. The eigenmodes were calculated as well, and it can be concluded that most of the lower frequency modes have been initiated during the flight tests and the flight simulations. This can also cause considerable discomfort.

Finally, it was determined that the pilot discomfort can be improved by lowering the amount of control inputs provided or by designing a helicopter with a low correlation coefficient. The correlation coefficient is a newly introduced tool that has been proven to be capable in indicating the sensitivity of a helicopter to vibrations. Low correlations can for example be obtained by increasing the weight of the helicopter, or by control gains tuning. The amount of pilot inputs provided can for example be limited by using seat vibration isolators, which will limit the biodynamic feedthrough.

A (mechanical) solution for ride quality improvement should certainly be one of the follow-up studies. The main focus of this work was to investigate the influence of the control inputs on the helicopter ride quality. The conclusions made during this thesis certainly provided conclusions on this topic. Main improvements that can be made for future studies are to study more manoeuvring flight tests and pilot models, and to optimize the gust model.

Finally, this thesis can be used as a stepping stone for some other studies. Many studies at the moment are for example focused on the identification of the turbulence level. Nowadays, at many companies this is still based on turbulence ratings provided by the pilot, which is rather subjective. It was observed that there seems to be relationship between the turbulence level and the amount of control inputs and the correlation coefficient. Further research can be performed on this, which could potentially be used as a powerful tool to assess the turbulence level. Unfortunately there were not enough flight tests which were rated moderate or high turbulent to investigate this at the moment. Furthermore, high pilot discomfort values also mean high whole body vibrations. This means that the unintentional inputs given due to biodynamic feedthrough is also higher. This could also be an interesting topic for the future.
Several potential solutions have been provided as well on how to decrease the amount of control inputs and how to obtain lower correlation coefficients. A (mechanical) solution to improve ride quality should certainly be one of the follow-up studies. The main focus of this thesis was to investigate the influence of the control inputs on the helicopter ride quality. The conclusions made during this thesis certainly provided further insights on this topic. Next to providing conclusions on a previously relatively unknown area about pilot comfort, the conclusions made, were actually also providing interesting insights in diminishing the vibration level in the lower frequencies in general.

Bibliography

[1] Al Sharman, M., Al Jarrah, M., and Abdel-Hafez, M. (2018). Auto takeoff and precision terminal-phase landing using an experimental optical flow model for gps/ins enhancement. *ASCE-ASME Journal of Risk and Uncertainty in Engineering Systems, Part B: Mechanical Engineering*.

[2] Arcidiacono, P. J., Bergquist, R. R., and Alexander, W. (1974). Helicopter gust response characteristics including unsteady aerodynamic stall effects. *Journal of the American Helicopter Society*, 19(4):34–43.

[3] Asuero, A., Sayago, A., and Gonzalez, A. (2006). The correlation coefficient: An overview. *Critical reviews in analytical chemistry*, 36(1):41–59.

[4] Bechhoefer, E. and Power, D. (2003a). Imd hums rotor track and balance techniques. *2003 IEEE Aerospace Conference Proceedings (Cat. No.03TH8652)*.

[5] Bechhoefer, E. and Power, D. (2003b). Imd hums rotor track and balance techniques. *2003 IEEE Aerospace Conference Proceedings (Cat. No.03TH8652)*.

[6] Bernaschek, V. (2017). Modelling and investigation of the impact of fundamental airframe dynamic characteristics on helicopter ride quality. Technical report, Technische Universität Braunschweig, Airbus Helicopters.

[7] Bilošová, A. and BIloš, J. (2012). Vibration diagnostics. *Ostrava*.

[8] Bramwell, A. R., Balmford, D., and Done, G. (2001). *Bramwell's helicopter dynamics*. Elsevier.

[9] Branco, N. C., Alves-Pereira, M., et al. (2004). Vibroacoustic disease. *Noise and Health*, 6(23):3.

[10] Chen, Y., Wickramasinghe, V., and Zimcik, D. (2009). Development of adaptive seat mounts for helicopter aircrew body vibration reduction. *Journal of Vibration and Control*, 15(12):18091825.

[11] de Waard, P. and Trouvé, M. (1999). Tail shake vibration. *Proceedings of the 55th American helicopter society, Montreal, Canada*.

[12] Drees, J. M. and Harvey, K. W. (1970). Helicopter gust response at high forward speed. *Journal of Aircraft*, 7(3):225–230.

[13] ELLIOTT, A. and CHOPRA, I. (1987). Hingeless rotor response to random gusts in forward flight. In *28th Structures, Structural Dynamics and Materials Conference*, page 954.

[14] Elliott, D. F. and Rao, K. R. (1983). *Fast transforms, algorithms, analyses, applications*. Elsevier.

[15] Eurocopter (2017a). H135 technical data. Technical report, Eurocopter.

[16] Eurocopter (2017b). H145 technical data. Technical report, Eurocopter.

[17] Friedmann, P., De Terlizzi, M., and Myrtle, T. (2001). New developments in vibration reduction with actively controlled trailing edge flaps. *Mathematical and Computer Modelling*, 33(10-11):1055–1083.

[18] Friedmann, P. and Shanthakumaran, P. (1984). Optimum design of rotor blades for vibration reduction in forward flight. *Journal of the American Helicopter Society*, 29(4):70–80.

[19] Fries, J. (2001). *Black Hawk Helicopter Vibration Analysis Due to Main Rotor Damage, Directional Constituents of the Resultant Vibrations*. Army research lab aberdeen proving ground md, United States.

[20] Galton, F. (1889). I. co-relations and their measurement, chiefly from anthropometric data. *Proceedings of the Royal Society of London*, 45(273-279):135–145.

[21] Ganguli, R. and Chopra, I. (1995). Aeroelastic optimization of a helicopter rotor with composite coupling. *Journal of Aircraft*, 32(6):1326–1334.

[22] Giurgiutiu, V. (2000). Review of smart-materials actuation solutions for aeroelastic and vibration control. *Journal of Intelligent Material Systems and Structures*, 11(7):525–544.

[23] Griffin, M., Parsons, K., and Whitham, E. (1982). Vibration and comfort iv. application of experimental results. *Ergonomics*, 25(8):721–739.

[24] Harvey, K. W., Blankenship, B. L., and Drees, J. M. (1969). Analytical study of helicopter gust response at high forward speeds. Technical report, BELL HELICOPTER TEXTRON INC FORT WORTH TX.

[25] Hoblit, F. M. (1988). *Gust loads on aircraft: concepts and applications*. American Institute of Aeronautics and Astronautics, Washington, D.C.

[26] Hunsaker, J. and Wilson, E. (1917). Report on behavior of aeroplanes in gusts. part i—experimental analysis of inherent longitudinal stability for a typical biplane. part ii—theory of an aeroplane encountering gusts. Technical report, NACA Report.

[27] Karakolis, T., Farrell, P., and Fusina, G. (2015). Neck overuse injury in ch-146 griffon helicopter aircrews. *Procedia Manufacturing*, 3:4205–4212.

[28] Kåsin, J. I., Mansfield, N., and Wagstaff, A. (2011). Whole body vibration in helicopters: risk assessment in relation to low back pain. *Aviation, space, and environmental medicine*, 82(8):790–796.

[29] Konstanzer, P., Enenkl, B., Aubourg, P., and Cranga, P. (2008). Recent advances in eurocopter's passive and active vibration control. In *Annual Forum Proceedings-American Helicopter Society*, volume 64, page 854. AMERICAN HELICOPTER SOCIETY, INC.

[30] Krehbiel, T. C. (2004). Correlation coefficient rule of thumb. *Decision Sciences Journal of Innovative Education*, 2(1):97–100.

[31] Kretz, M. (1975). Research in multicyclic and active control of rotary wings. *1st European Rotorcraft Forum (ERF)*.

[32] Lawrence, T. H., Corning, S., and Wharburton, F. (1991). Helicopter maneuverability and agility design sensitivity and air combat maneuver data correlation study. Technical report, UNITED TECHNOLOGIES CORP STRATFORD CT SIKORSKY AIRCRAFT DIV.

[33] Leatherwood, J. D., Dempsey, T. K., and Clevenson, S. A. (1980). A design tool for estimating passenger ride discomfort within complex ride environments. *Human Factors*, 22(3):291–312.

[34] Lee Rodgers, J. and Nicewander, W. A. (1988). Thirteen ways to look at the correlation coefficient. *The American Statistician*, 42(1):59–66.

[35] Loewy, R. G. (1984). Helicopter vibrations- a technological perspective. *American Helicopter Society, Journal*, 29:4–30.

[36] Lusardi, J. (2004). *Control equivalent turbulence input model for the UH-60 helicopter*. ProQuest Dissertations.

[37] Mannchen, T. and Weil, K. H. (2004). Helicopter vibration reduction and damping enhancement using individual blade control. *Journal of Guidance, Control, and Dynamics*, 27(5):760–767.

[38] Martin, F. (2016). Investigation on the impact of gusts on helicopter ride quality. Technical report, Ecole d'ingenieur-e-s. France, Airbus Helicopters.

[39] Mattaboni, M., Quaranta, G., Masarati, P., and Jump, M. (2009). Experimental identification of rotorcraft pilots' biodynamic response for investigation of pao events. *35th European Rotorcraft Forum*.

[40] Mayo, J. R. (1989). The involuntary participation of a human pilot in a helicopter. *Fifteenth European Rotorcraft Forum*, pages 81–93.

[41] Mcfarland, R. E. (1983). The n/rev phenomenon in simulating a blade-element rotor system. *NASA Ames Research Center, Moffett Field, CA, United States*.

[42] McRuer, D. T. and Jex, H. R. (1967). A review of quasi-linear pilot models. *IEEE Transactions on Human Factors in Electronics*, 3:231–249.

[43] MIL-HDBK, D. (1997). Flying qualities of piloted aircraft. *US Department of Defense*.

[44] MJ, G. (1990). *Handbook of Human Vibration*. Academic Press, London, England.

[45] Murthy, T. S. (1987). Design sensitivity analysis of rotorcraft airframe structures for vibration reduction. *Journal of Aircraft*.

[46] Nguyen, K. and Chopra, I. (1989). Application of higher harmonic control (hhc) to hingeless rotor systems. *30th Structures, Structural Dynamics and Materials Conference*.

[47] Padfield, G. D. (1989). *Helicopter handling qualities and control: international conference*. Royal Aeronautical Society, London.

[48] Padfield, R. R. (2013). *Learning to fly helicopters*. McGraw Hill Professional.

[49] Parsons, K. and Griffin, M. (1982). Vibration and comfort ii. rotational seat vibration. *Ergonomics*, 25(7):631–644.

[50] Pearson, J., Goodall, R., and Lyndon, I. (1994). Active control of helicopter vibration. *Computing and Control Engineering Journal*, 5(6):277–284.

[51] Rath, T. and Fichter, W. (2017). A closer look at the impact of helicopter vibrations on ride quality. *Journal of the American Helicopter Society*.

[52] Regan, C. D. and Jutte, C. V. (2012). Survey of applications of active control technology for gust alleviation and new challenges for lighter-weight aircraft. Technical report, NASA Dryden Flight Research Center, Edwards, CA, United States.

[53] Reichert, G. (1973). Basic dynamics of rotors; control and stability of rotary wing aircraft; aerodynamics and dynamics of advanced rotary-wing configurations(basic dynamics of rotary wings, mechanics of helicopter flight, and aerodynamic characteristics of advanced rotary wing concepts and configurations). *AGARD Helicopter Aerodyn. and Dyn. 50 p(SEE N 73-22948 14-01)*.

[54] Reichert, G. (1980). Helicopter vibration control: A survey. *6th European Rotorcarft And Powered Lift Aircraft Forum*.

[55] Repperger, D. W. (1984). Biodynamic resistant control stick. US Patent 4,477,043.

[56] Richter, P., Eisbrecher, H.-D., and Klöppel, V. (1990). Design and first tests of individual blade control actuators. *16st European Rotorcraft Forum (ERF)*.

[57] Robertson, D. G. E. and Dowling, J. J. (2003). Design and responses of butterworth and critically damped digital filters. *Journal of Electromyography and Kinesiology*, 13(6):569–573.

[58] Roth, G. (1993). Dynamisches Durchflussmodell nach Pitt/Peters fur die Bewegungssimulation von Hubschraubern im Zeitbereich. Technical report, Airbus Helicopters.

[59] Roth, G. (1996). Analytical model for flight characteristics and loads evaluation of the EC135. Technical report, Airbus Helicopters.

[60] Rutkowski, M. J. (1983). The vibration characteristics of a coupled helicopter rotor-fuselage by a finite element analysis. Technical report, NATIONAL AERONUATICS AND SPACE ADMINISTRATION MOFFETT FIELD CA AMES RESEARCH CENTER.

[61] Samuel T. Crews, D. W. D. L. (2006). Requirements for rotorcraft vibration specifications, modeling and testing. Technical report, United States army aviation and missile command aviation engineering directorate.

[62] Schäferlein, U., Keßler, M., and Krämer, E. (2017). Aeroelastic simulation of the tail shake phenomenon. *42st European Rotorcraft Forum (ERF)*.

[63] Seddon, J. M. and Newman, S. (2011). *Basic helicopter aerodynamics*, volume 40. John Wiley & Sons.

[64] Seher-Weiss, S. and Von Gruenhagen, W. (2012). Development of EC135 turbulence models via system identification. *Aerospace Science and Technology*, 23(1):43–52.

[65] Srinivasan, A., Cutts, D., Shu, H., Sharpe, D., and Bauchau, O. (1990). Structural dynamics of a helicopter rotor blade system. *Journal of The American Helicopter Society*, 35(1):75–85.

[66] Stewart, E. C. (1989). Evaluation of the ride quality of a light twin engine airplanes by means of a ride quality meter. Technical report, NASA Langley Research Center Hampton, Virginia.

[67] Stull, R. B. (1988). *An introduction to boundary layer meteorology*. Kluwer Academic Publishers.

[68] Technology, N. A. . (2009). *FLIGHT MANUAL BK 117 D-2*. Airbus Helicopters.

[69] Tienhaara, H. (2004). Guidelines to engine dynamics and vibration. *Wärtsilä Corporation*.

[70] Venrooij, J., Mulder, M., Van Paassen, M. M., Mulder, M., and Abbink, D. A. (2010). A review of biodynamic feedthrough mitigation techniques. *IFAC Proceedings Volumes*, 43(13):316–321.

[71] Venrooij, J., Pavel, M. D., Mulder, M., Van Der Helm, F. C., and Bülthoff, H. H. (2013). A practical biodynamic feedthrough model for helicopters. *CEAS Aeronautical Journal*, 4(4):421–432.

[72] Viswanathan, S. P. and Myers, A. W. (1980). Reduction of helicopter vibration through control of hub-impedance. *Journal of the American Helicopter Society*, 25(4):3–12.

[73] Wang, S.-T. and Frost, W. (1980). Atmospheric turbulence simulation techniques with application to flight analysis. Technical report, NASA George C. Marshall Space Flight Center, Alabama, w.

[74] Wickramasinghe, V. K. (2012). *Dynamics Control Approaches to Improve Vibratory Environment of the Helicopter Aircrew*. Carleton University.

[75] Wilbur, M. L., Mirick, P. H., Yeager, W. T., Langston, C. W., Cesnik, C. E., and Shin, S. (2002). Vibratory loads reduction testing of the nasa/army/mit active twist rotor. *Journal of the American Helicopter Society*, 47(2):123–133.

[76] Wright, J. R. and Cooper, J. E. (2008). *Introduction to aircraft aeroelasticity and loads*, volume 20. John Wiley & Sons.

[77] Ziemer, R. E., Tranter, W. H., and Fannin, D. R. (1998). *Signals and systems: continuous and discrete*, volume 4. Prentice Hall.

A

ISO2631-I weighting functions

The weighting functions described in ISO2631-I are explained in this section. In Table A.1 the weighting functions are shown in one-third octaves. The transfer function parameters are defined in Table A.2. By using these parameters, the functions required to build the total weighting function, shown in Equation A.1, can be defined. This can be done with Equations A.2 - A.5, which are formulated in the frequency domain where p_j is known as the Laplace variable $p_j = j2\pi f$

Table A.1: ISO 2631-1 Principal Frequency Weightings in One-Third Octaves

Frequency Band Number	Frequency $[Hz]$	Weighting function z-direction Factor: × 1000	$[dB]$	Weighting function x,y-directions Factor: × 1000	$[dB]$
-3	0.5	418	-7.57	853	-1.38
-2	0.63	459	-6.77	944	-0.50
-1	0.8	477	-6.43	992	-0.07
0	1	482	-6.33	1011	0.10
1	1.25	484	-6.29	1008	0.07
2	1.6	494	-6.12	968	-0.28
3	2	531	-5.49	890	-1.01
4	2.5	631	-4.01	776	-2.20
5	3.15	804	-1.90	642	-3.85
6	4	967	-0.29	512	-5.82
7	5	1039	0.33	409	-7.76
8	6.3	1054	0.46	323	-9.81
9	8	1036	0.31	253	-11.93
10	10	988	-0.10	212	-13.91
11	12.5	902	-0.89	161	-15.87
12	16	768	-2.28	125	-18.03
13	20	636	-3.93	100	-19.99
14	25	513	-5.80	80.0	-21.94
15	31.5	405	-7.86	63.2	-23.98
16	40	314	-10.05	49.4	-26.13
17	50	246	-12.19	38.8	-28.22
18	63	186	-14.61	29.5	-30.60
19	80	132	-17.56	21.1	-33.53

Table A.2: ISO 2631-1 Transfer Function Parameters

Weighting	Band-limiting		Acceleration-velocity transition			Upward step			
	f_1 $[Hz]$	f_2 $[Hz]$	f_3 $[Hz]$	f_4 $[Hz]$	Q_4 $[-]$	f_5 $[Hz]$	Q_5 $[-]$	f_6 $[Hz]$	Q_6
Weighting function z-direction	0.4	100	12.5	12.5	0.63	2.37	0.91	3.35	0.91
Weighting function x,y-directions	0.4	100	2.0	2.0	0.63	∞	-	∞	-

$$H(p_j) = H_h(p_j)H_l(p_j)H_t(p_j)H_s(p_j) \tag{A.1}$$

- Band-limiting: High pass

$$\left|H_h(p_j)\right| = \left|\frac{1}{1+\sqrt{2}\frac{2\pi f_1}{p_j}+(\frac{2\pi f_1}{p_j})^2}\right| \tag{A.2}$$

- Band-limiting: Low pass

$$\left|H_l(p_j)\right| = \left|\frac{1}{1+\sqrt{2}\frac{p_j}{2\pi f_2}+(\frac{p_j}{2\pi f_2})^2}\right| \tag{A.3}$$

- Acceleration-velocity transition

$$\left|H_t(p_j)\right| = \left|\frac{1+\frac{p_j}{2\pi f_3}}{1+\frac{p_j}{Q_4 2\pi f_4}+(\frac{p_j}{2\pi f_4})^2}\right| \tag{A.4}$$

- Upward step

$$\left|H_s(p_j)\right| = \left|\frac{1+\frac{p_j}{Q_5 2\pi f_5}+(\frac{p_j}{2\pi f_5})^2}{1+\frac{p_j}{Q_6 2\pi f_6}+(\frac{p_j}{2\pi f_6})^2}(\frac{2\pi f_5}{2\pi f_6})^2\right| \tag{A.5}$$

B

Complementary information per flight case

During the parametric study in Chapter 3 several flight tests are compared with each other. The helicopter type, the serial number and the flight test number of the different cases are shown in Table B.1 for traceability. In the parametric study of the atmospheric conditions, there are several flight tests in the same category. This means that the Power Spectral Densities and correlation coefficients per flight test are calculated first, after which they are averaged. The table is sorted based on first appearance in Chapter 3. The flight speeds are added as well.

Table B.1: Helicopter type, serial number and flight test number of the flight test data used during parametric studies

Case	Helicopter Type	Serial number	Flight test number
Section 3.4 (flight speed: 40kts)			
Spectral analysis	H145	20085	F0011_040k_0
Section 3.5.1 (mixed flight speeds)			
Rotorcraft configuration	EC135	1155	F0035, F0036, F0037, F0038, F0039
Rotorcraft configuration	H145	20007	F0092, F0095, F0096, F0099, F0192, F0193
Section 3.5.2 (flight speed: 80kts)			
Center of gravity (4.2 m from nose)	EC135	1112	F0058
Center of gravity (4.4 m from nose)	EC135	1112	F0062
Section 3.5.3 (flight speed: 120kts)			
Lower weight ($\approx$ 2700 kg)	H145	20001	F0446
Higher weight ($\approx$ 3800 kg)	H145	20001	F0447
Section 3.5.4 (flight speed: 40/80/110kts)			
Low speed (40 kts)	H145	20085	F0011_040k_0
Medium speed (80 kts)	H145	20085	F0011_080k_0
High speed (110 kts)	H145	20085	F0011_110k_0
Section 3.5.5 (mixed flight speeds)			
90 degrees lateral manoeuvre	EC135	0595	F0343
Level Flight	EC135	0595	F0225
Section 3.5.6 (flight speed: 130kts)			
Autopilot off	EC135	0886	F0702_130_0
Autopilot on	EC135	0886	F0702_130_1
Section 3.5.7 (mixed flight speeds)			
Turbulent	H145	20001	F0622
Calm	H145	20001	F0183, F0446, F0447, F0451
Turbulent	EC135	0886	F0220_HS, F0220_LS, F0220_MS, F0452, F0452_HS
Calm	EC135	0886	F0330_HS, F0330_LS, F0451, F0451_HS, F0461, F0461_HS, F0462, F0462_HS, F0463, F0463_HS, F0464, F0464_HS, F0488, F0489, F0490, F0491, F0492

C

Scientific Paper

In this appendix, the accompanying scientific paper is presented.

Investigation of the influence of (auto-)pilot control inputs on helicopter vibrations and ride quality

Bryan Kim Fon Yip*

Graduate Student
Delft University of Technology
Delft, The Netherlands

June 22, 2018

Abstract

Nowadays the origins and solutions for rotor-induced vibrations in helicopters are well-known. However, non-rotor induced low frequency vibrations still remain a topic of research, although it has proven that these tend to become a dominant source of pilot discomfort, especially in case of turbulence. Therefore, this research aims to come to a conclusion on the effect of (auto-)pilot control inputs on the low-frequency vibrations of the helicopter, and how these influence the ride quality, in calm and turbulent air. This will be done by calculating the correlation between control inputs and low-frequency vibrations. For this, Airbus Helicopters provides flight test data and a non-linear helicopter model. This work adds knowledge on how much the control inputs and vibrations are correlated and in which frequencies region they are correlated. Furthermore, the causes for correlations are investigated, which assist in finding solutions to improve the pilot comfort. Finally, new methods that will help in the process of designing a better ride quality are introduced, which includes the assessment of the power of the control inputs and the correlation coefficient.

I. Introduction

The cabin vibration levels of rotorcraft have always been higher than for aircraft. The main reason for higher vibrations is the complex aerodynamic flow field of the main rotor. This leads to the occurrence of rotor induced vibrations caused by periodic air loads on the rotor blades. Under calm flight conditions, power is generated by the individual rotor blades at multiples of the rpm (revolutions per minute) of the rotor system. Another important type of rotor-induced vibrations is caused by the imbalance and tracking errors of the main rotor. The non-uniformity is due to the variation in manufacturing, and uneven wear/fatigue of the blade as a result of usage [2, 6, 14]. These vibrations will influence the comfort of occupants. The latter is important as it can decrease the performance of the pilot. Long-term exposure to vibrations is known to contribute to aircrew occupational health issues including neck strain, back pain injuries and many other human-interface related issues in helicopter operations [4, 9, 10].

While the rotor-induced vibrations are well-understood nowadays, a lesser known area in this field is the influence of non-rotor induced vibrations. This area has been largely ignored in the past, but its contribution to vibrations is starting to become more relevant. Research by Rath [19] on this topic concluded that an analysis of flight test data reveals that apart from rotor harmonic vibration, there are other vibra-

*Supervisors:
Oliver Dieterich, Airbus Helicopter
Marilena Pavel, TU Delft
Rene van Paassen, TU Delft

tion sources that contribute significantly to the vibration discomfort. These vibrations mainly occur in the low frequency domain. The potential causes stated in the research are the elastic tailboom deformations and control inputs. It is also stated that with increasing turbulence, the selected non-rotor vibrations tend to dominate the discomfort of the helicopter occupants.

Recently, research was performed by Bernaschek [3] on the influence of the tailboom deformations on the vibrations. Using a FEM Eigenmode analysis and flight dynamics simulations, the different tailboom modes were identified with the corresponding vibration peaks. The research confirms not only that there is an influence of the tailboom modes on the vibrations and ride quality, but also gives recommendations on how to improve the helicopter ride quality based on parametric studies. In order to be able to alleviate low frequency vibrations, the origins of the low frequency vibrations should be well understood. So far, the influence of the control inputs on pilot comfort has yet to be investigated.

Therefore it is necessary to investigate the influence of the (auto)-pilot control inputs on the helicopter ride quality. Although the peaks are not the highest in amplitude compared to the harmonic loads, the affected bandwidth is larger and the vibrations are more in the range of the human sensitivity [16]. Furthermore, it would be interesting to investigate whether pilot comfort can be improved in the low frequency range. The main focus of this work will be on answering the following questions:

- What is influence of the control inputs on the helicopter ride quality during calm and during turbulent air?
- Why and where in the frequency domain do the control inputs correlate with the vibrations?
- How can the pilot comfort potentially be improved?

In this paper the methodologies to assess pilot comfort and to link the vibrations and the control inputs together are explained first. The experimental setup is based on the provided flight test data and non-linear helicopter model from Airbus Helicopters, which are discussed next. The results will determine the exact locations in the frequency spectrum where correlation between the helicopter control inputs and low frequency vibrations occur. An elaboration will be given on why there could be a correlation. And finally, this paper will provide some initial insights into potential solutions to improve the pilot comfort.

II. Methodolgy

The influence of (auto)-pilot control inputs on the helicopter ride quality is determined in two steps. First, fundamental knowledge about human perception of whole body vibration (WBV) is required to correlate the vibrations in helicopters with pilot comfort. Secondly, the pattern and the power of the control inputs and vibration signals are compared with each other.

i. Pilot comfort assessment

Research has been performed [16] on the relationship between the psychophysical amplitude, representing the human sensitivity, and the measured vibration amplitude. A constant input vibration amplitude in each frequency does not produce the same amount of whole body vibration in each frequency. At low frequencies, below 1 (for x,y-directions) or 2 Hz (for z-direction), the forces acting on the body and the input acceleration have an approximately linear relationship. At slightly higher frequencies, the motion will be amplified due to the occurrence of different body resonance. At even higher frequencies, attenuation will occur. The exact frequencies are dependent on a wide range of parameters, such as subject group, seating geometry and backrest conditions. In general, the maximum sensitivity to horizontal translational vibrations (x,y-directions) occurs in the area of 1-2 Hz if there is no backrest. In the vertical axis (z-direction), the maximum is around 2-6 Hz. Therefore, it can be concluded that the rotor-induced vibrations largely occur in the area of decreased

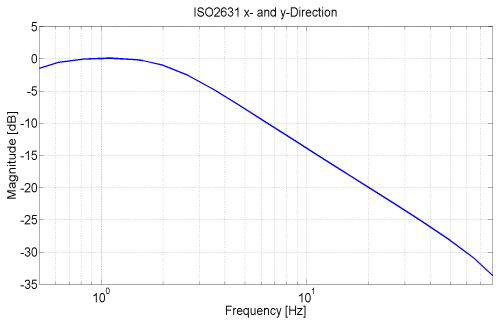

Figure 1: *Frequency weighting curve for x,y-directions*

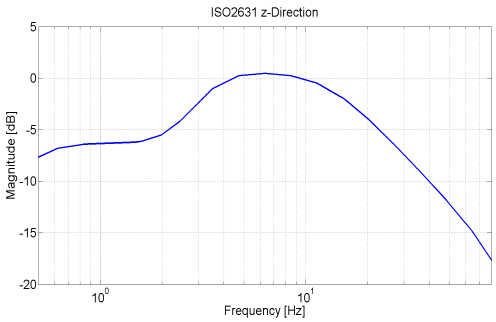

Figure 2: *Frequency weighting curve for z-direction*

sensitivity. This makes it even more important to investigate the non-rotor induced vibration, which are in the area of maximum sensitivity.

The sensitivity to rotational vibrations decreases with increasing vibration frequency. Furthermore, the sensitivity to rotational vibrations is dependent on the distance from the center of rotation. At distances larger than 1 m, and in many cases even a few centimeters, from the center of rotation, which is the case for pilots in cockpits, the translational vibrations dominates the human perception [7, 16, 18]. Therefore, the rotational vibrations are in general not taken into account when assessing the pilot discomfort.

Based on these findings, the ISO 2631-1(1997) [16] has described a method to combine the effects of vibrations from different axes in the form of one parameter a_v, the discomfort value. In contrast to some other pilot assessment methods, it does take into account the translational vibrations in all three directions. Furthermore, it takes into account a larger frequency range. The frequency sensitivity weighting curves are shown in Figure 1 for x,y-directions and in Figure 2 for z-direction. One can notice that the vibrations in x,y-directions are more important for the lower frequencies until approximately 3 Hz, with a peak sensitivity around 1 Hz. After that, the vibrations in z-direction will weight more in the calculation of the discomfort.

The translational acceleration signals are fed through the filters defined in ISO 2631-1 resulting in the weighted acceleration as a function of time ($\vec{a_w}(t)$). The key indicator for the discomfort level of a vibration signal is the weighted root-mean-square (r.m.s.) acceleration. This is defined as in Equation 1, where T is the duration of the measurements in seconds. The final evaluation is done by summing the weighted acceleration with a certain multiplying factor. The multiplying factors $k_x = k_y = 1.4$ and $k_z = 1$, as specified in ISO 2631-1 are used. By this definition, the missing influence of the backrest is taken into account. The final pilot discomfort value can be calculated with Equation 2. Acceptable values of vibration magnitude for comfort depend on many factors, which vary with each application. This is why fixed ranges for comfort ratings are hard to define. An indication defined by ISO 2631-I is shown in [16].

$$\vec{a_w} = (\frac{1}{T}\int_0^T \vec{a_w}^2(t)dt)^{\frac{1}{2}} \quad (1)$$

$$a_v = (k_x^2 a_{wx}^2 + k_y^2 a_{wy}^2 + k_z^2 a_{wz}^2)^{\frac{1}{2}} \quad (2)$$

ii. Correlation analysis

The control inputs influences the translational and rotational motion of a helicopter, which could lead to changes in the vibration level. Increased control inputs can be caused by (un)intentionally provided pilot inputs or inputs provided by the flight control system. In this research, the pattern and the power of both signals will be compared in the frequency spectrum. The control inputs and the vibrations are measured in different units. Therefore suitable

statistical methods should be found for comparison. Based on the mechanics and dynamics of a helicopter [17], the following combinations are investigated.

- Longitudinal cyclic - Vibrations in x,z-direction
- Lateral cyclic - Vibrations in y,z-direction
- Collective - Vibration in z-direction
- Pedals - Vibration in y-direction

The pattern in the frequency spectrum between the control inputs and the vibrations can be determined with the correlation coefficient. Correlation can be described as the degree of association between two variables [12]. The correlation coefficient is also independent of the magnitude of the signals, which means that a difference in the units of one or both signals does not influence the results. This calculation is shown in Equation 3. In this equation, $(x_1, ..., x_n)$ is the data set of one of the control inputs, and $(y_1, ..., y_n)$ is the data set of the vibration in one direction.

$$r_{xy} = \frac{\sum_{i=1}^{n}(x_i - \bar{x})(y_i - \bar{y})}{\sqrt{\sum_{i=1}^{n}(x_i - \bar{x})}\sqrt{\sum_{i=1}^{n}(y_i - \bar{y})}} \tag{3}$$

In general, a value of one means total positive linear correlation, minus one means total negative linear correlation and zero means that there is no linear association between the variables. The approximate strength of correlation is shown in Table 1.

Table 1: *Strength of correlation [1]*

Size of r_{xy}	Interpretation
0.90 to 1.00	Very high correlation
0.70 to 0.89	High correlation
0.50 to 0.69	Moderate correlation
0.30 to 0.49	Low correlation
0.00 to 0.29	Little if any correlation

For the correlation analysis, the correlation coefficient is calculated in small bandwidths in the frequency spectrum. The minimum amount of data points required per bandwidth can be estimated with Equation 4 [11]. This equation provides a rule of thumb, which links the number of data points to the reliability of the correlation coefficient. If one wants to have reliable coefficient from 0.3, at least 45 data points are required.

$$|r_{xy}| > \frac{2}{\sqrt{n}} \tag{4}$$

The intensity of a signal can be described with Power Spectral Density [5], as shown in Equation 5. This describes the power per Hz in the signal. To make the comparison easier, the Power Spectral Densities are integrated into bins of 0.1 Hz.

$$PSD = \frac{1}{Nf_s}\left|\sum_{n=0}^{N-1} x(n)e^{-j2\pi kn/N}\right|^2 \tag{5}$$

As you cannot compare the intensity of the two signals directly with each other due to the difference in units, an analysis will be performed on how both signals behave under different circumstances. This can be for example a change in flight condition or rotorcraft configuration. The increase or decrease in vibration level and control inputs is calculated per frequency bin, and it is determined whether there is a positive or negative relationship between the two variables. This means that a parametric study is performed. The correlation coefficient is also determined for each study. A list of different helicopter configurations and flight conditions taken into account in this parametric study is shown below:

- Weight
- Center of gravity
- Flight speed
- Rotor blade parameters
- Flight control system settings
- Atmospheric conditions (calm or turbulent flight)
- Rotorcraft mission (level flight or manoeuvre)

III. Data analysis and simulation set-up

In order to perform the correlation analysis, the flight test data of two different helicopter are used. The exploitation of flight test data is complemented by related flight dynamics simulations that identify the relationship between control inputs and vibrations under laboratory and thus reproducible conditions.

i. Flight test data

For this work, two four-bladed twin-engine civil light utility helicopters are investigated. These are the EC135 and H145 helicopter from Airbus Helicopters. For each helicopter, data of at least 50 flights tests is available. Between the flight tests, the helicopter configurations, flight missions pilot or flight conditions can be different. For each flight the pilot was asked to provide a rating for the turbulence level. Measurements of 200 seconds with a sampling rate (f_s) of 400 Hz are performed. The most important measurements for this thesis are listed below:

- Vibrations in x,y,z-direction: Measured at several locations in the cabin, including on the floor at the pilot location, which is required for the ISO2631-I calculation.
- Control inputs: Linear displacements of the 4 flight controls are measured at the main/tail rotor actuator. This means that the measured value is a combination of the pilot and autopilot control inputs.

ii. Helicopter dynamics simulation

A non-linear helicopter model including a flight control system and gust model is used for the correlation analysis. The behaviour of a helicopter in flight can be modelled as the combination of a large number of interacting subsystems. The contribution of the main rotor, the fenestron and the airframe is taken into account. As the frequency range of interest covers the lower range of the frequency domain, only rigid body motions are used. The rotor degrees of freedom considered in this work are the flapping, lead lag and rigid blade torsion. The Dryden wind turbulence model [8] is used to generate turbulence within the helicopter flight simulation. This gust model has been adapated to match the characteristics of a flight-test validated turbulence model developed by Seher-weiss and Gruenhagen [21]. The outputs of the non-linear helicopter are the rigid body accelerations in the center of gravity, which were then translated to the pilot's location. The control inputs are measured from the flight control system. The baseline settings of the simulation are listed in Table 2. Unless stated otherwise, these settings also hold for the flight tests. The pilot location is defined from the center of gravity in the body reference frame.

Table 2: *Baseline configuration: EC135*

Parameter	Input
Mass	2980 kg
Pilot Location (x/y)	1.7/0.39 m
Pressure altitude	3000 ft
Ambient temperature	9.06° C
Initial speed	120 kts

IV. Results

From the spectral analysis on the control inputs and the vibrations, it can be concluded that most of the control inputs indeed happen in the very low frequency domain, around 0-2 Hz, and that beyond 4 Hz, the amplitude of control signals is minimal. An example of a vibration spectrum in z-direction is shown in Figure 3. A spectrum of the longitudinal cyclic control is shown in Figure 4. Vibrations due to other sources are highlighted as well, including the rotor harmonic loads and the tailboom induced vibrations. As said before, although the amplitude of the vibration in the low frequency domain is lower, they occur over a larger frequency band. This means that these vibrations represent considerable energy. Furthermore, this occurs in the region of stronger human sensitivity. Both aspects have negative

consequences for the pilot comfort.

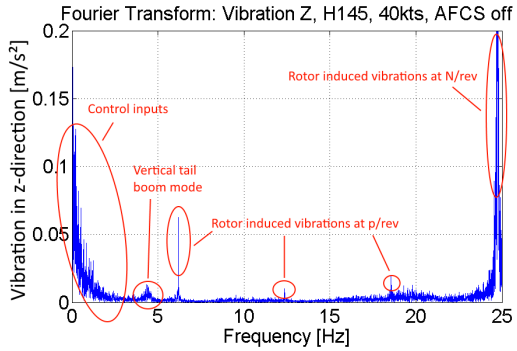

Figure 3: *Frequency spectrum of vibration in z-direction (flight test data H145, 40 kts)*

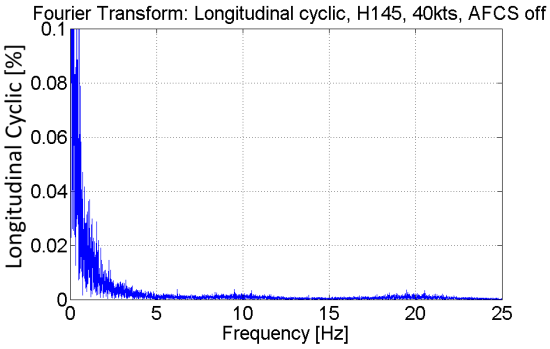

Figure 4: *Frequency spectrum of longitudinal cyclic (flight test data H145, 40 kts)*

Now the pattern is compared with the correlation coefficients for the flight test data. These are shown for the cyclic controls with the translational vibrations in Figures 5 - 7. The correlation coefficient is presented here for a range of 0 till 15 *Hz*. In these figures, several flight tests with different conditions or configurations are shown for the same series number. It can be seen that there is high correlation coefficient between the control inputs and the translational vibrations at the rotor harmonics and until approximately 5 *Hz* for the lateral cyclic and the vibration in y-direction, and until around 3-4 *Hz* for the longitudinal cyclic and the vibrations in x,z-directions. Therefore, the focus in this work is mainly on the 0-4 *Hz* frequency domain.

i. Parametric studies

The purpose of the parametric studies is to analyse where there is a high correlation between the control inputs and the vibrations. This is determined by comparing the power and the pattern of the signals. This analysis is then compared with the pilot discomfort value calculated with ISO 2316-I. The pilot discomfort in the lower frequency domain (0-4 *Hz*) is compared with the pilot discomfort at higher frequencies (>4 *Hz*). The results of the atmospheric condition change is elaborated to show the analysis approach. The outcome of the other parameters is summarized. But first the findings on the helicopter type and control inputs will be discussed.

Helicopter Type - *EC135/H145* - When comparing the correlation coefficients, there seems to be a comparable pattern within the same helicopter type. This suggests that part of the shape of the correlation coefficients is dependent of the rotorcraft configuration. Furthermore, the occurrence of negative correlation coefficients is negligible.

Control inputs - *Cyclic/collective/pedals* - The vibrations are more correlated with the cyclic control inputs than with the collective and the pedals. This was observed from the higher correlation coefficients between: lateral cyclic & vibration in y-direction, and longitudinal cyclic & vibrations in x,z-direction. Furthermore, it is noticed that the power of the vibrations and the cyclic control inputs consistently varies with flight condition or configuration alterations, while the relationship between the power of the vibrations and the collective and the pedals is more arbitrary. Therefore it can be concluded that the correlation of the latter two with the vibrations is negligible. The collective and pedal inputs are therefore not considered in the further discussion of this paper.

Atmospheric conditions - *Calm/turbulent* - Turbulence can affect the helicopter in

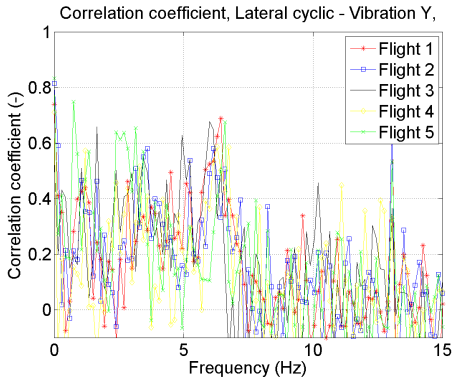

Figure 5: *Lateral correlation coefficient (Flight test data EC135, different flight conditions)*

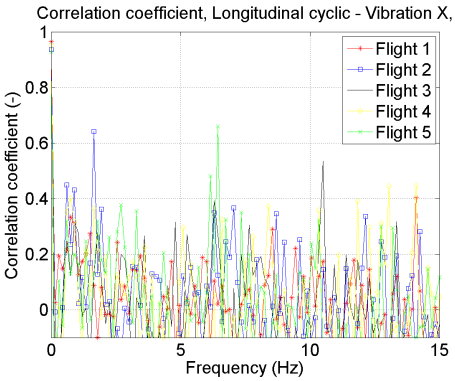

Figure 6: *Horizontal correlation coefficient (Flight test data EC135, different flight conditions)*

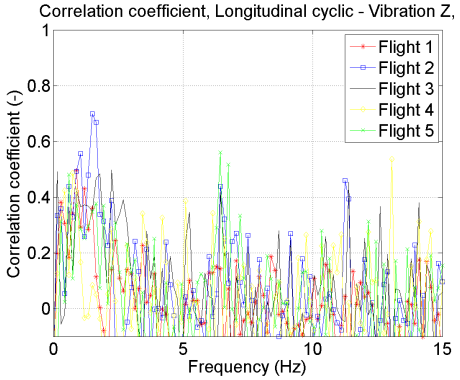

Figure 7: *Vertical correlation coefficient (Flight test data EC135, different flight conditions)*

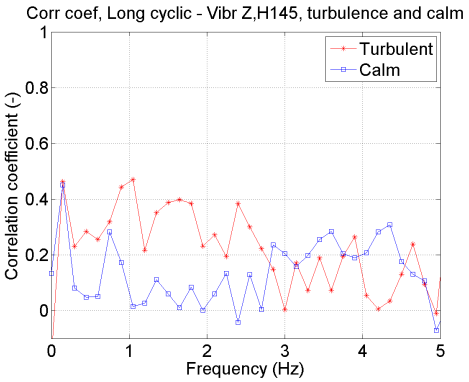

Figure 8: *Vertical correlation coefficient (Flight test data EC135, turbulent)*

two manners. It can both excite the structure directly and perturb the incident flow of the rotor blades. Furthermore, it can also affect the control inputs in different ways, which could lead to more or less vibrations. Firstly, if the frequency is low enough for a pilot to handle, the pilot's control input is higher. For higher frequencies, the pilot will try to keep the stick in the same position, in order to avoid amplifying the oscillations. Secondly, the autopilot will react to the disturbances and therefore provide more control inputs. Finally, biodynamic feedthrough can occur when the vibrations of the helicopter feed through the pilot's body and cause involuntary motions of limbs, which will result in involuntary control inputs. This can all lead to a higher vibration level, as shown in Figure 10. In the presence of turbulence, an increase in the cyclic controls up to 2.5 Hz can be noticed, which can be seen in Figure 9. In some cases, the eigenmodes are initiated more in case of turbulence. The correlation coefficients with the angular rates are in general higher, with the large increases generally up to 2.5 Hz, and even higher for the correlation coefficients with the translational vibrations, as can be observed from Figure 8. Finally, the pilot discomfort is calculated for both helicopter types and shown in Figure 11. The

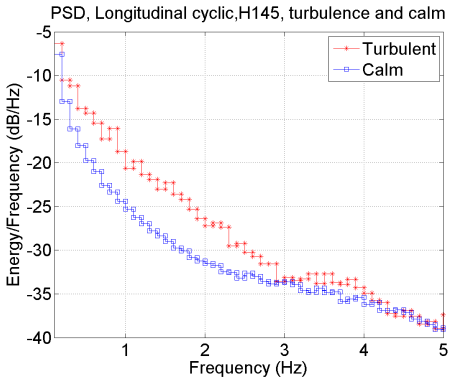

Figure 9: *Power spectral density: Longitudinal cyclic (Flight test data EC135, turbulent))*

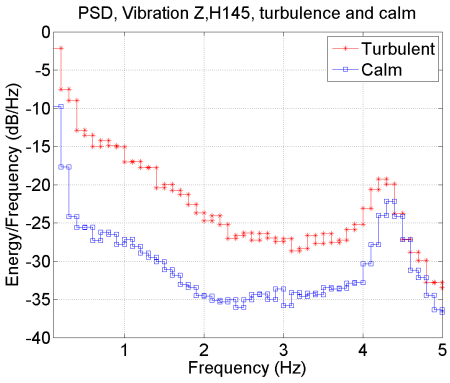

Figure 10: *Power spectral density: Vibration X (Flight test data EC135, turbulent))*

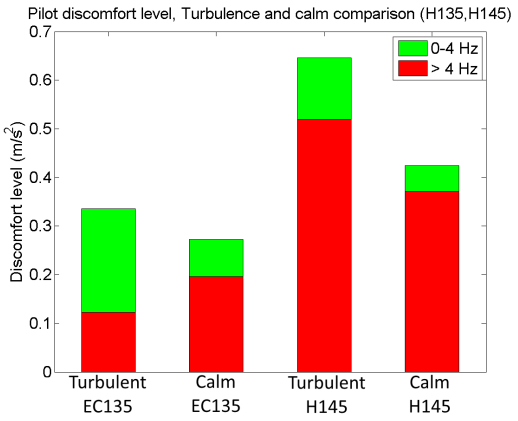

Figure 11: *Pilot discomfort level under turbulence and calm conditions*

statement from Rath [19] that in case of turbulence, the non-rotor induced vibrations could dominate the pilot discomfort, can be confirmed.

Weight - *EC135: 2980/1600, H145: 3800/2700, in kg* - It is concluded that the vibrations along the whole frequency range is larger for a lower weight helicopter. This is expected as a lower-weight helicopter is more sensitive to vibrations. The calculated pilot discomfort value is also higher. The amount of control inputs either remains almost equal or decreases in power due to higher manoeuvrability. The correlation coefficients are in general considerably higher for a lower weight helicopter, with among others a significant increase in the horizontal correlation coefficient. This is in contrast with the relatively lower horizontal correlation coefficients shown in Figure 6. This strengthens the idea that the correlation coefficient is partly a helicopter parameter and can possibly be used to indicate the sensitivity of a helicopter to vibrations due to control inputs. This also means that this parameter could be tunable per design. This hypothesis is tested later on.

Velocity - *40/80/110 kts* - Different velocities are compared with each other during level flight. It is expected that the aerodynamic disturbances are higher for higher flight speed, which was also the case. In general it can be said that the control inputs are also increasing in power for higher velocities. The only exception is for very low velocities, where much more control inputs are required to achieve certain movements. Here, the vibrations are high as well. The correlation coefficients are increasing slightly with higher velocities. The same relationship can also be seen in the pilot discomfort value.

Center of gravity - *4.2/4.4 m from nose* - Due to the offset of the thrust from the center of mass, the contribution of the rotor thrust is stabilizing for configurations

with a more forward center of gravity. It can be concluded that the more forward the center of gravity is, the more stable the helicopter is [17]. Furthermore, less control inputs are required, which leads to a slightly better pilot discomfort value. Some shifts in the peaks can be noticed in the correlation coefficients, but in general the magnitude remains the same.

Rotorcraft mission - *Level flight/90 degrees lateral movement* - During flights where more lateral manoeuvring is required, the lateral control input increases, as well as the vibrations. The correlation coefficients are also higher. Peaks in these values can be observed between zero and one Hz, which is logical, as a controlled manoeuvre does not require fast movements. The pilot discomfort value increases in this case.

Blade parameters - *10% increase/decrease: the flapping hinge, lead-lag damping, rotorblade mass and inertia* - Blade parameter modifications seems to have negligible influence on the longitudinal and vertical correlation coefficients. A slight shift can be seen in the lateral correlation coefficients. Furthermore, some blade parameters such as the flapping hinges do influence the damping of the eigenmodes and therefore the vibrations slightly. With huge changes in these blade parameters, the ride quality can be affected. However, with changes around the 5% w.r.t. the actual design parameters, the influence on the ride quality is almost negligible. This conclusion is solely based on the flight simulations.

Flight control system - *On/off and PID gain tuning* - During the flight test data analysis, it is concluded that the level of vibrations and control inputs are higher if the flight control system is not used. This means that in general the pilot provides more input than the flight control system. In most cases, the correlation coefficients are higher as well. The results also show that when more automation is used, the pilot discomfort value is lower. During the flight simulation analysis, the PID gains are tuned and the effects on the pilot discomfort are measured. It can be concluded that the gains influences either the correlation coefficients or the amount of control inputs or both. This leads to different results for the pilot discomfort value. This aspect is elaborated later on.

During the flight simulations, the influence of noise correlation and the sensor location is investigated as well. Noise can have an influence on the magnitude of the correlation. However, higher correlation peaks can still be noticed at the same frequencies. The same conclusion can be made by varying the sensor location.

ii. Causes of correlation peaks

The focus in this section is on the investigation whether the correlation methods used are providing logical and expected results. Knowing the causes of the correlations will help in the process of designing solutions. In terms of ride quality assessment, this work mainly focuses on vibrations up to 4 Hz, as this is the region where the pilot comfort is affected the most by the actively provided control inputs. To verify the method in general and to verify whether there is a correlation at the expected frequencies, the verification process will take into account vibrations up to 15 Hz. This is done as more knowledge is available in this frequency domain on the expected vibration sources. Examples of the PSD and correlation coefficient are shown in Figures 12 and 13. In Figure 12, peaks can be observed, which means an increase in control activity. In approximately the same frequencies, peaks can be observed in the correlation coefficient, shown in Figure 13, as well. The causes for these peaks are investigated in this section.

First the pilot model is discussed. Along the years analytical theory of manual control of vehicles has been developed. A useful and important research on this topic is performed by McRuer [15], who has proposed the crossover

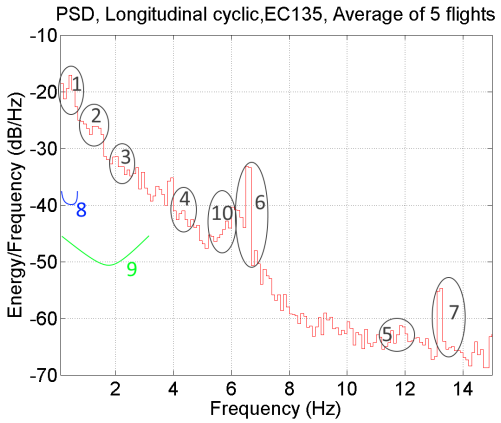

Figure 12: *Interesting peaks in Power Spectral Density*

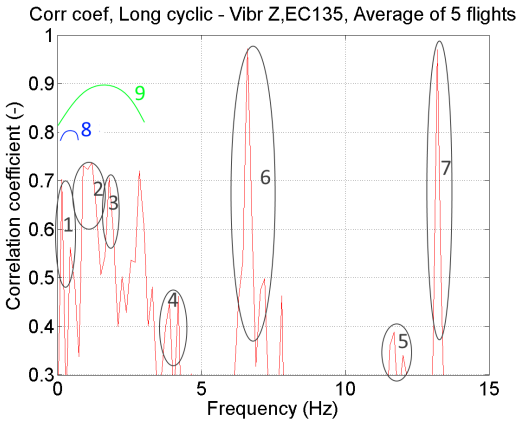

Figure 13: *Interesting peaks in Correlation coefficient*

model. In this model, the effect of the input of the pilot on the output is described for several different tracking tasks. From the crossover model, it is expected that most of the intentional pilot control inputs are below approximately 0.5 Hz in closed loop situations. Control inputs at higher frequencies could be possible during open loop situations, which is not expected during level flights. This model can explain the higher correlations in the frequency region of number **8** in Figures 12 and 13. This supports the fact that the control inputs and vibrations increases in that frequency area in case of a lateral manoeuvre. This also supports the point that the control inputs increases mainly up to 0.5 Hz in case the flight control system is not used. The flight control system mainly provides control inputs up to 4 Hz, but higher inputs are possible. These observations are based on the performed spectral analysis on the flight simulation outputs.

Next to these intentional inputs, the pilot also provides some unintentional inputs, in the form of biodynamic feedthrough. Biodynamic feedthrough occurs when the vibrations of a vehicle feed through the pilots body and cause involuntary motions of limbs, which will result in involuntary control inputs. This behaviour has been modelled by Mayo and Venrooij [13, 23]. From these results, the conclusion can be made that pilot inputs can be provided up to around 3 Hz. This is marked as number **9** in the figures. This means that vibrations up to that point can results in more control inputs, which will lead to more vibrations.

In order to investigate the influences of the body and rotor eigenmodes, linearisation is performed on the helicopter model for different conditions. The eigenmodes for the baseline configuration are calculated and shown in Table 3. It is determined that the short period and spiral mode do not have oscillatory parts in their eigenvalues, which means that their effect on the pilot discomfort is negligible. The main natural eigenmodes affecting the oscillations are the phugoid and the dutch roll. This is marked as number **1** in the figures. The roll subsidence mode is marked as number **2** in the figures.

The torsion eigenmodes of the rotor are all at very high frequencies, and their influence on the pilot discomfort is negligible. The regressive flapping mode occurs close to the natural eigenmodes. In many cases, around the first harmonic rotor load, the collective flapping mode can be found, and the progressive flapping mode is close to the second harmonic rotor load. These flapping modes are marked as numbers **1,6,7** respectively in the figures. In almost all Power Spectral Densities and correlation coefficient graphs, the regressive, collective, and progressive lead-lag modes can be found, which are marked as number **3,4,5**.

As a change in configuration can change the

Table 3: *Frequencies of the body and rotor eigenmodes (Flight simulation: calculated for EC135 baseline configuration)*

Eigenmodes	Frequency $[Hz]$
Phugoid	0.07
Regressive flapping mode	0.17
Dutch roll	0.27
Roll subsidence mode	1.08
Regressive lead-lag mode	2.23
Collective lead-lag mode	4.67
Collective flapping mode	6.82
Progressive lead-lag mode	11.6
Progressive flapping mode	13.3
Regressive torsion mode	28
Collective torsion mode	31.5
Progressive torsion mode	35

eigenmodes, the peaks can indeed be shifted, as can be seen in the parametric study on the center of gravity. This shift does not necessarily have to be attributed only to the change in configuration, as this eigenmode is also dependent on the thrust level, which is not constant during flight. Although the rotor speed is tried to be kept constant, small variations can still occur. These can also be the reasons that the peaks shown are not straight line peaks, but rather peaks with small bandwidths. Another reason could be the occurrence of spectral leakage.

Clear peaks can be noticed at the rotor harmonics. In some data sets, a slight influence can be seen from the tailboom induced vibrations. These can either be seen as a disturbance by the flight control system or added unintentionally by the pilot. The earlier described turbulence will influence the control inputs as well.

iii. Final evaluation on ride quality

Up to this point, the focus was on the correlation analysis between the vibrations and the control inputs. It was investigated where in the frequency spectrum there is high correlation and the causes of the peak correlations have been investigated as well. Now it would be interesting to know how this knowledge can be used for ride quality improvements.

It was suggested before that either high correlation coefficients or high control inputs can lead to high vibrations in the lower frequency domain. To investigate this further, the following sensitivity analysis is proposed and applied to the results of the parametric study:

1. The following **correlation coefficients** are taken into account: lateral cyclic & vibration in y-direction, and longitudinal cyclic & vibrations in x,z-direction. After they are calculated, the coefficients larger than 0.3 are summed and divided by the amount of bins. This value can be seen as an average value for the correlation coefficient.

2. The following calculation is applied on the **Power Spectral Density** of the lateral and longitudinal cyclic.

   (a) The Power Spectral Density of the lateral and longitudinal cyclic inputs are calculated in small bins.

   (b) The increase/decrease between each of the cases, as stated in the parametric study, is calculated with respect to the baseline case. This is done per bin. For example: the increase/decrease is calculated in the frequency range 0-0.1 Hz in the first iteration, until it reaches the bin 3.9-4 Hz in the final iteration.

   (c) These increases/decreases are summed and divided by the amount of bins. This is the average value of increase/decrease in the PSDs of the cyclic controls. With the normalization, it is avoided that the values in the first bins dominate the final value.

3. The ratio of the vibration levels between the investigated cases is estimated. This is done by multiplying the correlation coefficient with the power of the respective control input. This will be referred to as **'estimated vibration'**.

4. These estimated ratios are compared with the ratio's of the **measured vibration** levels. The latter are also estimated by determining the change between each of the cases with respect to the baseline case per bin, which is summed together.

The idea of this approach is not to try to estimate the actual vibration value, but rather to determine whether the power of the control inputs and the correlation coefficients can be used to determine which helicopter configuration or flight condition will be better in terms of ride quality. The reason is that this scaling will affect the absolute value of the vibrations but not ratio between the different cases. The upper frequency limit of this is taken to be 4 Hz, which is the area where most of the control inputs occur. It also includes the area of maximum human sensitivity. As the occurrence of large negative correlation coefficients was almost non-existent, these coefficients are not taken into account.

This sensitivity analysis is now be applied to the results of the atmospheric conditions comparison. Here, the turbulence level was assessed by a rating provided by the pilot. The power spectral densities and the correlations coefficient are calculated for several turbulent and calm flights. The different flights were then averaged per category (calm and turbulent). Using the described approach, the results are shown in Tables 4 and 5. It can be seen that the power of both control inputs increases. Furthermore, all correlation coefficients increase as well. This indicates that the estimated vibration level is higher in each direction in case of turbulence, which matches with the actual vibrations. One can further observe that the estimated and measured ratio's between the cases are not identical. As said before, this is also not expected. The multiplication of the power and the correlation coefficient is just to determine whether both factors will influence the vibrations.

The same approach is applied to the results of the weight comparison. It can be seen in Table 6 that the amount of control inputs are lower for a lower weight helicopter, but that the correlation coefficients are higher. The result is that the vibration levels are estimated higher, as can be seen in Table 7.

This sensitivity analysis can now be applied to the parametric studies of the flight control system tuning in order to test whether it can be used as a potential solution for ride quality improvement. It should be noted that the focus is solely on the vibrations and that the influence on other control and stability characteristics is not further analyzed. During the parametric study, it was concluded that increasing the PID gains by three will affect the correlation coefficients and the amount of control inputs, as shown in Table 8, and the pilot discomfort value. Ranking the different cases from highest discomfort: increasing all three PID gains, followed by the proportional gain, then the derivative gain and finally the integral gain. This also coincides with the ratio of the measured vibrations in Table 9. Based on the observations made from Tables 8 and 9, the following conclusions can be made:

- The case with increased PID gains has the highest correlation coefficients and amount of control inputs, which also results in the highest amount of vibrations.
- The amount of longitudinal control inputs of the baseline case and the case with increased I gain is comparable. However, the case with increased I gain has lower correlation coefficients between the longitudinal cyclic controls and vibrations in x-direction, which leads to relatively lower vibrations in x-direction.
- The correlation coefficients between the lateral cyclic and the vibrations in y-direction are almost equal for the baseline case and the case with higher P gain. However, the case with higher P gain has higher amount of lateral cyclic inputs, which leads to higher vibrations in y-direction.

These three conclusion strengthens the theory that the vibration level is dependent on the amount of control inputs, and is also reflected in the magnitude of the correlation coefficients.

Table 4: *Turbulence comparison: summations of correlation coefficients and Power Spectral Densities (Flight test data H145)*

Case	Correlation Coefficient			Power Spectral Densities	
	Lateral cyclic - Vibration Y	Longitudinal cyclic - Vibration X	Longitudinal cyclic - Vibration Z	Lateral Cyclic	Longitudinal Cyclic
Calm	0.0470	0.0360	0.0167	1.0000	1.0000
Turbulent	0.0533	0.0738	0.1333	3.5805	2.4027

Table 5: *Turbulence comparison: estimated vs measured vibrations (Flight test data H145)*

Case	Vibration X		Vibration Y		Vibration Z	
	Estimated	Measured	Estimated	Measured	Estimated	Measured
Calm	1.0000	1.0000	1.0000	1.0000	1.0000	1.0000
Turbulent	4.9250	2.4092	4.0596	6.8907	6.8170	9.2905

Table 6: *Weight comparison: summations of correlation coefficients and Power Spectral Densities (Flight simulation EC135)*

Case	Correlation Coefficient			Power Spectral Densities	
	Lateral cyclic - Vibration Y	Longitudinal cyclic - Vibration X	Longitudinal cyclic - Vibration Z	Lateral Cyclic	Longitudinal Cyclic
Baseline	0.2425	0.0827	0.0981	1.0000	1.0000
Lower weight	0.2955	0.1475	0.2723	0.8224	0.7654

Table 7: *Weight comparison: estimated vs measured vibrations (Flight simulation EC135)*

Case	Vibration X		Vibration Y		Vibration Z	
	Estimated	Measured	Estimated	Measured	Estimated	Measured
Baseline	1.000	1.0000	1.000	1.0000	1.000	1.0000
Lower weight	1.3652	4.3726	1.0021	3.7193	2.1254	2.9270

There are also some observations which have higher measured vibrations, while not showing a higher value in estimated vibrations. These are marked in red.

From these results it could indeed be concluded that the flight control system can be used as a potential solution for ride quality improvements. Both measurements on the power of the control inputs as well as the correlation coefficients can be used for this purpose. It can be noticed in this sensitivity analysis that increasing the P gain will lead to higher amount of control inputs, while increasing the D gain will mainly influence the correlation coefficients. Both parameters affect the pilot comfort significantly. Of course, a trade-off with the other design criteria should be made, which means that further investigations are required.

The advantage of using this approach over solely basing the pilot comfort on the discomfort value calculated with ISO2631-I is that the sources of discomfort here are based on the amount of control inputs given and the sensitivity of helicopter to low frequency vibrations, quantified with the correlation coefficients. So far, investigations were mainly based on calculating the total discomfort value under different conditions or for different configurations. However, now it would also provide more insights to why there is or there is not an increase in pilot discomfort. For example, the derivative gain tuning does not necessarily provide more control inputs than the baseline simulation, but due to the higher correlation coefficients, it does lead to higher vibrations. The added value of this approach is that the amount of control inputs, as well as the correlations coefficients, can be used to measure the sensitivity of the helicopter to lower frequency vibrations.

The correlation coefficient is based on helicopter configuration or flight condition. More explanation is provided on this. In general, the correlation coefficient measures how big the chance is that more control inputs will lead to more vibrations. Configuration-wise, a low weight helicopter is in general more sensitive to vibrations, therefore extra force inputs, caused by the control inputs, will easily cause more vibrations. Another example is the increase in derivative gain. This means that the flight control system will react stronger to the changes in the error. With the SAS mode, this means that in case of a disturbance, the derivative gain will directly sense a change in error and react to it quickly. The higher the gain, the higher the reaction will be. This means that the helicopter is more sensitive to vibrations. This discussion not only holds for different design parameters, but also for different flight conditions. In general, the aerodynamic forces (lift, drag) are dependent on the square of the velocity. This means that at high speeds, a change in helicopter orientation caused by a control input, will lead to changes in the different velocity components, which leads to extra vibrations. Therefore, at high speeds, the helicopter is more sensitive to vibrations. Another example is the occurrence of turbulence. Turbulence is able to perturb the incident flow of the rotor blades. This itself already leads to more vibrations, however this also means that if one adds more control inputs in this case, it will cause more disturbances. The reason why the correlation coefficient of the vibration in z-direction increases the most in case of turbulence, is that the lift force is probably affected the most. This means that the vertical movement is the most sensitive to vibrations. The latter point can be investigated in a future research. In order to improve ride quality, one can therefore use this coefficient to measure the sensitivity of a helicopter to low frequency vibrations. Potential solutions provided in this research are for example the tuning of the control system or to modify the weight of the helicopter. This of course should be a trade off with other design parameters, such as stability, fuel efficiency, et cetera.

From this research, it can also be concluded that the amount of control inputs provided should be lowered in order to improve the ride quality. The amount of pilot inputs can for example be limited by providing extra training on this to pilots. Furthermore, seat dampers can

Table 8: *Control gains comparison: summations of correlation coefficients and Power Spectral Densities (Flight simulation EC135)*

Case	Correlation Coefficient			Power Spectral Densities	
	Lateral cyclic - Vibration Y	Longitudinal cyclic - Vibration X	Longitudinal cyclic - Vibration Z	Lateral Cyclic	Longitudinal Cyclic
Baseline gain	0.2425	0.0827	0.0981	1.0000	1.0000
P gain ($\times$ 3)	0.2453	0.1643	0.0941	12.8597	3.0840
I gain ($\times$ 3)	0.0550	0.0516	0.0899	2.0190	1.0495
D gain ($\times$ 3)	0.2591	0.1782	0.1675	2.2486	1.6965
PID gain ($\times$ 3)	0.1843	0.2694	0.1393	17.9920	5.2858

Table 9: *Control gains comparison: estimated vs measured vibrations (Flight simulation EC135)*

Case	Vibration X		Vibration Y		Vibration Z	
	Estimated	Measured	Estimated	Measured	Estimated	Measured
Baseline gain	1.0000	1.0000	1.0000	1.0000	1.0000	1.0000
P gain ($\times$ 3)	6.1256	1.4207	13.0064	1.2199	2.9597	0.9893
I gain ($\times$ 3)	0.6548	0.9067	0.4582	0.9688	0.9617	0.9508
D gain ($\times$ 3)	3.6542	1.1414	2.4022	0.9547	2.8974	0.9828
PID gain ($\times$ 3)	17.2163	2.3898	13.6718	1.3419	7.5046	1.0640

be used to limit whole body vibrations, which may result in less biodynamic feedthrough. Finally, it is determined that in general using the autopilot will result in a decreased level of control inputs. The tuning of the flight control systems will also affect the control inputs provided by the system. It can for example reduce the vibrations caused by the eigenmodes and the 'strength' of the reaction to a tracking error.

V. Conclusion

The purpose of this work was to investigate the influence of the vibrations in the lower frequency domain on the pilot comfort. It was suspected that the vibrations were caused by the control inputs. The exact causes were unknown and so far no tools were directly available to analyse this. The main goal of this research was therefore to show where in the frequency domain there is a correlation between the control inputs and the vibrations, why there is a correlation and how the ride quality can be improved with this knowledge.

The measurements of the vibrations and control inputs were obtained from flight test data of the EC135 and H145 helicopters, and from flight simulations. For the correlation between the control inputs and the vibrations, the pattern is compared using correlation coefficients, and the intensity is compared using PSDs. To correlate the vibrations to the ride quality, human sensitivity weighting functions, as described in ISO2631-I, are applied. These two steps are applied in a parametric study, which includes different helicopter configurations and flight conditions. The important conclusions are listed below:

- It is determined that the cyclic control inputs and the vibrations are mainly correlated between 0-4 Hz. This is also the frequency domain where most of the control inputs occur. Peaks can be observed at the rotor harmonics as well.
- The vibrations in y-direction are mainly influenced by the lateral cyclic. The vibrations in x,z-direction are mainly influenced by the longitudinal cyclic. The correlation between the pedal and collective inputs and the vibrations is negligible.

- The correlation coefficient is influenced by a change in rotorcraft configuration and flight condition.
- The following parameters can negatively influence the ride quality: A more aft center of gravity, a lower-weight helicopter, higher flight speeds, a manoeuvring flight, no use of flight control system. Furthermore, it is determined that in case of turbulence, the non-rotor induced vibrations can indeed dominate the pilot discomfort.

The causes for high correlation are investigated. This is necessary to verify that the methods used are showing logical and expected results, especially the results from the correlation coefficients, which is an uncommonly used tool to analyse vibrations. Secondly, knowing the causes for correlation will help in the process of defining solutions. The following conclusion are made:

- Pilots are able to intentionally provide control inputs between 0-0.5 Hz during closed loops.
- The flight control system will provide most of the control inputs up to 4 Hz, although higher frequency inputs are possible.
- Biodynamic feedthrough occurs mostly in the region until 3 Hz, although amplifications at higher frequencies are possible.
- The eigenfreqencies are determined with a non-linear model and most peaks are identified in the correlation coefficient graphs and PSDs. Up till 4 Hz the phugoid, Dutch roll, roll subsidence mode, regressive flapping mode and regressive lead lag mode are identified.
- The exact range where the turbulence has influence on is hard to define, although most of it occurs below the 2.5 Hz. Turbulence is also a cause for initiating eigenmodes.
- Peaks can be observed around the rotor harmonic loads. This can be caused by the flight control system or biodynamic feedthrough.

The correlation coefficient is introduced in the research of pilot comfort assessment. During the parametric study it is observed that both a high amount of control inputs and a high correlation coefficient can indicate higher pilot discomfort. An analysis is performed to investigate this. The conclusions made are:

- Both the Power Spectral Density of the control inputs and the correlation coefficients can be used to approximate which helicopter design will have a lower vibration level between 0-4 Hz. This is also the frequency domain in which the maximum human sensitivity lies.
- The correlation coefficient can be used to measure the sensitivity of a helicopter to vibrations. A lower correlation coefficient will improve the helicopter ride quality.
  - This tool can for example compare different designs with each other during flight simulations. With this, the helicopter configuration with lower vibrations can be determined. Potential solutions provided in this study are for example the tuning of the control system or the modification of the weight of the helicopter.
  - For further research, it can be interesting to test some mechanical devices during flights tests. Examples are seat vibration isolators [24] and the biodynamic resistant control stick [20]. The correlation coefficient can measure the sensitivity to vibrations for flights with and without these devices.
- By lowering the amount of cyclic control inputs provided over the frequency range 0-4 Hz, the ride quality can be improved.
  - The amount of pilot inputs can for example be limited by providing extra training on this to pilots. An analysis between experienced and inexperienced pilots has not been performed in this research, which could be interesting to investigate.
  - Seat vibration isolation devices are able to limit the biodynamic

feedthrough by pilots. Another type of solution can be to restrain and immobilize body parts. Efforts has also been devoted to build a model-based cancellation approach, where the biodynamic feedthrough model is used to obtain a cancelling signal [22].

- It is investigated that in general using the autopilot will result in a lower amount of control inputs. The tuning of the flight control systems will also influence the control inputs provided by the system and therefore the ride quality.
- It is determined that shifting the center of gravity forward will increase the stability and decrease the amount of control inputs required.

A (mechanical) solution should certainly be one of the follow-up researches. Some potential solutions are provided in the list above.

As the correlation coefficient is a newly introduced statistical tool in rotorcraft applications and although it works well in many cases, conclusions should still be made with caution. Not all the peaks are identified yet and this coefficient is susceptible to noise correlation and is quite sensitive to the flight condition and helicopter configuration. Furthermore, the influence of spectral leakage is another nuisance factor that should be investigated. Therefore, a low correlation coefficient does not mean that there is no correlation between the control inputs and the vibrations.

Elastic motion and rotor harmonic loads are two assumptions made in the flight simulation model. As they occur in higher frequencies, where the amplitude of the control inputs are already considerably low, the influence of the added control inputs on the ride quality due to these phenomena is negligible. What is interesting to take into account in the flight simulation for future research, are pilot models. Pilots are one of the main contributors to a higher amount of control inputs, and it can therefore be investigated how this amount can be lowered. Furthermore, rotational gust speed components can be taken into account for more reliable results.

The results obtained during this work are mainly based on level flights. This means that the correlation between the vibrations and the pedal and collective inputs can become more significant in manoeuvring flights. In order to have a better estimation on how the control inputs influences the vibrations during a manoeuvre, more specific flight tests are required.

To conclude, the main focus of this work was to investigate the influence of the control inputs on the helicopter ride quality. It is investigated why and where in the frequency domain the correlation is. Furthermore, it provided stepping stones for future work on this topic.

References

[1] Asuero, A., Sayago, A., and Gonzalez, A. (2006). The correlation coefficient: An overview. *Critical reviews in analytical chemistry*, 36(1):41–59.

[2] Bechhoefer, E. and Power, D. (2003). Imd hums rotor track and balance techniques. *2003 IEEE Aerospace Conference Proceedings (Cat. No.03TH8652)*.

[3] Bernaschek, V. (2017). Modelling and investigation of the impact of fundamental airframe dynamic characteristics on helicopter ride quality. Technical report, Technische Universität Braunschweig, Airbus Helicopters.

[4] Branco, N. C., Alves-Pereira, M., et al. (2004). Vibroacoustic disease. *Noise and Health*, 6(23):3.

[5] Elliott, D. F. and Rao, K. R. (1983). *Fast transforms, algorithms, analyses, applications*. Elsevier.

[6] Fries, J. (2001). *Black Hawk Helicopter Vibration Analysis Due to Main Rotor Damage, Directional Constituents of the Resultant Vibrations*. Army research lab aberdeen proving ground md, United States.

[7] Griffin, M., Parsons, K., and Whitham, E. (1982). Vibration and comfort iv. application of experimental results. *Ergonomics*, 25(8):721–739.

[8] Hoblit, F. M. (1988). *Gust loads on aircraft: concepts and applications*. American Institute of Aeronautics and Astronautics, Washington, D.C.

[9] Karakolis, T., Farrell, P., and Fusina, G. (2015). Neck overuse injury in ch-146 griffon helicopter aircrews. *Procedia Manufacturing*, 3:4205–4212.

[10] Kåsin, J. I., Mansfield, N., and Wagstaff, A. (2011). Whole body vibration in helicopters: risk assessment in relation to low back pain. *Aviation, space, and environmental medicine*, 82(8):790–796.

[11] Krehbiel, T. C. (2004). Correlation coefficient rule of thumb. *Decision Sciences Journal of Innovative Education*, 2(1):97–100.

[12] Lee Rodgers, J. and Nicewander, W. A. (1988). Thirteen ways to look at the correlation coefficient. *The American Statistician*, 42(1):59–66.

[13] Mayo, J. R. (1989). The involuntary participation of a human pilot in a helicopter. *Fifteenth European Rotorcraft Forum*, pages 81–93.

[14] Mcfarland, R. E. (1983). The n/rev phenomenon in simulating a blade-element rotor system. *NASA Ames Research Center, Moffett Field, CA, United States*.

[15] McRuer, D. T. and Jex, H. R. (1967). A review of quasi-linear pilot models. *IEEE Transactions on Human Factors in Electronics*, 3:231–249.

[16] MJ, G. (1990). *Handbook of Human Vibration*. Academic Press, London, England.

[17] Padfield, G. D. (1989). *Helicopter handling qualities and control: international conference*. Royal Aeronautical Society, London.

[18] Parsons, K. and Griffin, M. (1982). Vibration and comfort ii. rotational seat vibration. *Ergonomics*, 25(7):631–644.

[19] Rath, T. and Fichter, W. (2017). A closer look at the impact of helicopter vibrations on ride quality. *Journal of the American Helicopter Society*.

[20] Repperger, D. W. (1984). Biodynamic resistant control stick. US Patent 4,477,043.

[21] Seher-Weiss, S. and Von Gruenhagen, W. (2012). Development of EC135 turbulence models via system identification. *Aerospace Science and Technology*, 23(1):43–52.

[22] Venrooij, J., Mulder, M., Van Paassen, M. M., Mulder, M., and Abbink, D. A. (2010). A review of biodynamic feedthrough mitigation techniques. *IFAC Proceedings Volumes*, 43(13):316–321.

[23] Venrooij, J., Pavel, M. D., Mulder, M., Van Der Helm, F. C., and Bülthoff, H. H. (2013). A practical biodynamic feedthrough model for helicopters. *CEAS Aeronautical Journal*, 4(4):421–432.

[24] Wickramasinghe, V. K. (2012). *Dynamics Control Approaches to Improve Vibratory Environment of the Helicopter Aircrew*. Carleton University.